UNIVERSITÀ DEGLI STUDI DI NAPOLI FEDERICO II

SCUOLA POLITECNICA E DELLE SCIENZE DI BASE

Dipartimento di Ingegneria Chimica, dei Materiali e della Produzione Industriale

DOTTORATO DI RICERCA IN INGEGNERIA DEI MATERIALI E

DELLE STRUTTURE

XXVIII CICLO

"An engineered driving plate for the electro-drawing of polymer microneedles with internal microstructure based on multiphase system templating"

Tutor
Ch.mo Prof. Ing. Paolo Antonio Netti

Candidata
Ing. Flavia Ruggiero

Co-tutors
Dr. Ing. Raffaele Vecchione
Dott.ssa Ing. Enza Torino

Coordinatore
Ch.mo Prof. Ing. Giuseppe Mensitieri

2013 - 2016

Preface

To date, transdermal delivery is recognized as a successful route for the administration of active compounds, overcoming most of the drawbacks affecting the traditional oral and parenteral routes. Patches made up of microscopic needles, namely microneedles, fabricated by means of several kinds of polymers, including biodegradable, biocompatible and water-soluble polymers, have been, in the last decade, developed and tested as effective and not-invasive devices for delivering therapeutic macromolecules across the skin. Anyway, some limitations associated to the fabrication techniques of biodegradable and dissolvable microneedles, such as stamp-based multistep sequences of process or high work temperatures, not suitable for encapsulating thermolabile drugs, have prevented their spreading on pharmaceutical market. Recently, a mold-free and mild temperature Electro-Drawing technique, has been proposed as viable route for the fabrication of biodegradable microneedles: it is based on the deformation of sessile drops of polymer solution, undergoing an electrohydrodynamic action generated from the electric field arising from a thermally stimulated pyroelectric crystal. The technique also allows tuning the internal microstructure of microneedles. In fact, as for other controlled release drug delivery systems, such as microparticles, also for polymer microneedles, the presence of an internal microstructure can lead to many advantages, for instance incremented loading efficiency, drug protection and tunable release kinetics.

The main goal of the thesis was to develop some technological advances for the Electro-Drawing technique, in order to extend it to an in parallel production of microneedles, together with some strategies for tuning their internal microstructure.

In the first chapter, an overview on the microstructured polymer systems mainly used in the biomedical field is provided, followed by a focusing on the fabrication techniques for biodegradable and dissolvable microneedles. In the second chapter, a novel set-up for the in parallel Electro-Drawing, based on an engineered driving plate, is presented. The third chapter deals with some strategies in order to tune the internal morphology of the Electro-Drawn microneedles. Finally, in the fourth chapter, the results of a work focused on the study of thermodynamics of polymer systems, useful for controlling the morphology of architectures obtained from phase separation processes, are presented.

Table of Contents

Abstract

In this study, a development of the Electro-Drawing (ED) technique is carried out, in order to extend its advantages to the in parallel fabrication of arrays of biodegradable microneedles for transdermal drug delivery. To this aim, a novel set-up, based on an engineered driving plate is proposed. In particular, the electric field needed for the shaping of microneedles from sessile drops, is generated from the heating of a pyroelectric crystal by means of an electric circuit directly patterned onto it. The circuit is designed, starting from simulation results, and fabricated, by means of laser writing and metal deposition, in order to obtain the homogeneous heating of an extended crystal surface area, such that a uniform and simultaneous electrohydrodynamic action can be activated on an array of sessile drops, generating the final microneedles. Further, this novel set up allows the microneedle shape modulation, in term of indenting cone height and tip radius of curvature. This new shape, joint to the interposition of a rapid dissolvable layer, allows the microneedles to separate from the patch few minutes upon application.

Further, several strategies for tuning the internal microstructure of the fabricated microneedles, in order to modulate their release properties, are proposed. In particular, it is demonstrated how it is possible to obtain different porosity features by electro-drawing sessile drops of emulsions with different formulations, or by inducing phase separations on the precursor solution. While in the first case a closed porous structure is achieved, in the second case an interconnected porosity is obtained.

In a final section of the work, it is proposed a strategy based on Isothermal Titration Calorimetry, in order to study the thermodynamics of ternary polymer systems, useful to gain information for the control of the morphology of porous polymer structures, obtained starting from controlled phase separation processes. A simulative approach, based on a Monte Carlo method, is also proposed as a complement to the strategy in the previous lines.

Chapter 1

Introduction

This first chapter is finalized to describe the scientific frame, starting from which the aims of the presented study were fixed, and within which the results described in the following chapters were developed.

In the first paragraph, an overview of the advantages of the controlled release systems as routes for drug administration with respect to the traditional ones will be provided, together with the explanation of the mechanisms of drug delivery from polymeric carriers. This overview will be followed by the one concerning the most widely employed polymer-matrix drug delivery systems (further referred to as DDSs), together with their applications. In particular, the attention will be focused on the following kinds of polymer DDSs:

- scaffolds for tissue engineering, widely employed for mimic the extracellular matrix and for delivery the growth factors needed for the cell proliferation and differentiation;
- microparticles for targeted delivery of manifold compounds of therapeutic interest;
- patches of microneedles for transdermal delivery of active macromolecules across the skin.

Among these DDSs, despite of their potential wide range of applications, polymer microneedles, as dissolvable or biodegradable carriers, still suffer of several limitations concerning their fabrication technologies reported in literature. For this reason, being the thesis work substantially focused on polymer microneedles as DDSs, a paragraph of this chapter will be completely dedicated to the description of these technologies, together with their limitations. The Electro-Drawing, recently proposed as viable route for overcoming the limitations of the previous fabrication techniques[1], among its advantages, offers the chance of engineering the internal microstructure of the produced biodegradable microneedles. In fact, the presence of an internal microstructure, as explained further, is a fundamental issue for a good DDS. For this reason, within the present chapter, a paragraph will be dedicated to reviewing the most widely used techniques in order to obtain porous polymer architectures for drug delivery. Even though these techniques were substantially tested for scaffolds and

microparticles, their study, as reported in this chapter, can be of precious value in order to gain information for further applications in biodegradable microneedle internal microstructure engineering. In the last paragraph, starting from what previously described, the aims of the thesis will be explained.

1.1 Controlled drug delivery systems

Nowadays, the continuous discovery of novel therapeutic active compounds, makes the development of efficient drug delivery systems one of the most challenging aims of research in the biomedical and pharmaceutical fields. To date, the most employed administration routes for the known active ingredients, belong to the oral and parenteral categories. Each of these latter traditional medication systems is obviously characterized by both advantages and drawbacks. In particular, if the absence of pain for the patient, the low costs and the exposure of large surface areas with high blood supply useful for the absorption represent some of the oral administration advantages, on the other hand, the possibility of drug degradation during the passage in the gastrointestinal tract and some factors affecting the absorption such as PH, food and mucus layers, represent some drawbacks for it[2,3]. On the contrary, if the rapid onset of the therapeutic action and the continuous administration by infusion of the active drug are advantages for the parenteral routes, the pain linked to the injection, the infection risks and the difficulties for high drug quantity administration are their point of weakness. In particular, these drawbacks, joined to the one-shot drug administration, concern also the hypodermic injection, nowadays still widely employed for various kinds of drug administration[2].

Despite of their large employment, these traditional systems may not allow the delivery of satisfactory concentrations of medication to the appropriate site. Drug delivery systems (DDSs) have been developed in the past decades, with the aim of altering the pharmacokinetics of drugs, in order to maintain a sustained therapeutic concentration at a specific location in the body, by minimizing the side effects[4]. The basic idea for the DDSs is linked to the creation of a matrix or a carrier which can increase the drug bioavailability while minimizing the drug waste. The matrix has to act as rate-controlling device for the delivery of bioactive compounds in a pre-determined part of the body, in order to keep the desired level of bioavailability of the drug over a certain time period[4]. This latter task

represents the fundamental improvement of the controlled release systems with respect to the traditional administration route: in this latter case, the desired level of drug is not constant in time, but has to be renewed with following administrations at fixed time periods. Further, the DDS matrix has also the task of protecting the encapsulated drugs from the body metabolic mechanisms. Also the targeting of the DDSs, i.e. the punctual delivery of the active compound to an organ, a tissue, or special cells, is one of their most important issues.

For the DDS matrix realization, several polymeric materials have been selected as drug carriers, because of their biocompatibility, biodegradability and hydrophilicity[5]. In fact, hydrophilicity or biodegradability are important properties in order to control the release mechanism of the active compounds, loaded within the polymer matrix. The different drug release mechanisms are summarized in Fig.1.1.

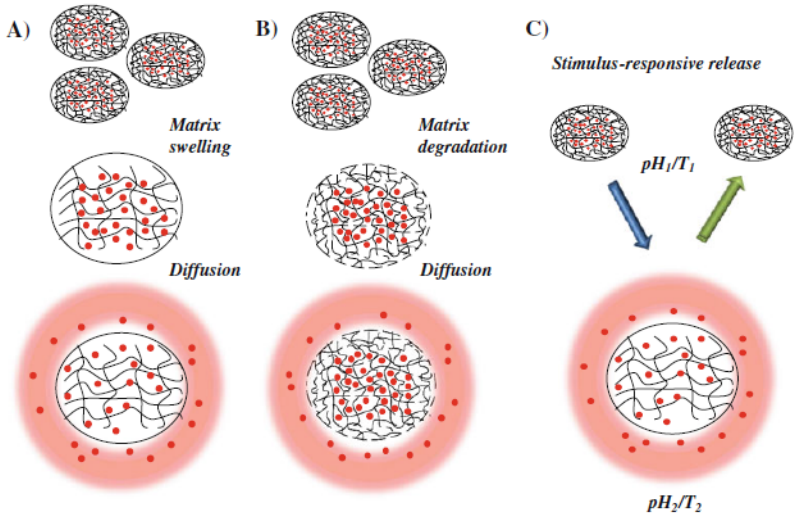

Figure 1.1*: Schematic representation of the different drug release mechanisms; a) swelling of the polymer matrix with consequent drug diffusion; b) matrix degradation followed by drug diffusion; c) drug release subsequent to the change in matrix properties, induced by an external stimulus (pH or temperature)*[4].

As summarized in Fig. 1.1, if the polymer matrix encapsulating the drug is of hydrophilic nature, the release of the active compound is controlled by diffusion phenomena due to the swelling of the matrix, following to the contact with biological fluids. With the same basic principles, in the case of biodegradable polymers, the drug release diffusion is controlled by the degradation rate of the encapsulating matrix[6]. In several cases, the drug release is ruled by external stimulus instead[7].

On the basis of what discussed in the previous lines, the properties of polymer structures of encapsulating active compounds and of releasing them following a specific kinetics, which

can be tuned by adjusting some matrix features (such as degradation times), can be employed for several applications. The specific features required for polymer DDSs, are strictly linked to their final application, in order to realize a controlled release of the drug as near as possible to the desired one. Among the examples of DDSs as biodegradable polymer architectures, there are scaffolds, microparticles and microneedles.

1.2 Scaffolds

Regenerative medicine represents a branch of medicine based on the goal of reconstructing damaged organs or tissues, as a consequence of a disease or an injury. This task is carried out by means of cells and/or growth factors. In particular, strategies linked to the direct application of progenitor cells or to the use of growth factors in order to make the cells repair tissues, are employed. For both the two strategies, often cells and/or growth factors are combined with three-dimensional polymer materials[4]. Growth factors are proteins capable of stimulating cellular proliferation, migration and differentiation into a specialized phenotype[8]. While for therapeutic cell administration, their confinement within a polymer shell, namely a polymer capsule, can be a suitable and helpful strategy, in the case of tissue regeneration by means of growth factors, the amount administered to cells, joint to the maintenance of their biological activity, has to be finely tuned. This latter task can be pursued by means of the encapsulation of these compounds within polymer matrices for drug delivery, referred to as scaffolds for tissue engineering. Indeed, biodegradable scaffolds are used in tissue engineering in order to create a desirable microenvironment for regeneration of damaged organs or tissues[9]. Scaffolds are biodegradable 3D supports, with a porous structure emulating the extracellular matrix, guiding cell adhesion, proliferation and differentiation[10]. The scaffolds must provide (1) a proper combination of physical properties, such as strength, stiffness and toughness; (2) adequate porosity, interconnectivity and permeability for nutrient delivery and metabolite removal; and (3) a controllable degradation rate in nontoxic products[11]. Several synthetic polymers, such as polylactic acid (PLA), polyglycolic acid (PGA), polycaprolactone (PCL) and their copolymers, such as polylactic-co-glycolic acid (PLGA) have been widely used to fabricate scaffolds, not only because of their characteristics of biodegradability and biocompatibility[12], but also for their availability, ease of processing and adjustable degradation[13]. The active compounds, such as

the growth factors mentioned above, are typically encapsulated within the scaffold matrix and then released to the desired site upon polymer degradation. There are two different kinds of polymer degradations: the first, so-called surface erosion, is the degradation of the matrix surface due to the contact with surrounding liquids, the second is the bulk degradation, which takes place in the whole polymeric domain. This latter mechanism is the one demonstrated to dominate for PLA and PLGA scaffolds.

1.3 Microspheres

Both for tissue engineering and other medical and pharmaceutical applications, microspheres have been widely used as successful carriers for drugs encapsulated within them[14]. In fact, formulations based on microparticles are characterized by a very wide range of chances of applications, being flexible for manifold deliveries: oral delivery, intramuscular injection, subcutaneous injection and targeted delivery[15]. These spheres, made of biodegradable polymer materials, allow releasing in a controlled manner the encapsulated drug, in order to maintain a constant therapeutic level in body fluids over a long period after administration[16]. Specific features are required for a suitable release from microspheres, such as high surface-to-volume ratio, low density and low coefficient of thermal expansion[17]. The chance of a localized delivery to a targeted area represents a further advantage in polymeric microsphere delivery systems. Among the others applications, microparticle based systems have been widely employed for the delivery of peptides and proteins[14]: because of their relatively large size, their bioavailability following the administration by the conventional route results to be too low. Further, these compounds are very sensitive to the environmental conditions, undergoing to degradation drawbacks.

1.4 Microneedles

The transdermal administration, i.e. the drug adsorption across the skin, realized by means of patches, in the two most common kinds “drug in matrix” and “drug in reservoir”, is characterized by some advantages such as absence of pain for the patient and chance to realize a drug controlled release[18]. Anyway, the transdermal delivery by means of patches is effective only for a limited class of active compounds, because of the barrier, represented

from the stratum corneum, imposed by the epidermis to the delivery of molecules across the skin[19]. Several have been the approaches developed within the last years, differing from each other only for the basic principle, but all finalized to stratum corneum "destruction", to the aim of creating local passage ways for the active compound macromolecules, but with dimension small enough to not induce clinical damages[20,21]. The alternative approach to the local destruction of the stratum corneum, is represented by the development of patches made up of two-dimensional arrays of microscopic needles, by means of which deliver drugs across the stratum corneum without any pain. The characteristic dimensions of microneedles are such that they result larger than the ones of the therapeutic macromolecules, supramolecular complexes or microparticles to be encapsulated and delivered, but also such that creating holes, when indenting skin, smaller than the ones produced by the common hypodermic needles. Anyway, even though microneedle patches have been proposed during 1970s, technological limitations, linked to the fabrication of structures with such small dimensions, determined that the first microneedles were realized at the end of 1990s[22]. Starting from those years, the availability of the microelectronics techniques, characterized by low costs and possibility of massive production, has made possible their fabrication by means of several materials. The transdermal delivery through the use of microneedles, with its advantages of absence of pain and first-pass metabolism, and lower microbial penetration with respect to the hypodermal needles, joint to the chance of controlling the drug release rate, has been tested both in vitro and in vivo for several applications, among which also the vaccines administration[23]. In this latter case, a better immunological reaction than the classic hypodermal route has been evidenced[24].

To date, the microneedles used and tested for transdermal delivery, can be associated to three main categories, differing from each other for the administration mechanism[25]: solid, hollow and dissolvable or biodegradable. The choice of the material suitable for the microneedle fabrication has to be fitted on several considerations, such as features of the biomolecules to administer, mechanical resistance for skin indentation and drug release modulation. Both metallic and silicon microneedles were fabricated and tested for the transdermal delivery of several biomolecules, such as proteins, vaccines, antibodies and DNA. They were realized both as hollow microneedles and as solid microneedles coated by means of the drug containing solution[2,26,27]. Anyway, for the coated microneedles the drug loading efficiency is rather low. On the other side, for the hollow microneedles the major

limitation is linked to the infusion system complexity. Further, the drawbacks concerning the high fabrication costs and to the dangers associated to the accidental breakage of the microneedle tips under the skin, because of the material fragility[25], promoted the development of novel fabrication techniques for polymer microneedles, with features of dissolvability or biodegradability. The testing of these latter microneedles demonstrated their capability of successfully releasing across the skin therapeutic molecules which transfer was not possible by means of the conventional transdermal techniques[28,29]. The mechanism of delivery from dissolvable or biodegradable microneedles is summarized in Fig. 1.2.

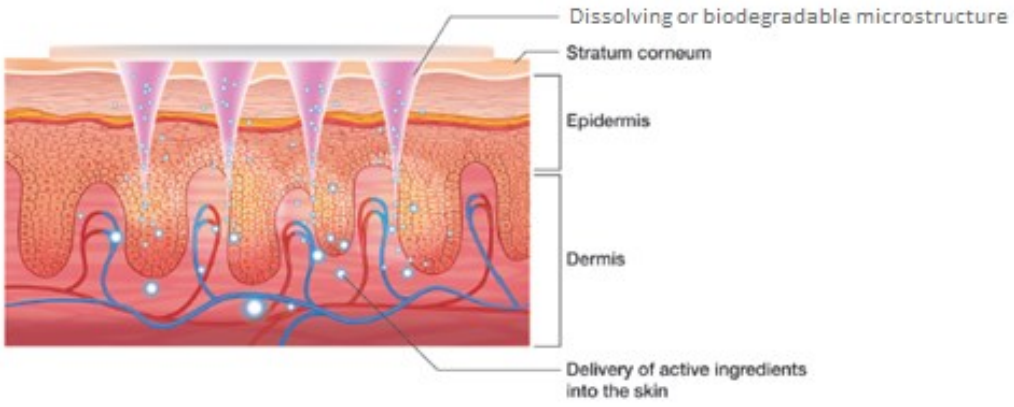

Figure 1.2*: Schematic diagram showing the mechanism of delivery from biodegradable or dissolvable microneedles; adapted from ref 30.*

1.4.1 Polymer microneedle fabrication techniques

Stamp-based techniques

As anticipated in the previous lines, the obstacle to the wide diffusion on the pharmaceutical market of dissolvable or biodegradable polymer microneedle patches is represented by the technological limitations which affect their fabrication processes.

Most of the fabrication processes proposed in literature are based on the preventive realization of a mold, by means of which a polymer melt, containing the active compound, is modeled and shaped into microneedles. These stamp - based techniques result in sequences of multi-step processes, economically and temporally expensive. More in detail, these processes can be summarized in the following steps: fabrication of the initial master structure, fabrication of the three-dimensional mold starting from the master, active compound encapsulation within a polymer material suitable for microneedle production,

polymer hardening and obtaining of the final microneedles from the mold. Among these steps, the master fabrication is characterized by peculiar difficulty. Fort this task, microfabrication processes, typical for MEMS devices, are commonly employed. In particular, the master fabrication can be divided in three principal steps: deposition, patterning and etching. The deposition consists in coating a substrate by means of a polymeric resist, with a layer thickness of few nanometers up to hundreds of microns. On the deposited layer, a pattern is then transferred by means of a lithographic technique (photolithography, e-beam lithography, x-ray lithography, etc.), consisting in the selective resist exposure to a radiative source. Finally, the etching process (dry or wet etching according to the employed agent) allows the selective removal of substrate portions, to the aim of transferring the desired pattern on it. After the master fabrication, the structure, typically realized in polydimethylsiloxane (PDMS), which will be the mold for the replication of microneedles, can be obtained starting from it, according to the flow chart summarized in Fig. 1.3.

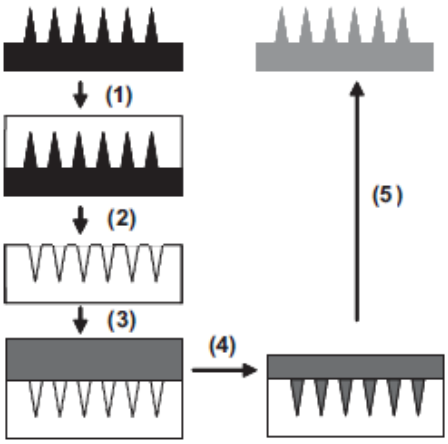

Figure 1.3: *Flow chart of the micro-molding technique; PDMS is poured onto the microneedle master structure (1); the PDMS mold is cured and peeled off (2); the drug-containing polymer melt is pipetted onto the mold (3); a vacuum is applied in order to pull the solution into the mold (4); the polymer melt is hardened and the microneedle patch is peeled out of the PDMS mold (5)*[31].

The described process flow chart was employed in several literature works[29,31-33], being in each case revised according to the kind of material and the desired shape for final microneedles.

Park et al.[29] fabricated biodegradable polymer microneedles with manifold shapes, made of polylactic acid (PLA), polyglycolic acid (PGA) and their copolymers, by means of a micro-molding technique. After the fabrication of a master structure made of polyurethane or SU-8

epoxy photoresist, and the PDMS mold realization starting from it, the mold was filled by polymer pellets and vacuum was applied joint to temperatures higher than the polymer melting point, in order to melt the pellets. The final freezing step allowed to obtain the final microneedles from the mold. The produced microneedles, with several tip shapes, are represented in Fig. 1.4.

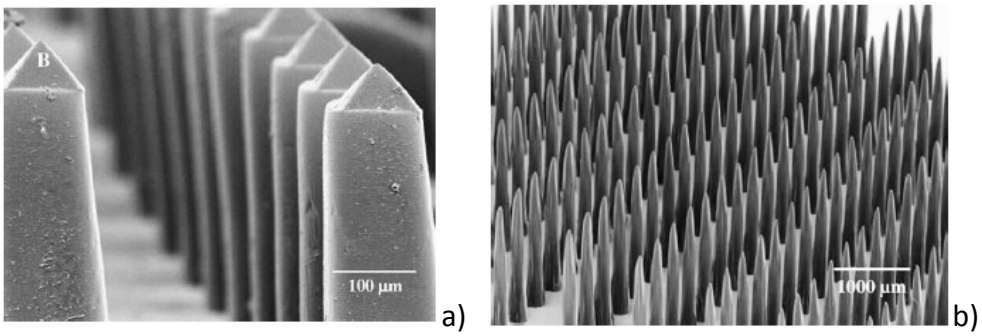

a) b)

Figure 1.4*: SEM images of PGA microneedles produced my micro-molding technique; a) chisel-tip microneedles; b) tapered cone microneedles*[29]*.*

Anyway, because of the microneedle high mechanical resistance needed for indenting the skin, only high molecular weight polymers are suitable for their fabrication. But, it is well known how the higher the polymer molecular weight, the higher is the melting point; in this way high process temperatures are imposed for molding. This issue is of crucial importance in sight of the encapsulation of thermolabile drugs, leading the micro-molding techniques to lack of versatility[34].

The inconvenient due to high process temperatures was underlined and circumvented by Sullivan et al.[31]. In their work, the authors fabricated polymer microneedles by means of a micro-molding technique again, but they pursued the polymer hardening by means of an in situ photopolymerization process at room temperature. The fabricated polyvinyl pyrrolidone (PVP) microneedles, represented in Fig. 1.5 a) were shown to successfully encapsulate an active protein, insert into the skin and delivery the active compound.

Anyway, this latter process was activated by means of UV radiations: the UV treatment can inhibit the activity of the therapeutic compound encapsulated within the polymer matrix, as well as photoinitiator residuals within the final microneedles can introduce dangers in terms of toxicity. On the other hand, solvent casting processes at ambient temperatures and in absence of UV resulted to be very complex and temporally expensive, because of the solvent long evaporation times needed[28]. Polymer microneedles fabricated by means of micro-molding and solvent casting are shown in Fig. 1.5 b).

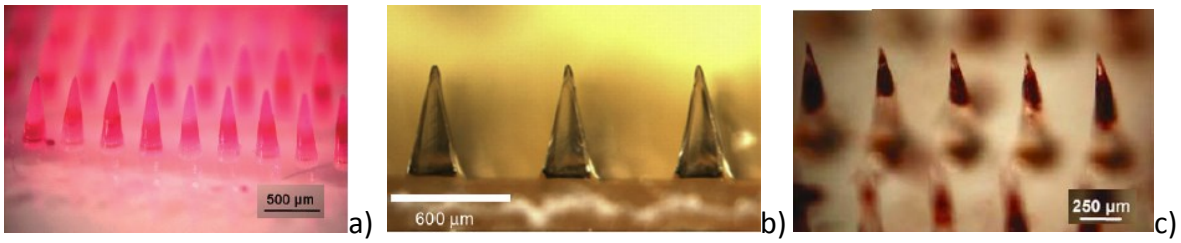

Figure 1.5*: a) PVP microneedles, encapsulating sulforhodamine, fabricated by in situ polymerization method*[31]*; b) CMC microneedles by solvent casting process*[28]*; c) PLGA microneedles, fabricated by micro-molding*[34]*.*

Therefore, nevertheless the stamp-based techniques are able to guarantee an optimal reproducibility on the shape of arrays of hundreds of microneedles, and in this way an easy chance of industrial scaling up production, the factors employed for polymer melting in order to fill the stamp or, vice versa, for its hardening, represent a crucial limitation.

Mold-free techniques

Recently, a new polymer microneedle fabrication technique, based on a drawing lithography process[35,36], has been proposed as potential solution for several of the technological limitations affecting the processes presented above. This latter technique is based on the elastic response of the polymeric material in its glass state, in particular by generating the three-dimensional shape characteristic of the microneedle by means of the application of an extensional deformation. The process is schematically shown in Fig. 1.6.

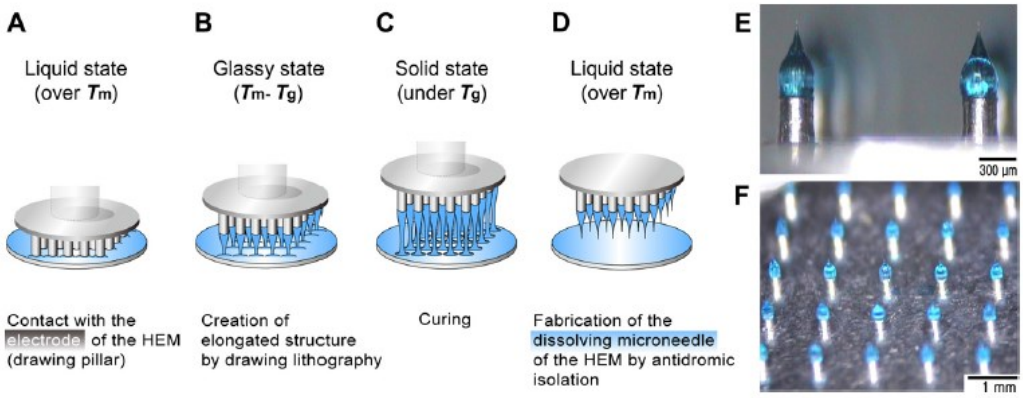

Figure 1.6*: Fabrication process of microneedles by means of drawing lithography; a) liquid maltose, at temperature higher than its melting point (T_m) is coated on a planar surface and contacted with a driving plate made up of an array of 5x5 pillars; b) the maltose at glassy state, at temperature between T_m and its glass transition temperature T_g, is elongated by means of the pillars; c) the elongated structures are cured to solid state; d) the coating on the flat surface is melted in order to isolate the 3D structures; e-f) images of the fabricated microneedles*[35].

Anyway the technique, being it based on the high viscosity variation experimented by the polymer near its glass transition, despite of the absence of master fabrication processes or replica molding, is again affected by the limits arising from the needing of high temperatures. Further, the features of reproducibility result to be lower than the stamp-based processes, being the shaping of microneedles induced by the dynamic interaction between the polymer melt and the employed set-up.

The drawing lithography technique has been recently revisited by Kim et al.[37]: in their work, the authors introduced a new stamp-free fabrication technique for polymer microneedles, based on the "Droplet-born Air Blowing" (DAB) method. According to this technique, drops of polymer solution are shaped into the 3D morphology of microneedles and then consolidated in their final shape by means of an air blow, avoiding in this way both high temperatures and UV. The solution drops are deposited in an array configuration onto two plates, by means of a dispenser equipped with automated stages for positioning. The two plates are then contacted with each other and elongated at a controlled rate, in order to realize an extensional deformation process on the contacted droplets. When the final distance between the plates is reached, the elongated polymer is hardened by means of the air blow and the microneedles are obtained starting from a final isolation step of the plates. The process flow chart is summarized in Fig. 1.7.

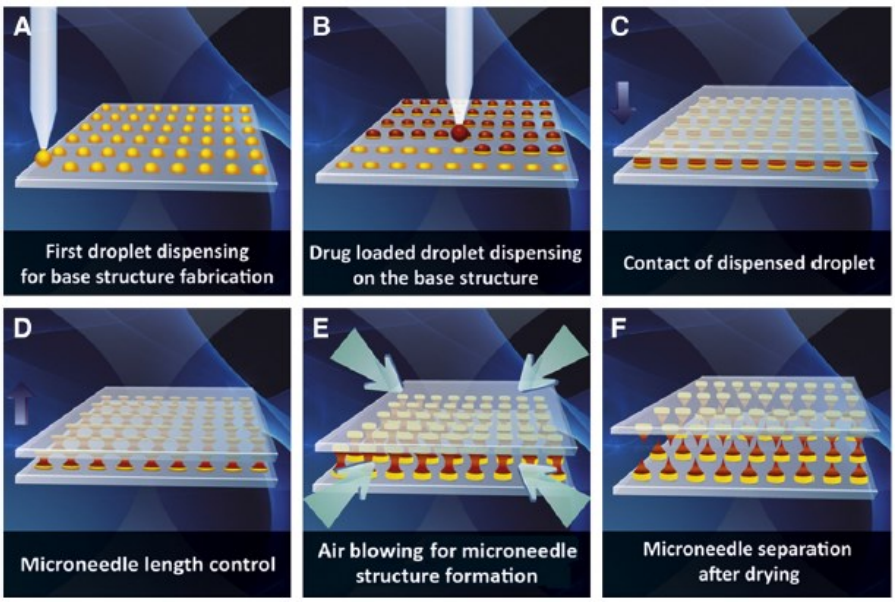

Figure 1.7*: Schematic flow chart of the droplet-born air blowing method for polymer microneedles*[37].

The technique has been employed for the fabrication of microneedles made of different biopolymers, i.e. carboxymethylcellulose (CMC), sodium hyaluronate (HA) and polyvinyl pyrrolidone (PVP). The control of drug dose within the dissolvable microneedles can be tuned by means of the control of drops volume and drug concentration within it. Some microneedles, fabricated by means of the DAB method, are shown in Fig. 1.8.

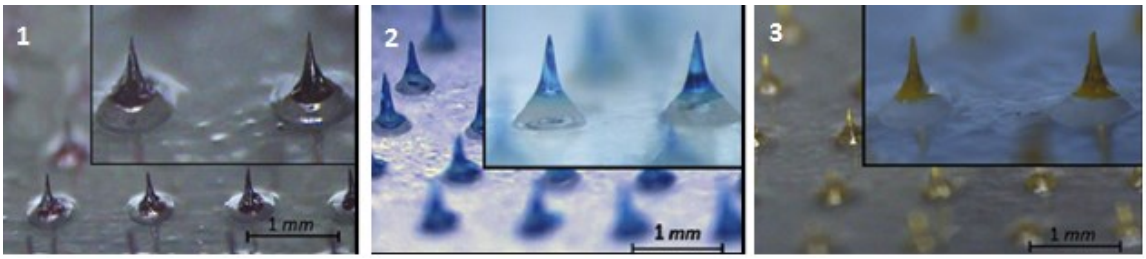

Figure 1.8: *Dissolvable microneedles, fabricated by means of droplet-born air blowing method; 1) CMC; 2) HA; 3) PVP*[37].

The droplet-born air blowing method has been recently combined with a cyclic contact and drying process on pillars (CCDP process, reported in Fig. 1.9)[38], in order to obtain patches of dissolvable microneedles, characterized by the possibility of rapid separation of microneedles from their backing film. These microneedles have been demonstrated to separate from the patch few seconds after the insertion in the skin, before their dissolution.

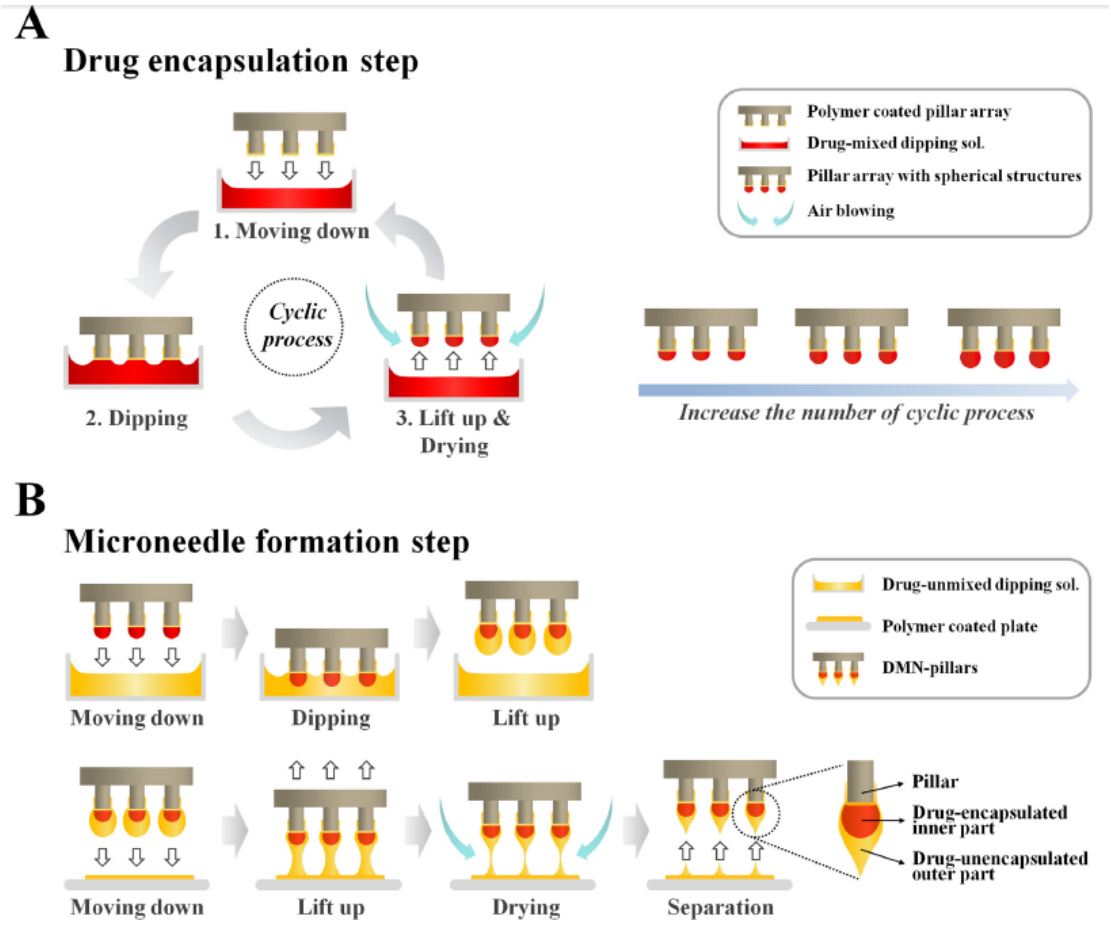

Figure 1.9: *Schematic flow chart of the CCDP process*[38].

Despite the CCDP technique is free from the limitation concerning the high process temperature affecting the traditional drawing lithography, the process is still affected by the drawbacks linked to the dynamic interaction with the contact plate. Further, the proposed solution seems to be not suitable for a uniform drug distribution within the microneedles, together with the not ideal radius of curvature of their tips.

The Electro-Drawing technique

The absence of multi-step sequences, based on molding processes, is one of the peculiar features of a novel fabrication technique for biodegradable polymer microneedles, recently proposed by Vecchione et al.[1]. The technique basic idea is the direct drawing of microneedles starting from sessile drops of polymer solution, by means of an electrohydrodynamic (EHD) action on them, overcoming in this way the limitations presented by the most of the technologies reported in literature. The technology is, in fact, free from high process temperature and UV radiations, being the biopolymers processed in

solution form, at temperatures between 20°C and 40°C, and shaped into microneedles in a single step procedure, under the effects of an external electric field. The technique was demonstrated to be suitable for the encapsulation of both hydrophilic and hydrophobic active compounds, in concentration of therapeutic interest.

The set-up for the electro-drawing (ED) process is based on the frontal exposure of a polar dielectric crystal (Lithium Niobate $LiNbO_3$ or Lithium Tantalate $LiTaO_3$) and a drop of polymer solution, at controlled distance. The basic principle of the fabrication technique is the *pyroelectric effect* of the dielectric crystal (i.e. the propriety of experimenting, as response to a temperature change, a change in spontaneous polarization), which acts in this way as guide for the microneedle drawing process[39]. Indeed, an appropriate thermal stimulus applied to the crystal, makes possible an electric field generation. Consequently, this electric field makes an EHD force arise, inducing an instability on the polymer solution drop and making it to assume the typical shape of a microneedle. In fact, it is well known how liquid meniscus undergoing to EHD forces generated by external electric fields, assume the shape of the so-called Taylor cone[40]: by properly tuning the electric field generated from the pyroelectric crystal, i.e. the EHD action, this latter shape can be modulated into a microneedle one. By depositing several drops onto a flexible polydimethylsiloxane (PDMS) substrate and applying the thermal stimulus on the crystal in correspondence of each drop, several microneedles can be obtained.

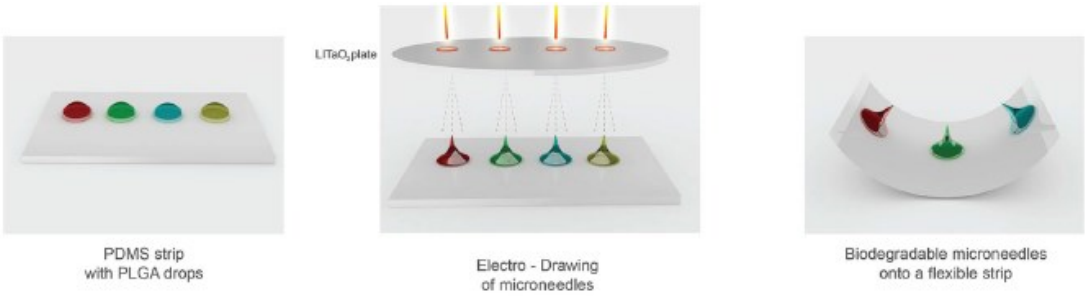

Figure 1.10*: Schematic flow chart of the electro-drawing of polymer microneedles*[1]*.*

As shown in Fig. 1.10, the ED technique can be summarized in three fundamental steps: deposition of the polymer solution drops, EHD force activation, solvent elimination by evaporation. Indeed, during the shaping process, the liquid cone solidifies following to the fast solvent evaporation, fixing in this way the microneedle desired shape. A final thermal treatment (40°C for 10 min) is carried out in order to improve the aspect ratio of the fabricated microneedle. The microneedle shape can be regarded as the result of the

competition between the surface tension of the liquid drop and the electrostatic attraction at which it undergoes. For this reason, the fabrication process, and therefore the final microneedle shape can be properly controlled by means of the modulation of the EHD action.

The technique was tested on polylactic-co-glycolic acid (PLGA) solutions, with dimethylcarbonate (DMC) as solvent for it and a third compound as model for the hydrophobic active compound to encapsulate. To the aim of better controlling the ED process, the PLGA drops was deposited onto PDMS pillars, in order to make the drop basis, and therefore the microneedles, be uniform. The technique was demonstrated to be suitable also for the production of microneedles encapsulating hydrophilic compounds: W/O emulsions, made up of water phase disperse within the PLGA matrix, were successfully electro-drawn, generating microporous microneedles.

As described in the previous lines, the ED appears a very suitable route for the fabrication of polymer microneedles overcoming the limitations of the classic techniques, such as the high process temperatures or the use of photoinitiators and/or UV radiations, as well as of complicated multistep mold fabrications. Being the biopolymers processed from their solution formulation, the technique also offers the chance of engineering the microstructure within the polymer matrix, with a high versatility in terms of tunable drug release kinetics. Anyway, in sight of the process parallelization, a novel approach, different from a punctual stimulus of the pyroelectric crystal in correspondence of each drop, for the EHD activation is needed. Further, the presence of a basis pedestal for the fabricated microneedles, should be removed in order to avoid loss of drug during administration.

1.4.2 Applications for polymer microneedles

Conventionally, the administration of immunobiologicals is carried out via the subcutaneous, intramuscular or intradermal route, in order to avoid infectious diseases. Anyway, the phobia and the pain associated with the needle employment, has encouraged the development of vaccinations by means of microneedles, in order to pursuit lack of pain, self-administration and quick delivery of the vaccine. Among the immunobiologicals used for testing microneedle administration, there are influenza vaccine, hepatitis B vaccine, human IgG and tetanus toxoid[24,41-43]. In particular, it was shown how a single vaccine dose

administered with polymer microneedles induces a protective immune response superior to the one obtained by means of intramuscular injection at the same dose, including lung viral clearance.

The properties of microneedles of successfully delivery molecules of large sizes across the skin were also taken for the administration of biopharmaceuticals such as human growth hormone, heparin, calcein, insulin, vitamins and bovine serum albumin[28,34,37,44-46]. For these biomolecules, the administration by means of microneedles showed an increasing of absorption, bioavailability and stability, together with a rapid onset of the action and a controlled release over long times, if compared with the administration by traditional parenteral routes.

Nowadays, delivery technologies based on microneedles are developed also for cosmetic aims, such as wrinkle reduction, freckle and acne treatment. In fact, it is estimated how, generally, only a minor fraction (about 0.3%) of the active compounds contained within creams, gels and lotions can penetrate deep into the skin: dissolvable microneedles can be a viable route, without causing epidermal damages. About that, in 2014, Raphas' beauty patch product Acropass, based on dissolvable microneedles, was approved by the Chinese CFDA because of its safety and high quality[30].

1.5 Fabrication of microstructured DDSs

In the previous paragraphs, it has been anticipated how PLA, PGA and their copolymers, especially PLGA, show the desired features not only of biocompatibility and biodegradability, but also of availability, ease of processing and adjustable degradation, for successful controlled drug delivery. For this reason, these materials have been widely employed for the fabrication of scaffolds[47,48], microparticles[49,50] and microneedles[1]. In the case of scaffolds and microparticles, the importance of a well distributed porosity within the polymer matrix has been widely recognized as fundamental issue in order to modulate the encapsulated drug release kinetics and its protection against the microenvironment[51]. It appears clear as this latter concept has to be extended also to the delivery systems based on biodegradable polymer microneedles. The task of engineering the internal microstructure of polymer microneedles has been introduced recently with the ED development[1]; anyway, further developments in order to optimize the drug release kinetics of these microneedles can be

useful in order to make the technology gain in versatility. In the following lines, some of the most widely used technique used in order to create a porosity within a polymer matrix are summarized.

Manifold ways to produce porous architectures from polymer-containing systems have been developed: among the others, there are expansion in high pressure gas[52], emulsion freeze drying[53], salt leaching[54], or 3D printing[55]. Anyway, one of the most successful techniques is represented by the Thermally Induced Phase Separation (TIPS)[47], being this latter a reliable, flexible and cost-effective process for the control of microstructures. This latter technique is based on the controlled thermodynamic demixing of a homogeneous polymer solution, in order to obtain two liquid immiscible phases, with different compositions: a polymer-rich phase and a polymer-lean phase. To obtain this demixing, the starting monophasic system is quenched, in order to reach its thermodynamic instability. The polymer-rich phase is then stabilized as porous structure by removing the residual solvent, by means of freeze drying or leaching. Among the other advantages of TIPS technique, there is the chance to obtain systems with a very large variety of pore size and pore interconnectivity, by varying the process parameters[11]. Examples of polymer porous architectures obtained by means of TIPS are shown in Fig.1.11[12].

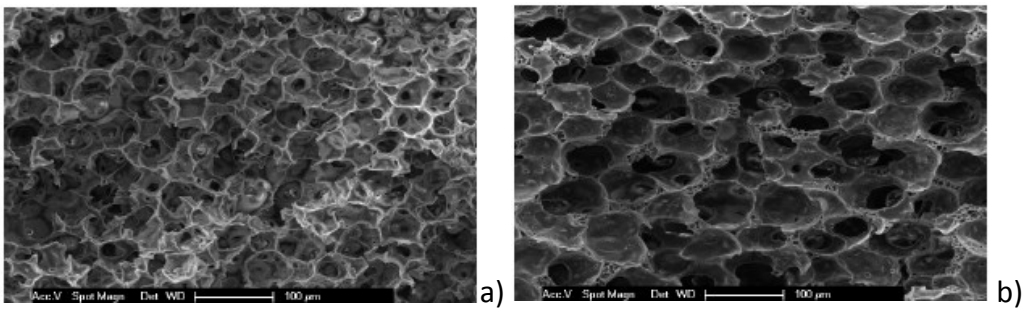

Figure 1.11*: SEM images of polymer scaffolds prepared by means of TIPS, starting from different composition of the polymer solution and with different quenching final temperature; a) 95/5 PLLA/PLA, 87/13 dioxane/water, demixing T = 20°C; b) 95/5 PLLA/PLA, 84.5/15.5 dioxane/water, demixing T = 45°C*[12]*.*

TIPS processes have been widely used also for fabrication of polymeric microspheres. In fact, the control of their internal and external morphology can be used in order to influence their interaction with the encapsulated drug, as well as with the microenvironment after administration in the body. In particular, the introduction of porosity within microspheres

can considerably increase their loading capacity while also allowing the regulation of release kinetics by means of their diffusion processes. As well as for scaffolds, this technique has been successfully employed for fabrication of PLGA microspheres, as represented in Fig. 1.12[56].

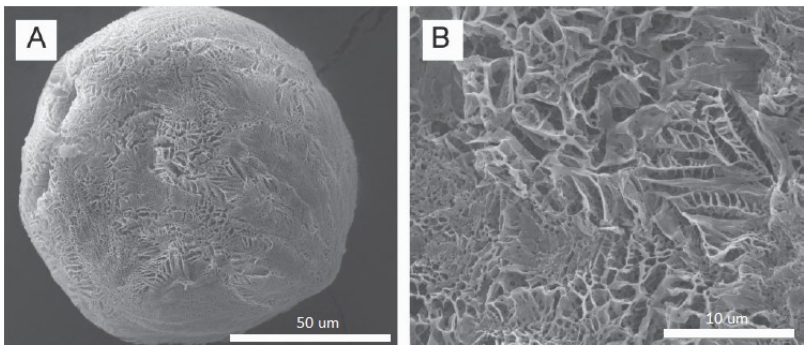

Figure 1.12*: SEM images of a PLGA microsphere produced by TIPS; a) overall image; b) detail of the microstructure*[56].

As alternative route to TIPS, approaches based on the emulsion freezing have been employed for porous polymer system fabrication[53,57]. They consist in creating an emulsion which continuous phase is represented by a solution of the chosen biodegradable polymer, followed by the solvent and the inner phase removal by freeze drying. Also in this latter case, the technique offers a high versatility in terms of tuning of porosity level and distribution, by means of the starting emulsion features, such as the volume ratio between the two phases, the interfacial tension, the relative viscosity and the diffusion rate of the disperse phase within the continuous one.

1.6 Aims of the thesis

On the basis of the concepts described in the previous paragraphs, among the different DDSs for controlled release, the microneedles seem to be one of the most promising transdermal delivery routes for manifold applications in pharmaceutical and biomedical field. Particularly promising are the devices based on patches of biodegradable and dissolvable polymer microneedles. Anyway, limitations affecting their fabrication technologies are crucial for their spreading on medical device market. Among the mold-free fabrication techniques, the recently proposed Electro-Drawing (ED) contact-free technique represents an alternative solution to the limitations of the other ones, allowing the microneedle fabrication in a single

drawing step, in absence of UV or high temperatures. In sight of the scaling up of the ED technology for industrial production, the process parallelization results of remarkable interest. This task consists in elaborating a strategy in order to simultaneously activate the pyroelectric effect of the driving plate on two-dimensional arrays of drops, in order to homogeneously activate the EHD action on them. This latter task has to be joint to the achieving of a controlled deposition of a two-dimensional array of drops on the PDMS substrate.

If the parallelization is a desired improvement for the ED technique from a technological point of view, the microneedle internal microstructure engineering represents a further intriguing task in order to extend their potential application fields. On the way of what done in previous literature works for other polymer architectures used in drug delivery, strategies based on multiphase system processing can be employed for controlling the internal structure of microneedles. These strategies can be substantially recognized in emulsion freezing and TIPS processes.

TIPS processes can be often complicated because of the need of information about the thermodynamic properties of the processed polymer system, in order to control the morphological features of the final porous architectures. A strategy, based on both experimental and simulative approaches, for a rapid investigation of thermodynamics of polymer solutions, especially for ternary systems, can be an interesting task in order to give support to many TIPS processes.

References

[1] R. Vecchione, S. Coppola, E. Esposito, C. Casale, V. Vespini, S. Grilli, P. Ferraro, P.A. Netti, Electro-Drawn Drug-Loaded Biodegradable Polymer Microneedles as a Viable Route to Hypodermic Injection, Advanced Functional Materials, 24 (2014) 3515-3523.

[2] H.S. Gill, M.R. Prausnitz, Coated microneedles for transdermal delivery, Journal of Controlled Release, 117 (2007) 227-237.

[3] Y. Xie, B. Xu, Y. Gao, Controlled transdermal delivery of model drug compounds by MEMS microneedle array, Nanomedicine : nanotechnology, biology, and medicine, 1 (2005) 184-190.

[4] E.R. Balmayor, H.S. Azevedo, R.L. Reis, Controlled Delivery Systems: From Pharmaceuticals to Cells and Genes, Pharmaceutical Research, 28 (2011) 1241-1258.

[5] P.B. Malafaya, G.A. Silva, R.L. Reis, Natural-origin polymers as carriers and scaffolds for biomolecules and cell delivery in tissue engineering applications, Advanced Drug Delivery Reviews, 59 (2007) 207-233.

[6] W.L. Jiang, S.P. Schwendeman, Stabilization and controlled release of bovine serum albumin encapsulated in poly(D, L-lactide) and poly(ethylene glycol) microsphere blends, Pharmaceutical Research, 18 (2001) 878-885.

[7] Y.P. Wang, J.D. Byrne, M.E. Napier, J.M. DeSimone, Engineering nanomedicines using stimuli-responsive biomaterials, Advanced Drug Delivery Reviews, 64 (2012) 1021-1030.

[8] E. Anitua, M. Sanchez, G. Orive, I. Andia, Delivering growth factors for therapeutics, Trends in Pharmacological Sciences, 29 (2008) 37-41.

[9] Y.H. Chen, S.W. Zhou, Q. Li, Microstructure design of biodegradable scaffold and its effect on tissue regeneration, Biomaterials, 32 (2011) 5003-5014.

[10] F.C. Pavia, V. La Carrubba, S. Piccarolo, V. Brucato, Polymeric scaffolds prepared via thermally induced phase separation: Tuning of structure and morphology, Journal of Biomedical Materials Research Part A, 86A (2008) 459-466.

[11] Y.S. Nam, T.G. Park, Porous biodegradable polymeric scaffolds prepared by thermally induced phase separation, Journal of Biomedical Materials Research, 47 (1999) 8-17.

[12] V. La Carrubba, F.C. Pavia, V. Brucato, S. Piccarolo, PLLA/PLA scaffolds prepared via Thermally Induced Phase Separation (TIPS): tuning of properties and biodegradability, International Journal of Material Forming, 1 (2008) 619-622.

[13] L.S. Nair, C.T. Laurencin, Biodegradable polymers as biomaterials, Progress in Polymer Science, 32 (2007) 762-798.

[14] C.Y. Dai, B.C. Wang, H.W. Zhao, Microencapsulation peptide and protein drugs delivery system, Colloids and Surfaces B-Biointerfaces, 41 (2005) 117-120.

[15] L. Brannonpeppas, Recent advances on the use of biodegradable microparticles and nanoparticles in controlled drug-delivery, International Journal of Pharmaceutics, 116 (1995) 1-9.

[16] R. Sinha, G.J. Kim, S.M. Nie, D.M. Shin, Nanotechnology in cancer therapeutics: bioconjugated nanoparticles for drug delivery, Molecular Cancer Therapeutics, 5 (2006) 1909-1917.

[17] M. Enayati, Z. Ahmad, E. Stride, M. Edirisinghe, One-step electrohydrodynamic production of drug-loaded micro- and nanoparticles, Journal of the Royal Society Interface, 7 (2010) 667-675.

[18] B.J. Thomas, B.C. Finnin, The transdermal revolution, Drug Discovery Today, 9 (2004) 697-703.

[19] P.H. Lambert, P.E. Laurent, Intradermal vaccine delivery: Will new delivery systems transform vaccine administration?, Vaccine, 26 (2008) 3197-3208.

[20] A.C. Williams, B.W. Barry, Penetration enhancers, Advanced Drug Delivery Reviews, 64 (2012) 128-137.

[21] A.R. Denet, R. Vanbever, V. Preat, Skin electroporation for transdermal and topical delivery, Advanced Drug Delivery Reviews, 56 (2004) 659-674.

[22] S. Henry, D.V. McAllister, M.G. Allen, M.R. Prausnitz, Microfabricated microneedles: A novel approach to transdermal drug delivery, Journal of Pharmaceutical Sciences, 87 (1998) 922-925.

[23] G. Widera, J. Johnson, L. Kim, L. Libiran, K. Nyam, P.E. Daddona, M. Cormier, Effect of delivery parameters on immunization to ovalbumin following intracutaneous administration by a coated microneedle array patch system, Vaccine, 24 (2006) 1653-1664.

[24] S.P. Sullivan, D.G. Koutsonanos, M.D. Martin, J.W. Lee, V. Zarnitsyn, S.O. Choi, N. Murthy, R.W. Compans, I. Skountzou, M.R. Prausnitz, Dissolving polymer microneedle patches for influenza vaccination, Nature Medicine, 16 (2010) 915-U116.

[25] S.H. Bariya, M.C. Gohel, T.A. Mehta, O.P. Sharma, Microneedles: an emerging transdermal drug delivery system, Journal of Pharmacy and Pharmacology, 64 (2012) 11-29.

[26] Y.C. Kim, F.S. Quan, R.W. Compans, S.M. Kang, M.R. Prausnitz, Stability Kinetics of Influenza Vaccine Coated onto Microneedles During Drying and Storage, Pharmaceutical Research, 28 (2011) 135-144.

[27] M.W. Ashraf, S. Tayyaba, A. Nisar, N. Afzulpurkar, D.W. Bodhale, T. Lomas, A. Poyai, A. Tuantranont, Design, Fabrication and Analysis of Silicon Hollow Microneedles for Transdermal Drug Delivery System for Treatment of Hemodynamic Dysfunctions, Cardiovascular Engineering, 10 (2010) 91-108.

[28] J.W. Lee, J.H. Park, M.R. Prausnitz, Dissolving microneedles for transdermal drug delivery, Biomaterials, 29 (2008) 2113-2124.

[29] J.H. Park, M.G. Allen, M.R. Prausnitz, Biodegradable polymer microneedles: Fabrication, mechanics and transdermal drug delivery, Journal of Controlled Release, 104 (2005) 51-66.

[30] Transdermal delivery & Microneedles, in, On Drud Delivery Magazine, 2015.

[31] S.P. Sullivan, N. Murthy, M.R. Prausnitz, Minimally invasive protein delivery with rapidly dissolving polymer microneedles, Advanced Materials, 20 (2008) 933-+.

[32] S.D. Gittard, A. Ovsianikov, N.A. Monteiro-Riviere, J. Lusk, P. Morel, P. Minghetti, C. Lenardi, B.N. Chichkov, R.J. Narayan, Fabrication of polymer microneedles using a two-photon polymerization and micromolding process, Journal of diabetes science and technology, 3 (2009) 304-311.

[33] L.Y. Chu, M.R. Prausnitz, Separable arrowhead microneedles, Journal of Controlled Release, 149 (2011) 242-249.

[34] J.H. Park, M.G. Allen, M.R. Prausnitz, Polymer microneedles for controlled-release drug delivery, Pharmaceutical Research, 23 (2006) 1008-1019.

[35] K. Lee, J.D. Kim, C.Y. Lee, S. Her, H. Jung, A high-capacity, hybrid electro-microneedle for in-situ cutaneous gene transfer, Biomaterials, 32 (2011) 7705-7710.

[36] K. Lee, H. Jung, Drawing lithography for microneedles: A review of fundamentals and biomedical applications, Biomaterials, 33 (2012) 7309-7326.

[37] J.D. Kim, M. Kim, H. Yang, K. Lee, H. Jung, Droplet-born air blowing: Novel dissolving microneedle fabrication, Journal of Controlled Release, 170 (2013) 430-436.

[38] M. Kim, H. Yang, S. Kim, C. Lee, H. Jung, The Troy Microneedle: A Rapidly Separating, Dissolving Microneedle Formed by Cyclic Contact and Drying on the Pillar (CCDP), Plos One, 10 (2015) 14.

[39] P. Ferraro, S. Coppola, S. Grilli, M. Paturzo, V. Vespini, Dispensing nano-pico droplets and liquid patterning by pyroelectrodynamic shooting, Nature Nanotechnology, 5 (2010) 429-435.

[40] J.U. Park, M. Hardy, S.J. Kang, K. Barton, K. Adair, D.K. Mukhopadhyay, C.Y. Lee, M.S. Strano, A.G. Alleyne, J.G. Georgiadis, P.M. Ferreira, J.A. Rogers, High-resolution electrohydrodynamic jet printing, Nature Materials, 6 (2007) 782-789.

[41] H. Hirschberg, G. de Wijdeven, H. Kraan, J.P. Amorij, G.F.A. Kersten, Bioneedles as alternative delivery system for hepatitis B vaccine, Journal of Controlled Release, 147 (2010) 211-217.

[42] G.H. Li, A. Badkar, S. Nema, C.S. Kolli, A.K. Banga, In vitro transdermal delivery of therapeutic antibodies using maltose microneedles, International Journal of Pharmaceutics, 368 (2009) 109-115.

[43] H. Hirschberg, G. de Wijdeven, A.B. Kelder, G. van den Dobbelsteen, G.F.A. Kerstena, Bioneedles (TM) as vaccine carriers, Vaccine, 26 (2008) 2389-2397.

[44] K. Fukushima, A. Ise, H. Morita, R. Hasegawa, Y. Ito, N. Sugioka, K. Takada, Two-Layered Dissolving Microneedles for Percutaneous Delivery of Peptide/Protein Drugs in Rats, Pharmaceutical Research, 28 (2011) 7-21.

[45] Y. Ito, A. Murakami, T. Maeda, N. Sugioka, K. Takada, Evaluation of self-dissolving needles containing low molecular weight heparin (LMWH) in rats, International Journal of Pharmaceutics, 349 (2008) 124-129.

[46] J.H. Oh, H.H. Park, K.Y. Do, M. Han, D.H. Hyun, C.G. Kim, C.H. Kim, S.S. Lee, S.J. Hwang, S.C. Shin, C.W. Cho, Influence of the delivery systems using a microneedle array on the permeation of a hydrophilic molecule, calcein, European Journal of Pharmaceutics and Biopharmaceutics, 69 (2008) 1040-1045.

[47] L.M. He, Y.Q. Zhang, X. Zeng, D.P. Quan, S. Liao, Y.S. Zeng, J. Lu, S. Ramakrishna, Fabrication and characterization of poly(L-lactic acid) 3D nanofibrous scaffolds with controlled architecture by liquid-liquid phase separation from a ternary polymer-solvent system, Polymer, 50 (2009) 4128-4138.

[48] K.C. Shin, B.S. Kim, J.H. Kim, T.G. Park, J. Do Nam, D.S. Lee, A facile preparation of highly interconnected macroporous PLGA scaffolds by liquid-liquid phase separation II, Polymer, 46 (2005) 3801-3808.

[49] V. Lassalle, M.L. Ferreira, PLA nano- and microparticles for drug delivery: An overview of the methods of preparation, Macromolecular Bioscience, 7 (2007) 767-783.

[50] F. Danhier, E. Ansorena, J.M. Silva, R. Coco, A. Le Breton, V. Preat, PLGA-based nanoparticles: An overview of biomedical applications, Journal of Controlled Release, 161 (2012) 505-522.

[51] H. Ghanbar, C.J. Luo, P. Bakhshi, R. Day, M. Edirisinghe, Preparation of porous microsphere-scaffolds by electrohydrodynamic forming and thermally induced phase separation, Materials Science & Engineering C-Materials for Biological Applications, 33 (2013) 2488-2498.

[52] D.J. Mooney, D.F. Baldwin, N.P. Suh, L.P. Vacanti, R. Langer, Novel approach to fabricate porous sponges of poly(D,L-lactic-co-glycolic acid) without the use of organic solvents, Biomaterials, 17 (1996) 1417-1422.

[53] K. Whang, C.H. Thomas, K.E. Healy, G. Nuber, A NOVEL METHOD TO FABRICATE BIOABSORBABLE SCAFFOLDS, Polymer, 36 (1995) 837-842.

[54] A.G. Mikos, A.J. Thorsen, L.A. Czerwonka, Y. Bao, R. Langer, D.N. Winslow, J.P. Vacanti, PREPARATION AND CHARACTERIZATION OF POLY(L-LACTIC ACID) FOAMS, Polymer, 35 (1994) 1068-1077.

[55] A. Park, B. Wu, L.G. Griffith, Integration of surface modification and 3D fabrication techniques to prepare patterned poly(L-lactide) substrates allowing regionally selective cell adhesion, Journal of Biomaterials Science-Polymer Edition, 9 (1998) 89-110.

[56] D.P. Go, D.J.E. Harvie, N. Tirtaatmadja, S.L. Gras, A.J. O'Connor, A Simple, Scalable Process for the Production of Porous Polymer Microspheres by Ink-Jetting Combined with Thermally Induced Phase Separation, Particle & Particle Systems Characterization, 31 (2014) 685-698.

[57] R.A. Jain, The manufacturing techniques of various drug loaded biodegradable poly(lactide-co-glycolide) (PLGA) devices, Biomaterials, 21 (2000) 2475-2490.

Chapter 2

Electro-drawing of microneedle arrays by means of an engineered *driving plate*

Part of the results presented in this chapter are currently being organized for the production of a journal contribution, in collaboration with the institutes IMM and ISASI of CNR in Naples.

2.1 Introduction

Many application fields, such as inkjet printing[1,2], film deposition[3] and spray coating[4], are based on the generation of fine liquid droplets from capillaries or nozzles by means of the electrohydrodynamic (EHD) jetting technique. Among these applications, the EHD atomisation has been widely used in the biomedical field, in order to produce near-monodisperse micro and nano particles, starting from polymer solutions, for drug delivery[5,6] or scaffold assembly[7]. An example of these processes is schematically shown in Fig. 2.1. The advantages of this technique are linked to its versatility, and to the chance of processing a variety of solutions and emulsions of different polymers and therapeutic agents under ambient conditions. In order to obtain the particles, the EHD process is desired to be carried out in the cone-jet mode[8]. In this latter configuration, the fluid meniscus formed at the tip of a capillary nozzle, undergoing to an internal charging process due to the application of an electric field, shapes itself in a Taylor cone[9], from the tip of which a fine jet is generated. This jet subsequently breaks up, giving rise to fine polymeric droplets, which will finally be the particles. Therefore, a stable cone-jet is the most desirable EHD jetting condition for the generation of monodisperse spherical particles.

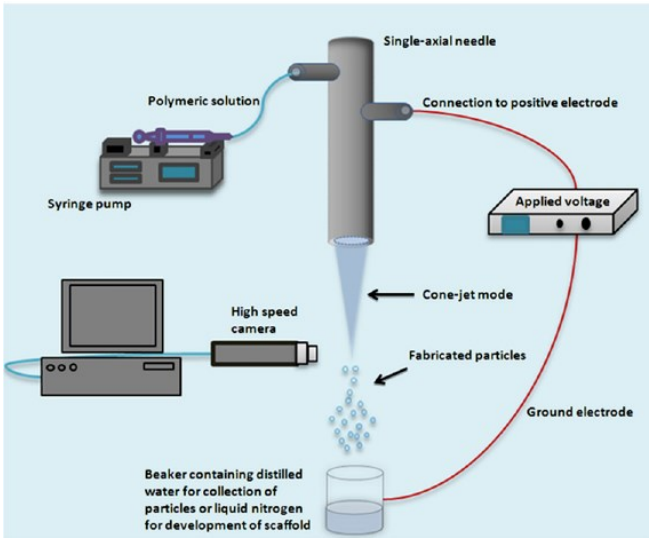

Figure 2.1: *Schematic diagram of EHD jetting process for microparticle fabrication*[7].

In these processes, the electric field needed for the shaping of the Taylor cone, is achieved by means of an experimental set up equipped with appropriate electrodes and high voltage circuits between the liquid source and the droplet collector, with remarkable set up complications. Recently, a novel and easier set up for the EHD jetting has been conceived and employed for the direct drawing and dispensing of droplets with controlled volumes, starting from sessile liquid drops or films[10]. The technique, schematically summarized in Fig. 2.2, is free from electrodes, high voltage circuits and nozzles, because of the employment of the electric field generated from the heating of a pyroelectric substrate, namely lithium niobate (LN). This pyro-EHD shooting systems has been demonstrated to be very suitable for liquid patterning on functionalized substrates.

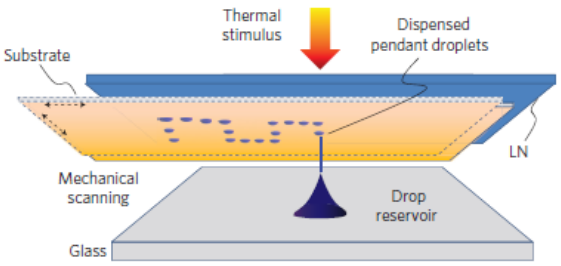

Figure 2.2*: Schematic representation of the pyro-EHD shooting set-up from ref. 10.*

The pyro-EHD system has been recently used for diverse applications[11-13]. Among these latter, there is the electro-drawing (ED) of polymer microneedles for transdermal delivery[14], on which the main part of this thesis work is focused. As described in the previous chapter, the pyro-EHD action has been employed for the shaping into the Taylor cone of PLGA

solution drops. The cones have been then consolidated in order to obtain the desired final microneedles. For this latter application, conversely to the microparticle fabrication principles and the liquid patterning described above, for which the breaking up of the cone is desired in order to produce the droplets, the cone formation, and therefore the electric field pyroelectrically generated, has to be finely controlled because the cone jetting mode would determine a loss of polymer solution, i.e. a loss of drug encapsulated within it. In the microneedle ED, such as in the other pyro-EHD applications mentioned in the previous lines, the heat local stimulus to the pyroelectric crystal was pursued by means of a hot tip or by an infrared laser, allowing the deformation of a single cone at time: it appears clear as this latter methodology is a limit for the process parallelization. This would be a crucial drawback for the ED of microneedles, in sight of a scaled-up production.

In this chapter, after a brief theoretical background, the design, the fabrication and the testing of an engineered driving plate for the ED is be presented. The device is made up of an integrated circuit directly patterned onto the pyroelectric crystal, in order to achieve its heating by means of Joule effect. The circuit allows heating a large surface area of it, in order to extend the process to the in parallel ED of microneedles under an array configuration. Also a more accurate control of the pyroelectric effect can be achieved by means of the engineered device. Further, the morphology of the microneedles fabricated on this novel ED set up can be optimized and coupled with a rapid dissolvable layer interposed between the needles and their substrate, providing the possibility of removing the patch few minutes after its application, leaving the needles inserted within the skin.

2.2 Theoretical background

2.2.1 Pyroelectricity

Pyroelectric materials represent a subgroup of piezoelectric materials, and therefore, more in general, of ferroelectric materials, with the property of undergoing to a spontaneous polarization by means of a change in temperature. The changes in polarization and in temperature are linearly related, according to the following tensor relation[15]:

$$\Delta \boldsymbol{P_s} = \boldsymbol{p}\Delta T \tag{2.1}$$

where $\boldsymbol{P_S}$ and $\boldsymbol{p}$ are the spontaneous polarization and the pyroelectric coefficient vectors respectively, and T the absolute temperature of the crystal. In lithium tantalate (LT), this property is due to the possibility of displacement of lithium and tantalum ions, relative to the layers on which the oxygen atoms lie[15]. Because of the mobility of these ions only in one direction, which is conventionally assumed as the z direction of a Cartesian system, the pyroelectric coefficients vector assumes the forms:

$$\boldsymbol{p} = \begin{bmatrix} 0 \\ 0 \\ p \end{bmatrix} \tag{2.2}$$

i.e. the spontaneous polarization arises only in the z direction, and it is proportional to the change in temperature by means of the coefficient *p*. In other words, the z direction is conventionally chosen as coincident with the c direction of the crystal, i.e. the only direction of ions mobility. The sense of the z direction is chosen according to the following convention: the +z axis is directed out of the z face that becomes more positively charged upon cooling the crystal[16]. The x direction of the Cartesian system is conventionally chosen as the one perpendicular to the mirror plane of symmetry of the crystal, while the y direction is chosen such as the system is right handed[15]. For the commercial use, the pyroelectric crystals are identified as x-cut, y-cut and z-cut, the letter indicating the direction normal to the largest wafer surface.

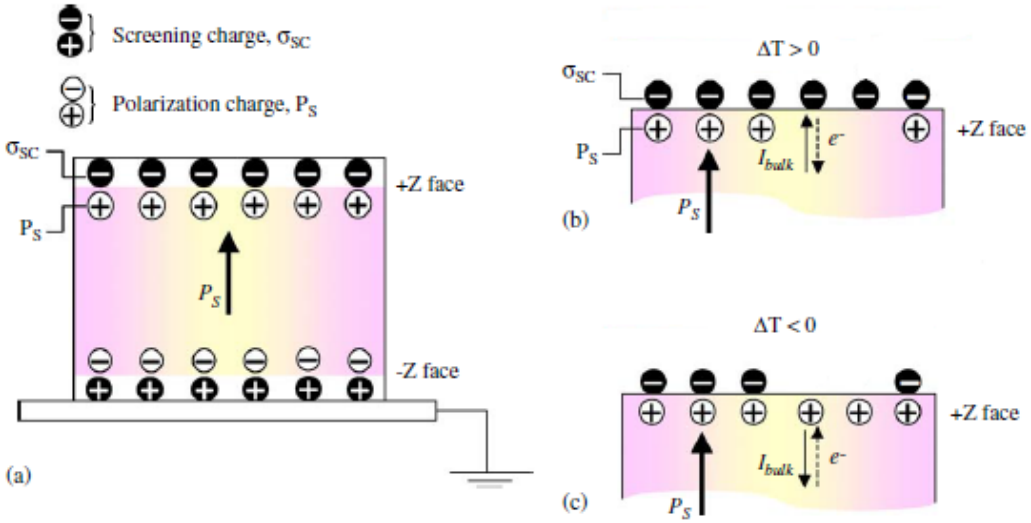

Figure 2.3*: Schematic diagram of the electrostatic state of surface charges onto a pyroelectric crystal: a) the equilibrium condition with no electric field; b) – c) under heating or cooling, the unbalanced surface charges produce an electric field; diagram adapted from ref. 17.*

The Fig. 2.3 schematically shows the electrostatic field generation from the change in temperature experimented by a pyroelectric crystal. At the equilibrium state (Fig. 2.3 a), the polarization charges P_S on the surface of the crystal are completely screened from the charges σ_{SC} and no electric field exists. When the crystal experiments a change in temperature (Fig. 2.3 b-c), the change in its polarization determines a perturbation of the equilibrium state because of the incomplete screening of the uncompensated charges P_S. These uncompensated charges are of opposite sign on the two main crystal surfaces, generating an electric field, which lines are generated from the surface +z and are closed on the –z surface. Anyway, the duration of this electric field is linked to the characteristic times for the screening of charges: the electric field intensity becomes zero when all the uncompensated charges have been screened. This screening process can mainly take place following two different mechanisms: screening from bulk crystal charges and screening with charges absorbed from the surrounding medium. Anyway, because of the high characteristic relaxation time of the bulk crystal, the contribution arising from the first of these two mechanism can be neglected. In other words, the electric field intensity decrease in time, mainly according to the dielectric properties of the surrounding medium.

2.2.2 Electrohydrodynamic (EHD) deformation of sessile drops

When a sessile drop is subjected to the action of an external electric field, its surface experiments a deformation process, which is the result of the interaction between electric and viscous forces. In particular, the modification of the interface is due to the competition between the surface tension, the hydrostatic pressure and the electrostatic stress.

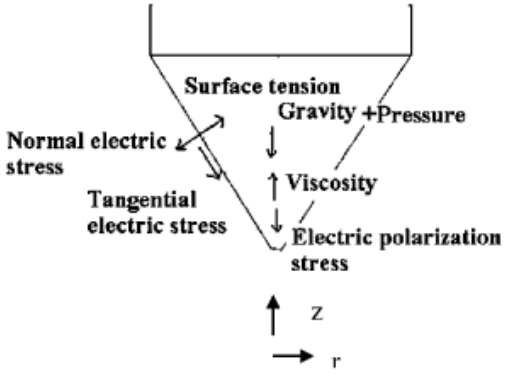

Figure 2.4*: Stresses acting on the sessile drop surface when an external electric field is applied; schematic representation adapted from ref. 18.*

In Fig. 2.4 there are summarized the principal forces acting during the drop deformation. The relevant stresses are electric polarization stress $\boldsymbol{\sigma_p}$, normal electric stress $\boldsymbol{\sigma_e}$, tangential electric stress $\boldsymbol{\tau_e}$, normal viscosity stress $\boldsymbol{\sigma_\mu}$ and tangential viscosity stress $\boldsymbol{\tau_\mu}$. Chosen as reference the axes in Fig. 2.4, these stress contributions can be expressed by means of the following relations[18,19]:

$$\sigma_p = \frac{(\varepsilon_r - 1)\varepsilon_0 {E_T}^2}{2} \tag{2.3}$$

$$\sigma_e = \frac{{E_N}^2}{2\varepsilon_r} \tag{2.4 a}$$

$$\tau_e = \varepsilon_0 E_T E_N \tag{2.4 b}$$

$$\sigma_\mu = 2\mu \frac{\partial v_z}{\partial z} \tag{2.5 a}$$

$$\tau_\mu = \frac{3\mu(\partial v_z/\partial z)(dr/dz)}{1+(dr/dz)^2} \tag{2.5 b}$$

where v_z, E_T, E_N are respectively the fluid velocity in the axial direction, the tangential and the normal component of the imposed electric field. In particular, during the ED of microneedles, these latter components are the ones of the electric field generated by the uncompensated polarization charges arising from the heating (or the cooling). The other parameters contained in the equation are: the fluid viscosity μ, its relative dielectric constant ε_r and the vacuum dielectric constant ε_0. For this reason, the final shape of the deformed droplet can be mainly attributed to the fluid viscosity, dielectric properties and surface tension, a part from the electric field intensity. In other words, the applied electric field generates normal and tangential electric stresses, which consequently generate viscous stresses both normal and tangential to the fluid interface, causing the evolution of its shape. About the effects of the dielectric properties on the final shape, results reported in literature[19] show substantial differences between conductive and dielectric fluids. In particular, in the case of conductive liquids, the electric stress components vanish at any time within the deforming droplets, because of the screening charges arising from the conduction of charges within the fluid. For this latter reason the elastic response of the interface dominates, leading the droplets to the equilibrium state after the initial cone deformation. The situation is completely different in the case of dielectric liquids. In this case, the charges within the droplets are transferred mainly by convection. For this reason, the electric stresses at the interface never vanish because of lack of screening charges. Consequently, the fluid inertia makes the viscous stresses increase, counteracting the elastic response of the interface. For this reason, dielectric fluids result suitable for the ED of microneedles.

2.3 Design and fabrication of the engineered driving plate

2.3.1 Device concept and mathematical model

The basic idea of the integrated device is to pattern a metallic circuit directly onto the pyroelectric crystal, in order to realize its heating by the Joule effect following the current circulation within the circuit. The modulation of the voltage applied to the circuit allows, in this way, the control of the heating of the crystal and, by consequence of the electric field generated from its pyroelectricity. The basic elements of the circuit were chosen to be in a spiral shape, in order to concentrate a high resistance, and so a high thermal dissipation, in a small area, without completely cover the crystal surface with metals to avoid electrical discharges. The dissipative elements were individually characterized, and then an expanded circuit based on their series and/or parallels was designed, to the aim of employing the device for the in parallel ED of microneedles.

The main goal of the engineered driving plate can be summarized as follows:

- ✓ the extended array of dissipative elements has to ensure the uniform heating of a crystal area corresponding to the one of the final microneedle desired patch, in order to activate a uniform electric field. In this way all the deposited droplets will experiment an EHD action with the same intensity.

For the circuit material, titanium (Ti) was chosen, because of its high mechanical strength and its excellent thermal stability[20]. About the Ti thin film thickness, a value of 200 nm was chosen as a good compromise between technological and physical aspects.

In order to individuate the best features of the final circuit, the Joule heating of the pyroelectric substrate was simulated by means of the Finite Element Method (FEM). The numerical simulations were carried out by coupling the Alternate Current/Direct Current (AC/DC) and the Heat Transfer modules of the commercial software COMSOL Multiphysics (version 4.4).

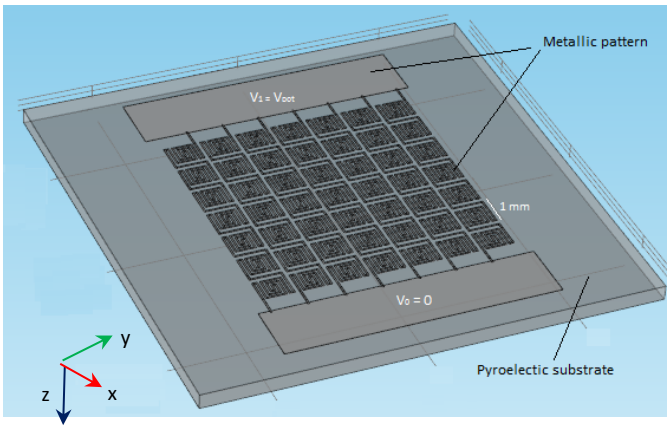

Figure 2.5*: Schematic representation of the calculation domain for the integrated device; the origin of the reference system was chosen coincident with the crystal center.*

In Fig. 2.5 there is the schematic representation of a typical calculation domain for the simulated system, differing the other ones from it only for the geometry of the integrated circuit. The three-dimensional geometry is made up of a rectangular subdomain, representing the pyroelectric crystal, and of a circuit made up of series and/or parallels of spirals. For the rectangular and the circuit subdomains the physical parameters of LT and Ti were respectively used as inputs (for Ti thin film: electrical conductivity 3.5 · 10^5 S/m).

For both subdomains, the electrical current circulation was modeled by means of the *continuity equation* for the *electric charge* in the form:

$$\frac{\partial \rho}{\partial t} + \nabla \cdot \mathbf{J} = 0 \tag{2.6}$$

coupled with the *Ohm's law*:

$$\mathbf{J} = \left(\sigma + \varepsilon_0 \varepsilon_r \frac{\partial}{\partial t}\right) \mathbf{E} \tag{2.7}$$

being **J** and **E** respectively the current intensity and the electrical field vectors, defined in every point of the calculation domain, ρ the electrical charge density, σ the material electric conductivity, ε_0 e ε_r the vacuum dielectric constant and the relative dielectric constant of the medium. For all the domain boundaries, except for the circuit terminals for which the zero potential and the applied voltage V_{pot} were respectively fixed, the condition of electric insulation was applied. Obviously in the case of stationary studies, the accumulation term in the eq. (2.6) vanishes and no initial conditions are needed. The heat transfer within the domains was modeled by means of the *energy continuity equation*, in the following form:

$$\rho C_p \frac{\partial T}{\partial t} + \rho C_p \boldsymbol{u} \cdot \nabla T = \nabla \cdot (k \nabla T) + Q \tag{2.8}$$

ρ, C_p and k respectively being the density, the specific heat at constant pressure and the heat conductivity of the medium, $\boldsymbol{u}$ the velocity vector, T the absolute temperature and Q an equation term comprehensive of all the thermal source differing from the convective or the conductive one. To all the domain boundaries, the thermal insulation condition was applied, with exception for the crystal and circuit faces at the atmosphere: for these ones, the latter condition was substituted with the one expressing the convective flux with the environment. The temperature distributions obtained from the described method were employed in order to estimate the intensity of the electric field generated by the pyroelectric crystal, within a spatial domain around it. In particular, the crystal surface charge distribution P_S was obtained by means of the following relation, peculiar for the pyroelectric materials:

$$\mathrm{P}_S = p \cdot \Delta T \tag{2.9}$$

being p and ΔT the crystal pyroelectric coefficient (for LT p = -2.3 · 10^-4 C K^-1 m^-2)) and the difference in temperature experimented by it, following the Joule heating process.

As boundary conditions for the electric charge conservation law, used for electric field calculation, the surface charge distributions given by the equation (2.9) were applied to the two main crystal surfaces, while for the other boundaries the zero potential conditions were fixed.

To the aim of discretizing the calculation domain for the solution of the model equations, a mesh-grid made up of tetrahedral elements was generated. The convergence of the mesh was ensured by evaluating the temperature profiles along the crystal thickness.

2.3.2 Simulation results

The first simulation results were aimed to characterize the Joule heating of the pyroelectric crystal by means of the single spiral circuit working as a microheater. Also the electric field generated by the system was numerically characterized. The simulation results, together with the schematic representation of the spiral element patterned at the center of the crystal, are shown in Fig. 2.6.

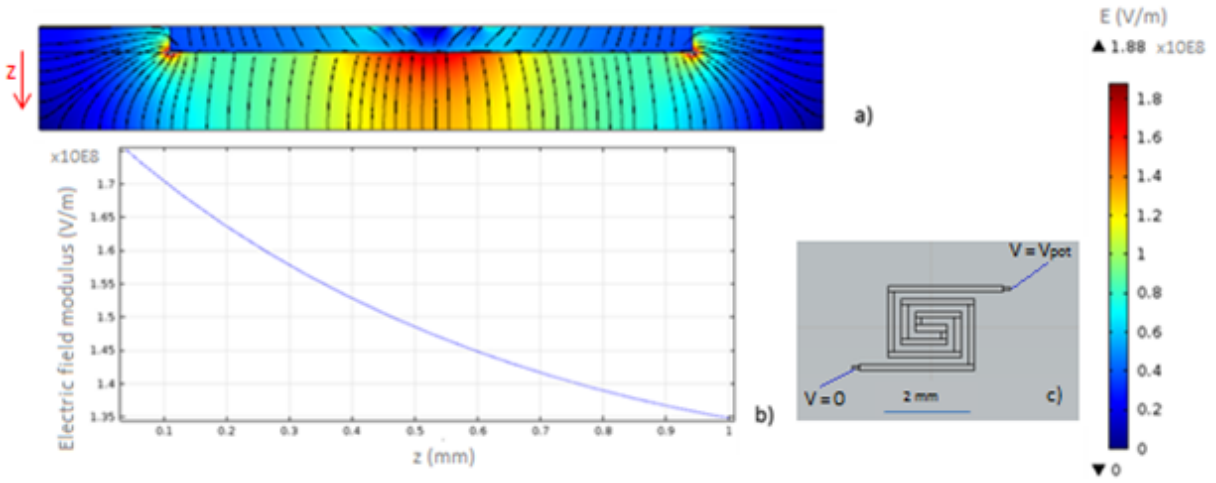

Figure 2.6: *Simulation of the electric field generated in the surrounding space by the pyroelectric crystal, heated by a spiral microheater patterned at its center; a) colormap of the electric field modulus and electric field lines in the central crystal section; b) electric field modulus trend with the distance from the crystal bottom surface, in correspondence of its center; c) schematic representation of the spiral element.*

The results in Fig. 2.6 were obtained by choosing the voltage applied to the circuit such that the maximum value of the T distribution on the bottom surface of the crystal was 60°C. This value was chosen because of the need of mild working temperature in sight of the encapsulation of thermolabile drugs within the microneedles. It is possible to notice how, in the case of heating the crystal by means of a thin metallic layer, a strong electric field arises nevertheless the mild temperature registered to the bottom of the crystal.

This electric field, stronger than the one produced by means of the hot tip in constancy of the bottom crystal surface temperature (previously obtained from simulations), can be attributed to a different arrangement of the charges in the crystal. The temperature gradient arising within the crystal from the Joule heating, and so to the polarization gradient following it, causes the presence of a volume charge, which originates an enhancement of the pyroelectric effect and, consequently, of the electric field intensity in the gap between the crystal surface and the PDMS pillars surface. In this way, a lower surface temperature of the crystal is needed in order to achieve the same electric field intensity, preserving it from breakage under the high temperature stress; in this way, also the temperature experimented by the shaping microneedle will be lower, preserving the advantages of the ED for thermolabile drugs. Further, this solution allows electro-drawing microneedles starting from sessile droplets by keeping constant the distance between the crystal surface

and the drop basis during the deformation process, without reaching the very high temperature needed with the hot tip in order to realize the same process. This result is highly significant in view of extending the electro-drawing technique to the fabrication of arrays of microneedles, but also in view of the process automatization needed for its scale-up, because it ensures the reproducibility of the microneedle shapes.

After the characterization of the single heater, a two-dimensional array of these elements, with scaled dimensions, was optimized, in order to extend the advantages of the electro-drawing technique to the fabrication of two-dimensional patches of polymer microneedles. Simulations, in terms of temperature distribution on the crystal surface, were carried out in order to choose the best configuration of the array, in terms of size of the elements, distribution of their centers and connections, in order to give a uniform heating in an surface of 1 cm^2, which will correspond to the final microneedle patch area.

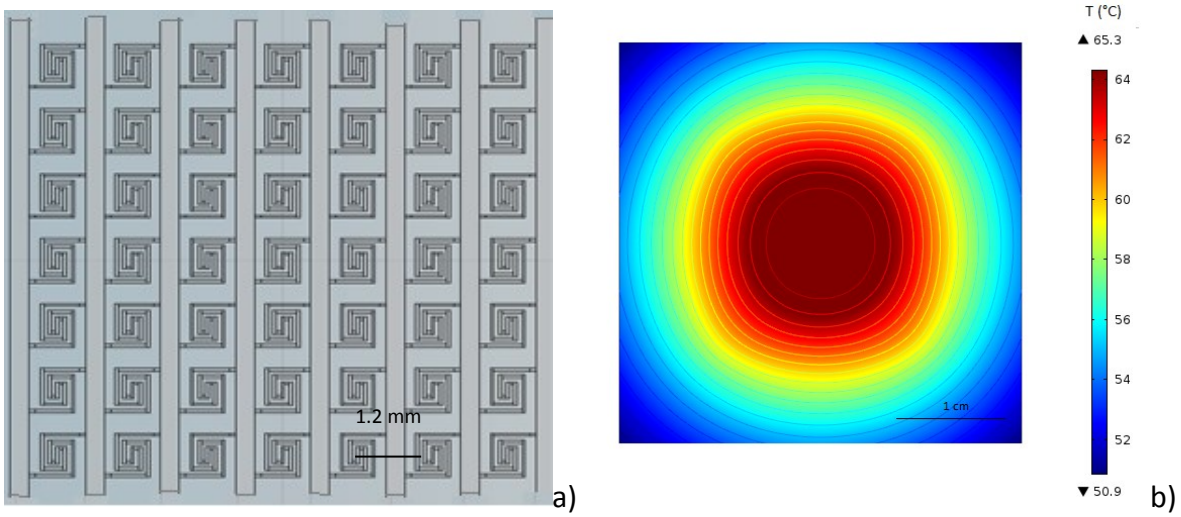

Figure 2.7: *Simulation results for the expanded array of heaters; a) detail of the layout of the circuit; b) temperature distribution at the bottom surface of the crystal.*

In Fig. 2.7 a) there is schematically shown a detail of the proposed solution for the engineered driving plate for the in parallel electro-drawing. It consists of a circuit made up of the series of 14 moduli, each made up of the parallel of 14 spiral elements. As simulations result, the distance between the centers of two following spiral elements was chosen to be 1.2 mm, in order to guarantee a uniform T distribution. The Fig. 2.7 b) shows the colormap of the temperature distribution onto the bottom surface of the crystal: it is possible to notice how the temperature is almost uniform in the area lying down the circuit, with the exception of the two most external crowns of elements. This latter circumstance is clearly due to the fact that these elements experiment a thermal diffusion effect consequent to a

number of neighbors which is smaller than the central elements. Therefore, these latter crowns will not be useful for the electro-drawing of microneedles, but they will have the aim of making the electric filed uniform within the area corresponding to the deposited droplets.

2.3.3 Materials

The fabrication of the integrated circuit was carried out on pyroelectric substrates provided by Altechna (Lithium Tantalate $LiTaO_3$ optical grade wafers, z-cut, 0.5mm thick, double side polished). For the high resolution laser lithography process, the positive AZ® ECI 3012 photoresist was purchased from Microchemicals, and chosen for its high resolution capability and its good thermal stability, in sight of the following metal deposition process by means of thermal evaporation. Also the AZ 351B developer was purchased from Microchemicals, and diluted in deionized water in ratio 1 : 4 before using. 2-Propanol, for wafer cleaning, and acetone for lift off process, were both purchased from Sigma Aldrich. Titanium pellets (purity 99.95%) for the metal deposition were provided by Kurt J. Lesker Company. Wrapping wires and silver conductive paint for circuit connections were purchased from RS Components.

2.3.4 Fabrication process

The integrated device fabrication process was carried out following a typical flow chart for microelectronic device fabrication. It is schematically summarized in Fig.2.8.

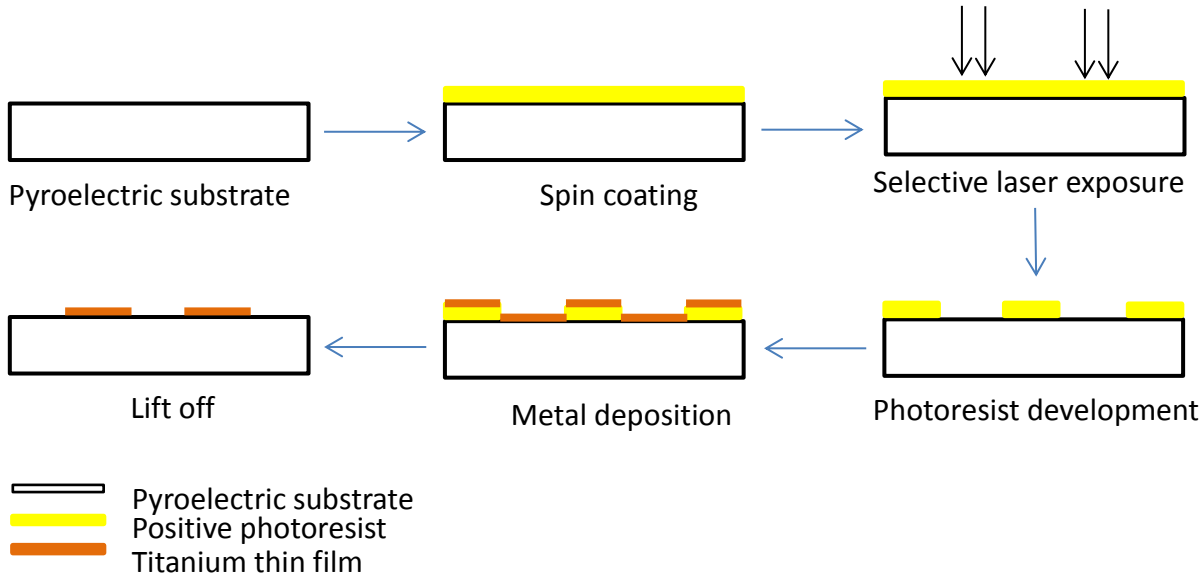

Figure 2.8: *Schematic fabrication process flow chart.*

A thin layer of photoresist was deposited onto the pyroelectric crystal (preventively cleaned and dried) by means of a spin coater (Laurell Technologies Corporation). The process was carried out for 60 s, with a spin speed of 3000 rpm. These parameters determined a photoresist thickness of 1.1±0.05 µm, as result of a profilometer (Veeco Dektak 150) analysis. A soft bake step was carried out before laser exposure, in order to complete the resist layer drying. For this step, because of the pyroelectricity of the substrate, in order to avoid the drawback of its damage with electric discharges, a temperature ramp of 1 min and 30 s was carried out from room temperature to 86 °C. The sample was left to rest at the reached temperature for further 30 s and then gradually acclimatized again.

The selective exposure of the photoresist for realizing the lithographic pattern, was carried out by a direct laser writer system (DWL 66fs, Heidelberg Instruments Mikrotechnik). The exposure parameters were set as follows: 90% for the beam intensity and 15% for the focus. These two parameters were identified by means of a preventive exposure dose test on the chosen photoresist: several couples of values were tested and the best one in terms of structure resolution was chosen. A post-exposure bake treatment was carried out, following the same thermal ramp of the soft-bake step. The exposed sample was then immersed into the developer for 60 s and then cleaned in deionized water. Some details of the realized lithographic patterns are shown in Fig. 2.9.

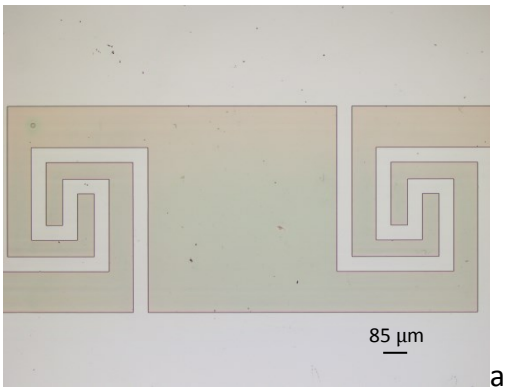

a)
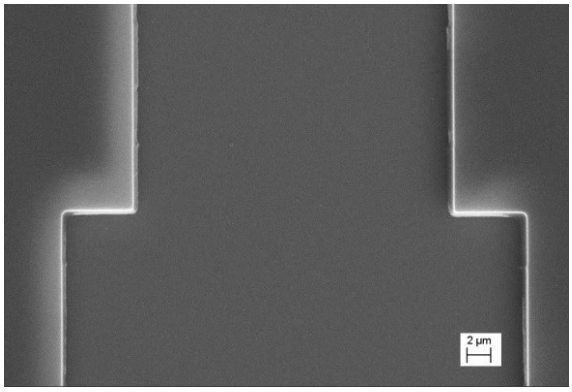

b)

Figure 2.9: *Lithographic pattern details after the photoresist development; a) optical image; b) SEM image (7 nm gold sputter coated sample).*

From the Fig. 2.9 a), it appears clear how the lithographic process guarantees good results in terms of pattern resolution. It is well know from literature[21] how, in order to ensure a good quality for the lift off process, the side walls of the photoresist after development, in the case of a single layer, have to show in the best case a negative slope, or alternatively have to

be vertical. At this aim, a SEM characterization of the lithographic pattern was carried out. A top view of a pattern detail is shown in Fig. 2.9 b).

After the post-exposure bake step, a thin titanium layer was deposited onto the patterned crystal. The titanium thickness was set to 200 nm, in order to have the desired specific resistance. The metallic deposition was carried out by means of a thermal metallic evaporator, equipped with a thickness controller (Inficon). On the metallized wafer, a lift off process allowed the removal of the residual photoresist, covered by Ti, in order to obtain the desired metallic pattern. The lift off was realized, with the help of a sonicating bath, by immersing the sample in pure acetone. The treatment was carried on for 20 minutes in order to test the metal adhesion to the substrate. The sample was finally cleaned, in order to remove the redeposited metal debris. The set thickness for the Ti layer was then confirmed on the final sample by means of profilometer measurements. Some details of the metallic pattern are shown in Fig. 2.10.

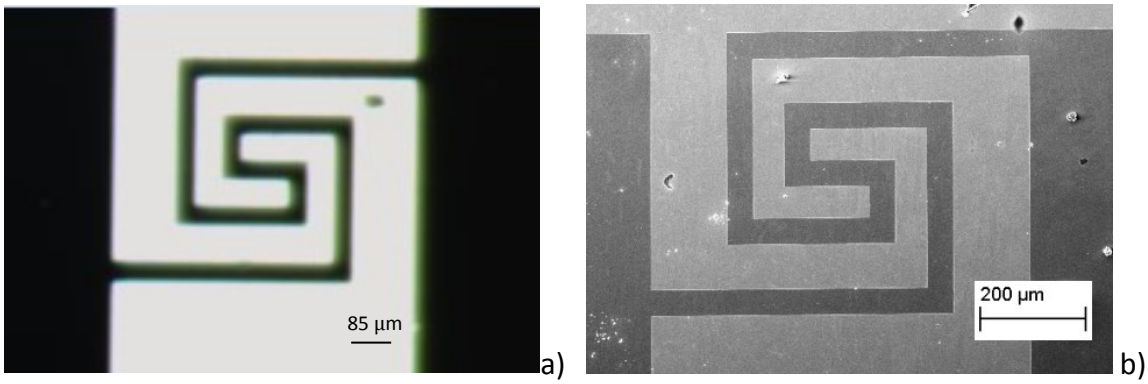

a) b)

Figure 2.10: *Optical (a) and SEM (b) images of some pattern details after the thin film metal deposition process.*

The SEM image also shows how the sample is free from the so-called “rabbit ears”, i.e. the photoresist thickness and the resolution of its vertical walls are good enough to ensure a successful lift off process, for the chosen metal layer thickness. In fact, a wrong choice on the photoresist thickness or a not good vertical resolution of its side walls, can determine a continuum metallic layer; in this latter case, the photoresist dissolution during the lift off process can determine the removal of the whole metallic layer, determining the absence of the desired pattern.

The fabrication process was finalized by the welding of the connection wires, carried out by means of a silver conductive paint, being the high temperatures reached in conventional welding processes not compatible with the pyroelectric device.

2.4 Microneedle morphology control

2.4.1 Materials and methods

Fabrication of flexible arrays of pillars and deposition vessels

Polymethyl methacrylate (PMMA) substrates, with thickness varying from 1 to 5 mm according to the use destination, were purchased from Goodfellow and milled following the desired geometry by means of a micromilling machine (Minitech CNC Mini-Mill). The obtained PMMA mold was then sonicated in water for 10 min and then dried with compressed air, in order to remove the residual debris from the milling process. The mold was used for obtaining a polydimethylsiloxane (PDMS) master, according to the following procedure. Dow Corning Sylgard 184 Silicone elastomer was carefully mixed with curing agent in the ratio 10 : 1 in weight. This recipe was modified by adding the surfactant Silwet L77 (3% wt/wt) and the curing agent in the ratio 10 : 2 in order to produce long lasting hydrophilic PDMS for the vessel employed for aqueous solutions deposition, as explained in the following paragraphs. The mixture was then degassed in a vacuum chamber for 20 min in order to remove air bubbles arisen from the mixing process. The degassed mixture was then poured onto the PMMA mold and degassed again for 10 min in order to remove the air bubbles eventually arisen from the pouring step. The PDMS was cured within the mold for 45 min at 80°C (this latter temperature was chosen being below the PMMA melting temperature, which is around 95°C, in order to ensure the absence of mold deformation). After curing, the PDMS master was gently peeled off from the PMMA mold. About the geometries used as inputs for the milling processes, the following choices were done: for the deposition vessels, square pools with edge of 1.5 cm and depth of 3 mm were used, while for pillars, array 10x10 of cylinders, being the distance between the centers of two following elements equal to 1.2 mm, with basis diameters ranging from 300 μm up to 600 μm and height of 500 μm were fabricated.

Microneedle patch fabrication

Poly(lactic-co-glycolic acid) with molecular weight in the range 38000 – 54000 Dalton (PLGA or RESOMER® RG 504 H), purchased from Evonik Industries, was used as biopolymer for the microneedles. Their precursor solution was made up of PLGA dissolved in Dimethyl Carbonate (DMC, provided by Sigma Aldrich), which is a solvent for it, with the compositions 20 - 25 - 30 – 35 - 40 % wt/v. Nile Red (Technical Grade, Sigma Aldrich) was used as model compound for hydrophobic drugs within the PLGA solution. For the rapid dissolution hydrophilic layer, interposed between the PDMS pillars and the microneedles, Polyacrylamide (PAA) with average numerical molecular weight 150000 Dalton was provided from Sigma Aldrich and diluted in deionized water in percentage 15% wt/v. Sulforhodamine B (Sigma Aldrich) was used as labelling compound for this latter layer. Gelatin from bovine skin, Type B, (Sigma Aldrich) was dissolved in pure water (10% wt/w), poured into a PDMS vessel and consolidated for 30 min, for testing the release of microneedles following the dissolution of the PAA layer.

Characterization of PLGA solutions

The studied PLGA solutions were characterized in terms of viscosity and surface tension. For the viscosity, the flow curves of the samples were obtained by means of a stress-controlled rheometer (MCR 302 rheometer, Anton Paar), fitted with a double gap concentric cylinder geometry (DG 27, Anton Paar) in order to avoid DMC evaporation during the measurements. Temperature was kept at 25°C, with an accuracy of $\pm$0.1°C, during the measurements by means of an Anton Paar Peltier temperature device for concentric-cylinder system, equipped with a water circulating bath. All the samples were placed in the double gap cylinder measuring system and left to rest for 2 min for structure recovery and temperature equilibration. The viscosity was measured for shear rate ranging from 0.01 s^{-1} to 100 s^{-1}. The surface tension of the PLGA solutions was measured by means of an Optical Tensiometer, (Attension Theta Lite, Biolin Scientific) according to the pendant drop method. The drop images were recorded and analysed by means of the Attension Theta Software, by using as input parameters the densities of the phases, previously measured. The Young – Laplace curve fitting method was employed and the measurements repeated at least three times, each time on a sample made up of ten drops.

2.4.2 Results and discussion

Microneedle shape optimization

The fabricated integrated devices were tested for the modulation and the optimization of the morphology of the final microneedles. These tests were carried out on the production of single microneedles, before extending the solution to in parallel electro-drawing. In particular, the features of the electric field generated from the pyroelectric crystal, heated by means of the metallic pattern, were employed for minimizing the formation of the pedestal at the microneedles basis, to the aim of making their cone entirely suitable for indentation. This improved morphology, joint to the presence of a rapid dissolvable hydrophilic layer interposed between the PDMS pillar and the PLGA microneedle, allows the removal of the patch few minutes after the microneedle insertion into the skin.

The first tests were focused on the formation of single microneedles on pillars with base diameter ranging from 600 μm to 300 μm, starting from sessile drops of polymer solution individually deposited. The microneedles were produced by means of an experimental set-up with the engineered crystal lying under the PLGA droplets, so as to develop the microneedle with its tip pointing downwards. The advantage of this latter configuration is related, further to the future extension of the process to two-dimensional arrays of microneedles, to the synergic action of the gravitational force with the EHD deformation.

The drop deformation process under the electric field action was carried out following a "*double step*" protocol:

1) during the first step of deformation, the microneedles were fabricated by fixing the distance between the crystal surface and the pillars one to 1.3 mm. This distance was as compromised between an efficient electro-drawing process, which allows obtaining microneedles with tips characterized by a small radius of curvature, and a too fast deformation, which can determine an excessive elastic response of the material;
2) in the second step, the now formed microneedles were moved, by means of the motion of a programmed stage, to a distance of 1.5 mm with respect to the starting position, to the aim of morphology consolidation under the electric field action, without experimenting further deformations.

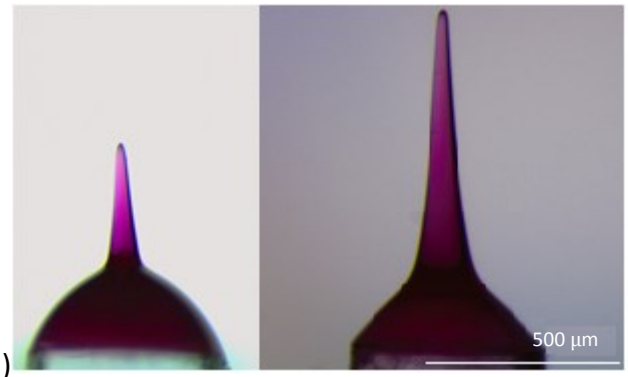

Figure 2.11*: Optical images of PLGA microneedles fabricated by means of the single step protocol (a) and the double step protocol (b).*

From the observation of the Fig. 2.11, it appears clear as the introduction of the second step allows not only the reduction of the pedestal at the basis of the indenting cone, i.e. the rapid necking between the basis and the cone, but also allows to reduce the loss of shape following the drying process. Indeed, during the second step, it is possible to consolidate the microneedle shape obtained during the first step, by counteracting the electric field action to the elastic response of the polymer solution used as precursor for the microneedles. This fact happens because during the second step, most of the solvent present in the starting solution evaporates, minimizing the plasticity of the just formed microneedles, and by consequence of the chance of changing its shape during the final drying step. Further, also the final pedestal reduction can be related to the minimized elastic response of the material under deformation. On the contrary, by stopping the electric field action just after the first deformation step, the microneedle tends to minimize its surface, leading to a morphology characterized by an almost spherical pedestal with a very short cone, with an increase of the PLGA useless for the indentation, i.e. the loss of drug within it.

A further controlling parameter for the process can be identified in the voltage applied to the integrated circuit or, if better, to the dissipated power within it. In particular, fixed the distance between the crystal and the microneedle basis, this parameter has been demonstrated to be crucial for obtaining low curvature radii for the microneedle tips. Anyway, a too high dissipated power will increase the temperature experimented by the shaping microneedles, with the mentioned above drawbacks for thermolabile drugs. For this reason, such a power that ensures a crystal surface temperature of 60°C was chosen.

The effects of the pillar diameter were studied in terms of microneedle shape. The results are summarized in Fig. 2.12.

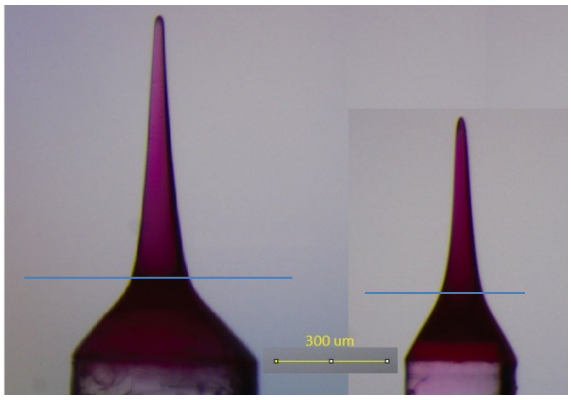

Pillar diameter (µm)	Total height (µm)	Cone basis (µm)	Tip radius of curvature (µm)
300	667	115	9
500	950	150	13

Figure 2.12: *Effects of the pillar diameter on the microneedle morphology; data obtained as mean values on population made up of 20 microneedles; the blue straight lines ideally "separates" the cone basis from the tip.*

As it is possible to notice from the Fig. 2.12, the pillar diameter is a crucial parameter for controlling the final microneedle height, i.e. the best application fitted from it. The smaller is the pillar diameter the smaller is the contraction between the basis and the indenting cone, thus the loss of drug. Further, pillar dimension is linked to the choice of the best PLGA solution concentration, in order to reach a good tip sharpness. The microneedles in Fig. 2.12 on pillars of 500 µm and 300 µm are respectively obtained starting from a 40% and a 30% PLGA solution, which percentages resulted the best ones for the two pillar dimensions taken into account. In fact, assuming that no significant variation in dielectric properties is registered in the studied range of solution concentrations, if higher polymer percentages are desired for reducing the loss of microneedle shape, linked to the shrinkage following the final drying process, on the other hand smaller drops on pillar have a higher surface-to-volume ratio, i.e. a faster solvent evaporation process. About the surface tension characterization for the PLGA solutions at different concentrations, from the tensiometry measurements a very small difference between the samples has been found (all the measured surface tensions were in the range 29 – 32 mN/m). For this reason, the smaller are the drops, the higher is their elastic response due to the interfacial tension. This increase has to be counteracted by a reduction of the viscosity, in order to successfully shaping the drops in microneedle. The results of the viscosity characterization are summarized in Fig. 2.13.

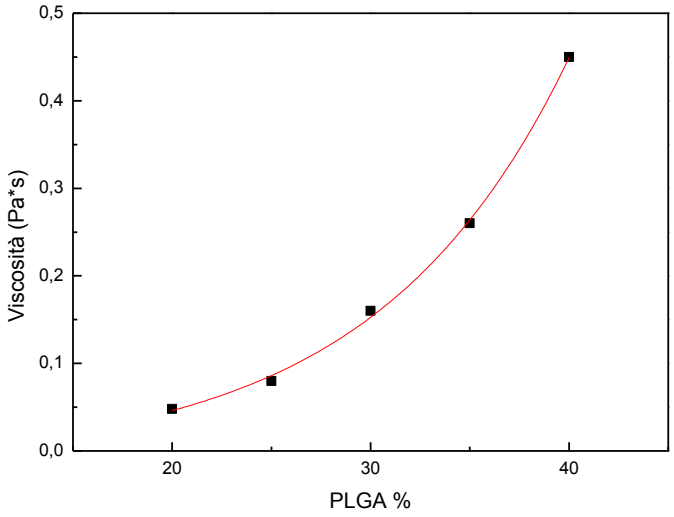

Figure 2.13: *Viscosity of the PLGA solution as function of its polymer percentage.*

Coating of pillars

To the aim of creating a microneedle array with a patch which can be removed from the skin few minutes after its application, leaving the microneedles inserted into the tissue, a rapid dissolving hydrophilic coating onto the PDMS pillars was created, according to the scheme in Fig. 2.14.

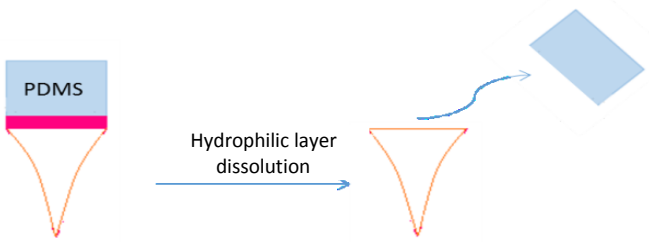

Figure 2.14: *Schematic concept of the microneedle release following the dissolution of the hydrophilic layer.*

By means of the motorized stages of which the ED set-up is made up, the PDMS pillars were contacted with the PAA solution, contained within a hydrophilic PDMS vessel, fabricated as described in the materials section, and then lift off again, following a micro-contact procedure. The PAA solution droplets deposited in such way, were then left to dry for 3 min, in order to let evaporate the most of the solvent, but maintaining the plasticity of the polymeric material. In a second step, the pillars were contacted with a flat PDMS layer,

previously treated with a silane solution, to the aim of obtaining a flat PAA coating onto the pillars. The final results are shown in Fig. 2.15.

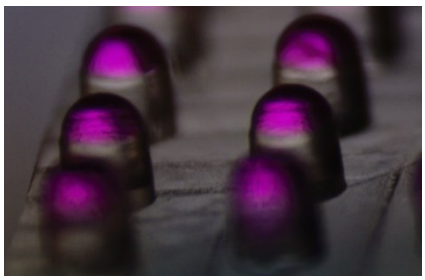
a)

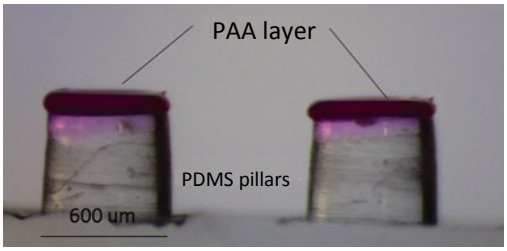

b)

Figure 2.15: PAA coating of PDMS pillars; a) just deposited droplets; b) lateral view of the final dried layer.

The release of microneedles following the PAA layer dissolution, was tested by inserting the patch within a gelatin matrix. As shown in Fig. 2.16, after 30 min from the insertion of microneedles, it was possible to remove the PDMS substrate, without microneedles, which were still inserted within the gelatin.

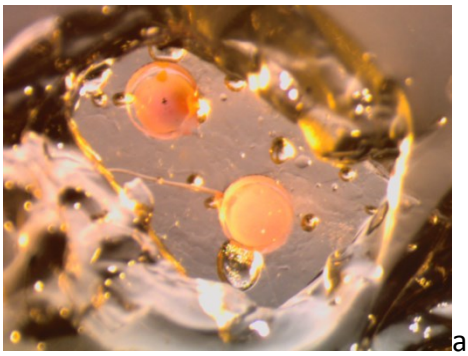
a)

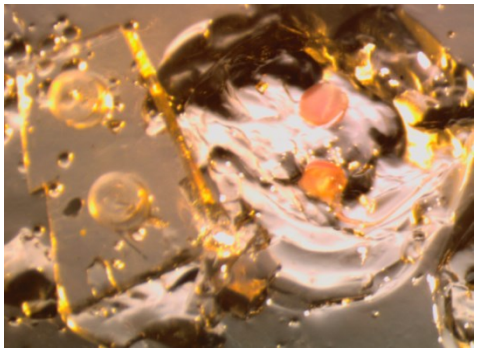
b)

Figure 2.16: *Microneedle release within a gelatin matrix; a) top view of a microneedles patch indenting the gelatin substrate; b) microneedles release after 30 min from the indentation.*

In parallel electro-drawing of microneedles

To the aim of electro-drawing simultaneously an array of microneedles, a solution based on the micro-contact technique was adopted in order to deposit droplets with homogeneous volume on the pillar array. Unlike the other techniques for liquid dispensing, such as the ink-jet printing, the micro-contact technique appears suitable also for the dispensing of polymer solutions with high viscosity, such as the PLGA/DMC solution used as precursor for microneedles. Like for PAA depositions, by means of motorized stages, the PDMS pillars were contacted with the PLGA solution contained within a PDMS vessel and then lifted up again at controlled rate.

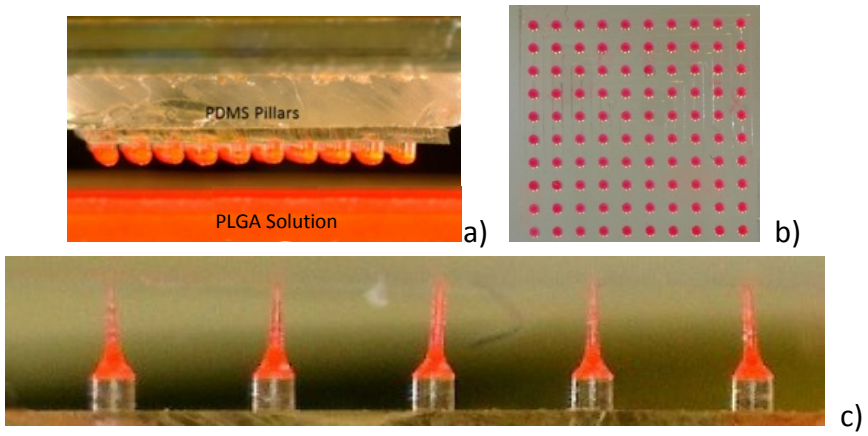

Figure 2.17: *Micro-contact deposition of the PLGA solution drops and in parallel electro-drawing; drops on pillars: lateral view (a) and top view (b); detail of in parallel electro-drawn microneedles on pillars with 300 μm basis diameter (c).*

From the Fig. 2.17 a-b), it appears clear as the μ-contact process was optimized in order to obtain 100 drops quite homogeneous in volume each other, showing, in particular, a contact angle with the pillar surface near to 90°. This latter value results to be the best for obtaining the desired morphology for the microneedles. The array of drops was employed for testing the in parallel electro-drawing, by means of the integrated device, designed and fabricated as described in the previous paragraphs, consisting of a pyroelectric driving plate with a metallic pattern of an array of spiral elements. The process was carried out by applying process parameters and results obtained for single ED, summarized in the previous lines. The result is shown in Fig. 2.17 c): both the deposited sessile drops and the pyroelectric effect activation, are homogeneous enough to guaranty a satisfactory reproducibility of the simultaneous electro-drawing of several microneedles.

2.5 Conclusions

In this chapter, a novel set up for the electro-drawing of polymer microneedles is presented. This set up is based on an engineered driving plate, made up of an integrated electrical circuit directly patterned onto the pyroelectric crystal, allowing in this way the control of the generated electric field by means of the voltage applied to the circuit. It is shown how this configuration determines an optimized shape for microneedles, in terms of sharp tip and absence of spherical basis pedestal. This latter shape, joint to the presence of a rapid dissolvable hydrophilic layer interposed between the microneedles and the PDMS substrate,

allows the complete release of microneedles from the patch after indentation. Further, the in parallel ED of microneedles in an array configuration has been demonstrated by combining the engineered driving plate with a micro-contact deposition of precursor drops.

References

[1] C. Wei, H.T. Qin, N.A. Ramirez-Iglesias, C.P. Chiu, Y.S. Lee, J.Y. Dong, High-resolution ac-pulse modulated electrohydrodynamic jet printing on highly insulating substrates, Journal of Micromechanics and Microengineering, 24 (2014) 9.

[2] O.A. Basaran, H.J. Gao, P.P. Bhat, Nonstandard Inkjets, in: S.H. Davis, P. Moin (Eds.) Annual Review of Fluid Mechanics, Vol 45, Annual Reviews, Palo Alto, 2013, pp. 85-113.

[3] K.L. Choy, B. Su, Growth behavior and microstructure of CdS thin films deposited by an electrostatic spray assisted vapor deposition (ESAVD) process, Thin Solid Films, 388 (2001) 9-14.

[4] R.L. Hines, Electrostatic atomization and and spray painting, in, Journal of Applied Phisics, 1996, pp. 2730.

[5] L. Ding, T. Lee, C.H. Wang, Fabrication of monodispersed Taxol-loaded particles using electrohydrodynamic atomization, Journal of Controlled Release, 102 (2005) 395-413.

[6] R. Pareta, M.J. Edirisinghe, A novel method for the preparation of biodegradable microspheres for protein drug delivery, Journal of the Royal Society Interface, 3 (2006) 573-582.

[7] H. Ghanbar, C.J. Luo, P. Bakhshi, R. Day, M. Edirisinghe, Preparation of porous microsphere-scaffolds by electrohydrodynamic forming and thermally induced phase separation, Materials Science & Engineering C-Materials for Biological Applications, 33 (2013) 2488-2498.

[8] C.J. Luo, S. Loh, E. Stride, M. Edirisinghe, Electrospraying and Electrospinning of Chocolate Suspensions, Food and Bioprocess Technology, 5 (2012) 2285-2300.

[9] G.I. Taylor, A.D. McEwan, The stability of a horizontal fluid interface in a vertical electric field, in, Jornal of Fluid Mechanics, 2006, pp. 1 - 15.

[10] P. Ferraro, S. Coppola, S. Grilli, M. Paturzo, V. Vespini, Dispensing nano-pico droplets and liquid patterning by pyroelectrodynamic shooting, Nature Nanotechnology, 5 (2010) 429-435.

[11] S. Grilli, S. Coppola, V. Vespini, F. Merola, A. Finizio, P. Ferraro, 3D lithography by rapid curing of the liquid instabilities at nanoscale, Proceedings of the National Academy of Sciences of the United States of America, 108 (2011) 15106-15111.

[12] S. Coppola, V. Vespini, G. Nasti, O. Gennari, S. Grilli, M. Ventre, M. Iannone, P.A. Netti, P. Ferraro, Tethered Pyro-Electrohydrodynamic Spinning for Patterning Well-Ordered Structures at Micro- and Nanoscale, Chemistry of Materials, 26 (2014) 3357-3360.

[13] S. Coppola, V. Vespini, S. Grilli, P. Ferraro, Self-assembling of multi-jets by pyro-electrohydrodynamic effect for high throughput liquid nanodrops transfer, Lab on a Chip, 11 (2011) 3294-3298.

[14] R. Vecchione, S. Coppola, E. Esposito, C. Casale, V. Vespini, S. Grilli, P. Ferraro, P.A. Netti, Electro-Drawn Drug-Loaded Biodegradable Polymer Microneedles as a Viable Route to Hypodermic Injection, Advanced Functional Materials, 24 (2014) 3515-3523.

[15] R.S. Weis, T.K. Gaylord, LITHIUM-NIOBATE - SUMMARY OF PHYSICAL-PROPERTIES AND CRYSTAL-STRUCTURE, Applied Physics a-Materials Science & Processing, 37 (1985) 191-203.

[16] G.D. Boyd, R.C. Miller, K. Nassau, W.L. Bond, A. Savage, LINBO3 - EFFICIENT PHASE MATCHABLE NONLINEAR OPTICAL MATERIAL (UNIAXIAL PIEZOELECTRIC OPTICAL PARAMETRIC EFFECTS E), in, Applied Physics Letters, 1964, pp. 234-236.

[17] E.M. Bourim, C.W. Moon, S.W. Lee, I.K. Yoo, Investigation of pyroelectric electron emission from monodomain lithium niobate single crystals, Physica B-Condensed Matter, 383 (2006) 171-182.

[18] J.L. Li, On the meniscus deformation when the pulsed voltage is applied, Journal of Electrostatics, 64 (2006) 44-52.

[19] O. Gennari, L. Battista, B. Silva, S. Grilli, L. Miccio, V. Vespini, S. Coppola, P. Orlando, L. Aprin, P. Slangen, P. Ferraro, Investigation on cone jetting regimes of liquid droplets subjected to pyroelectric fields induced by laser blasts, Applied Physics Letters, 106 (2015) 5.

[20] Y.L. Jeyachandran, B. Karunagaran, S.K. Narayandass, D. Mangalaraj, T.E. Jenkins, P.J. Martin, Properties of titanium thin films deposited by dc magnetron sputtering, Materials Science and Engineering a-Structural Materials Properties Microstructure and Processing, 431 (2006) 277-284.

[21] G.Y. Jung, W. Wu, S. Ganapathiappan, D.A.A. Ohlberg, M.S. Islam, X. Li, D.L. Olynick, H. Lee, Y. Chen, S.Y. Wang, W.M. Tong, R.S. Williams, Issues on nanoimprint lithography with a single-layer resist structure, Applied Physics a-Materials Science & Processing, 81 (2005) 1331-1335.

Chapter 3

Tuning of the internal microstructure of PLGA microneedles by multiphase system templating

Part of this chapter is based on the paper *"Room temperature consolidation of porous PLGA matrix by addition of maltose in the water phase",* Esposito E., Ruggiero F., Vecchione R., Netti P.A.*,* submitted to *Materials*

3.1 Introduction

Among the other biodegradable polymer materials, poly(lactic-co-glycolic) acid (PLGA) are widely used for several applications in the biomedical field, including the fabrication of scaffolds for tissue engineering[1-3] and drug delivery systems, such as micro and nano carriers[4,5]. In both cases, the introduction of a porosity, represents a good issue for several advantages deriving from it. In particular, in the case of scaffolds, the presence of void compartments within the polymer matrix is of fundamental importance for cell growth, adhesion and proliferation[6]. On the other hand, in the case of drug delivery systems, the presence of a high porosity can dramatically increase their loading capacity, as well as allow to tune their release kinetics, by means of the pore distribution and interconnectivity[7]. Further advantages in confining the drug within void compartments are linked to the chance of avoiding the burst effect and to a better protection of it from degradation, both during storage and after administration. These advantages linked to the introduction of porosity within the polymer structure of drug delivery systems, can be of practical interest also in the case of electro-drawn biodegradable PLGA microneedles. In fact, the addition of void compartments within them, gives the possibility of loading, protecting and delivering hydrophilic compounds, despite of the intrinsic hydrophobic features of PLGA[8]. Also the introduction of a dispersion of pores filled with a lipid phase can be useful to extend the biodegradable microneedle application fields to the delivery of lipid high soluble therapeutic compounds, such as, for example, Vitamin E which is one of the most used natural antioxidants in pharmaceutical industries[9]. These compounds are in fact almost insoluble in

water, leading to insufficient bioavailability after oral or parenteral administration and very often below the therapeutic level.

Among the other techniques presented in literature[3], the fabrication of porous structures starting from multiphase systems, seems to be a very promising route, because of its flexibility in terms of final morphologies and ease of process[10]. Emulsions represent an example of multiphase systems used as template for microstructured polymer matrices. In fact, disperse compartments within a polymer matrix can be obtained by fixing the continuous phase of an emulsion (typically by in situ polymerization or freezing by rapid solvent extraction), followed by the removal of the internal disperse phase when required[3]. In this case, fundamental parameters for the process control are the formulation of the starting emulsion, in terms of compositions of the immiscible phases and their reciprocal volume ratio, and the procedure used for consolidating the continuous phase. In particular, these are the factors determining the final morphology of the porous system and, as a consequence, its possible applications. The Thermal Induced Phase Separation technique, widely used for the fabrication of both PLA and PLGA porous scaffolds and microparticles[6,11-13], consists in inducing the thermodynamic destabilization of a polymer solution upon a change in its temperature, leading, by means of a controlled process, to the formation of a polymer-rich and a polymer-lean phase. The final porous structure is then obtained by polymer-lean phase removal, typically carried out by vacuum freeze-drying[14]. Therefore, in TIPS prcesses, the formation of the two immiscible phases is pursued by the destabilization of a kinetically and thermodynamically stable system. On the contrary, in the emulsion templating, the process is carried out starting from a system which is characterized by an intrinsic instability, i.e. it tends to spontaneously evolve towards a configuration with two immiscible phases, completely stratified one above the other. In order to counteract this phenomenon or, if better, to make the complete phase separation becoming a slower process, it is possible to act on the kinetics of the emulsion phase separation. A viable route could be a fast thermal treatment of the emulsion, in order to rapidly remove the solvent in continuous phase and “freeze” the internal microstructure. Anyway, this latter strategy appears not suitable for systems finalized to drug delivery, such as polymer microneedles or microspheres, because of the possibility of damaging encapsulated thermolabile molecules. A possible alternative to the “high” temperature treatment, can be the improved kinetical stability of the emulsion, by acting on its formulation. In the work presented in this chapter,

the improved stability of emulsions made up of an aqueous phase dispersed in a PLGA solution, is obtained by means of a densifying agent dissolved into the inner phase. The stability is improved enough for allowing a room temperature drying process, with a good final level of porosity. The improved stability is first experimentally shown by means of morphological analysis of the consolidated PLGA matrices, and then explained by means of argumentations based on both tensiometry and rheology. The new formulated emulsion is then tested for the electro-drawing of polymer microneedles, in order to demonstrate the applicability of the proposed solution. As a complement to the proposed study, the possibility of creating lipid compartments within the PLGA microneedles, by means of emulsion templating is also demonstrated. In the last paragraph of the chapter, a technique based on TIPS is then shown to be useful for creating interconnected porosities within both PLGA matrices and electro-drawn microneedles.

3.2 Materials

As in the previous chapter, the polymeric porous matrices, and afterwards the porous microneedles, were made of Poly(lactic-co-glycolic acid) purchased from Evonik Industries (PLGA or RESOMER® RG 504 H, copolymers ratio 50 : 50). Both Dimethyl Carbonate (DMC), used as solvent for it and maltose monohydrate, used as additive in the water phase emulsified within the polymer solution, were provided by Sigma Aldrich. For the water disperse phase, Millipore® Milli-Q water was used. Egg lecithin (Lipoid E80), used as surfactant for stabilizing the emulsions, because of its biocompatibility and biodegradability, was purchased from Lipoid. Soybean oil, used for lipid compartments within the PLGA matrix was provided from Sigma Aldrich. Polydimethylsiloxane (PDMS, Dow Corning Sylgard 184 Silicone elastomer) mixed with curing agent in ratio 10 : 1 was used for including the samples before their sectioning.

3.3 Experimental details

3.3.1 Emulsion preparation

For all the studied emulsions, the continuous phase was obtained by dissolving PLGA in DMC in the percentage of 25% wt/v. About the disperse phase, three different batches were used:

1. pure water/lecithin solution (surfactant concentration: 180 mg/ml);
2. maltose-containing water (maltose dissolved in quantity 360 mg/ml, corresponding to saturation level), with lecithin in concentration 180 mg/ml;
3. soybean oil/lecithin solution (surfactant concentration: 120 mg/ml).

For the pure water containing emulsions, several samples with different disperse phase contents were prepared: the aqueous phase was added in 30%, 60%, 80% and 100% wt/wt compared to PLGA. For the maltose-containing systems, the 80% composition was chosen starting from the first experimental observation carried out on the sample prepared with the pure water phase. Finally, for the soybean oil containing system, a 10% v/v ratio between the disperse and the continuous phase was set.

For all the emulsions, the disperse phase was emulsified within the continuous one, by means of an immersion sonicator (Ultrasonic Processor VCX500, Sonics and Materials Inc.) for 20 s, with a sonication amplitude of 30%, by keeping the processed sample within an ice bath, in order to avoid solvent evaporation due to the high temperature reached during the sonication.

3.3.2 Thermal treatments

For the two kinds of water containing samples, a comparison between the internal morphologies obtained after some different thermal treatments was carried out on PLGA films, each obtained by consolidating a volume of 15 µl of the starting emulsion within a 6 mm diameter PDMS pool. For the samples with disperse phase 1, a comparison between the porosities obtained on samples consolidated at room temperature and on samples consolidated at 50°C in oven, in both cases for 24 h, was carried out: obviously, a faster solvent extraction for the 50°C treatment was expected. For the samples with disperse phase 2, the comparison between films consolidated at 30°C with atmospheric pressure and films consolidated at 30°C under vacuum (around 100 mbar) was carried out: in this case the vacuum may accelerate the solvent extraction.

3.3.3 Interfacial tension measurements

Interfacial tension measurements between the PLGA/DMC continuous phase and the two aqueous dispersed phase, respectively made up of lecithin added to pure water in one case and to maltose containing water in another case, with the composition indicated in the "emulsion preparation" paragraph, were carried out by using of an Optical Tensiometer, (Attension Theta Lite, Biolin Scientific) by means of the reverse pendant drop method. After the stabilization of their shape under the surfactant action, drop images were recorded and analysed by means of the Attension Theta Software, by using as input parameters the densities of the phases, previously measured. The Young – Laplace curve fitting method was employed. The measurements were repeated at least three times, each time on a sample made up of ten drops.

3.3.4 Rheological measurements

The viscoelastic properties of PLGA emulsions with aqueous disperse phases, were measured by means of a stress-controlled rheometer (MCR 302 rheometer, Anton Paar), fitted with a double gap concentric cylinder geometry (DG 27, Anton Paar) in order to avoid DMC evaporation during the measurements. Temperature was kept at 25°C, with an accuracy of $\pm$0.1°C, during the measurements by means of an Anton Paar Peltier temperature device for concentric-cylinder system, equipped with a water circulating bath. All the samples were placed in the double gap cylinder measuring system and left to rest for 2 min for structure recovery and temperature equilibration. Dynamic oscillatory measurements were carried out for the frequency sweep tests. The viscoelastic linear region was preliminary determined by means of amplitude sweep tests (0.01 – 100% strain, 0.1 Hz), in order to choose a suitable value for the following frequency sweep tests. From this latter ones, ranging from 1 to 0.01 Hz at a strain of 10%, viscoelastic parameters of the emulsions, such as storage (G') and loss (G'') moduli were determined, in order to theoretically investigate the differences between the maltose containing and the maltose non containing systems. All the measurements were repeated three times on each sample.

3.3.5 Fabrication of porous matrices via TIPS

PLGA/DMC solutions were prepared with polymer contents corresponding to 15% and 20% wt/v. Starting from these solutions, flat matrices as explained in the previous lines, and electro-drawn microneedles were prepared. These systems, just after their preparation, were immersed in a liquid nitrogen bath, in order to realize their rapid quenching and thermally induced phase separation. The solvent was then removed from the polymer samples, in order to obtain the desired porosity, by vacuum freeze-drying for 18 h.

3.3.6 Analysis of internal microstructure

The consolidated PLGA films and microneedles were included in a PDMS matrix and cured at room temperature for 24 h. The PDMS blocks, containing the PLGA films or microneedles, were frozen at -140°C in liquid nitrogen and sectioned, by means of a cryo-ultramicrotome set up (Leica EM-FC7-UC7), with a slice thickness of 5 μm. The slices were coated with a 15 nm thick gold layer by means of a sputter coater (Cressington), and then observed by means of a scanning electron microscope (Ultra Plus, Zeiss), imposing a 5 kV voltage for the gun, in order to capture pictures of the internal porosity. Image analysis was carried out by means of the software Fiji, in order to calculate the percentage of porosity and the pore dimensional distribution. For this latter task, a population of at least 200 pores has been taken into account for each sample.

3.4 Results and discussion

3.4.1 Thermal treatment effects on porosity

First of all, the effects of the consolidation temperature, i.e. of the solvent extraction speed, on the final matrix porosity were observed as a function of the starting emulsion formulation in terms of aqueous dispersed phase percentage. The results are summarized in Fig.3.1.

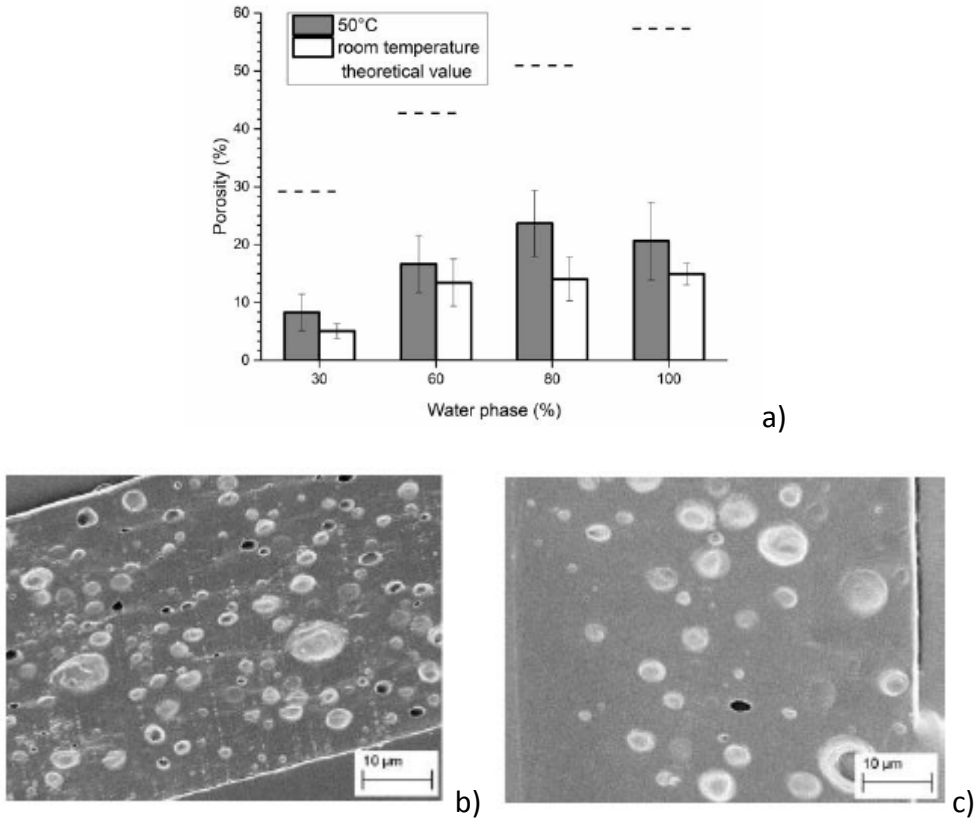

Figure 3.1: *Porosity percentage obtained from the analysis of SEM images of sections of matrices obtained consolidating emulsions with different percentages of pure water dispersed phase, for two different hardening procedures (a); SEM images of sectioned matrices obtained from emulsions with 80% of pure water phase, respectively dried at 50°C (b) and at room temperature (c) at atmospheric pressure.*

As shown in the bar diagram of Fig. 3.1 a), for all the studied composition of the starting emulsion, the higher is the temperature employed for the consolidation process, the higher is the porosity level preserved within the polymer matrix. In fact, the higher temperature determines a faster solvent extraction, i.e. a faster continuous phase viscosity increase until its consolidation, reducing the creaming tendency for the disperse droplets.

From the data in Fig. 3.1 (a), it is possible to notice how by increasing the water content above 60%, the porosity level does not increase appreciably in the case of room temperature consolidation, while by forcing by means of the temperature the rapid freezing of the matrix morphology, an increase in matrix porosity is observed up to the 80% of water phase. Anyway, the observed porosity level appears always slower than the theoretical one, calculated from the starting emulsion composition, due to the intrinsic phase separation tendency of the studied emulsions. This latter loss seems to be a very important drawback

for the studied biodegradable porous polymer matrix in reference to drug delivery applications, such as for polymer electro-drawn microneedles, because of the lower quantity of drugs which can be loaded and released. Furthermore, even if an increase in hardening temperature appears as a suitable strategy for decreasing the loss of porosity following the emulsion destabilization, it is not compatible with thermolabile drug encapsulation determining a loss of generality in terms of applicability for the final porous PLGA matrix.

3.4.2 Maltose-containing systems

Internal morphology

As an alternative strategy to the rapid quenching of the porous structure by rapid solvent extraction at high temperature, the densification of the disperse phase by means of the addition of a water-soluble species was tested. Maltose was chosen as densifying agent, because of its biocompatibility. In this way, by lowering the density difference between the continuous and the disperse phase, the emulsion creaming tendency can be reduced. Emulsions were prepared by adding water phase in percentage 80% wt/wt with respect to PLGA.

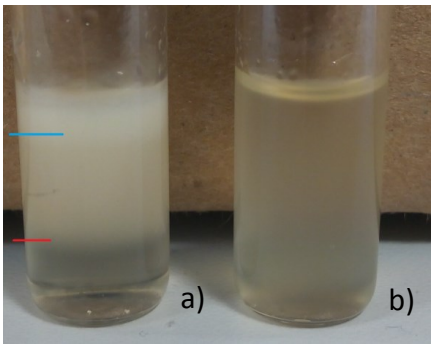

Figure 3.2: *Macroscopic comparison, after one week from their preparation, between emulsions obtained by emulsifying in the PLGA solution a water phase containing lecithin (a) and a water phase containing lecithin and maltose (b). The demarcation lines clearly indicate the phase separation process.*

In order to test the improved emulsion stability before proceeding with the morphological analysis of the matrices, the emulsions respectively with and without maltose were monitored for several days after their preparation. From the Fig. 3.2, it appears clear as after one week from the preparation, the maltose containing sample appeared homogeneous while the emulsion without maltose showed tangible signs of phase separation.

To the aim of comparing the porosity of the PLGA matrices, the consolidation of the maltose containing and not containing samples was carried out at 30° C, in order to avoid critical temperatures for thermosensitive drugs preloaded in the matrix. The consolidation was realized both at atmospheric pressure and under vacuum, in all cases for 1 h (indeed, by monitoring the weight of the matrices under consolidation, its stabilization was found in this short time, allowing to assume the morphology blocked).

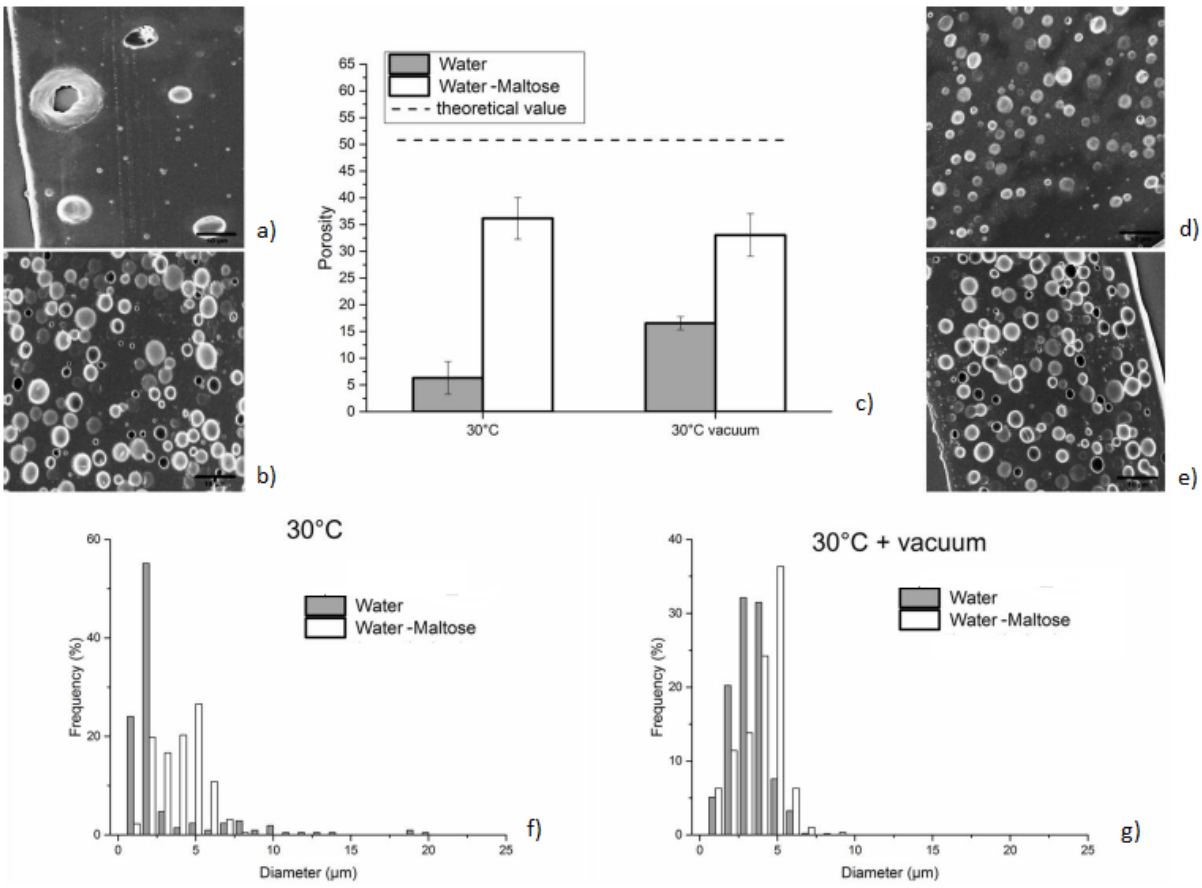

Figure 3.3: *SEM images of sections of the porous matrices obtained from the consolidation of emulsions hardened at 30°C; maltose not containing system hardened at atmospheric pressure (a) and under vacuum (d); maltose containing system hardened at atmospheric pressure (b) and under vacuum (e); porosity levels (c) and size pore distributions (f – g) of the mentioned systems; scale bars of the SEM images are 10 µm.*

From the analysis of the SEM images in Fig. 3.3 (a) and in Fig. 3.3 (d), it appears clear as the introduction of the vacuum in the matrix consolidation process determines an improvement of the final system porosity, because of the acceleration of the solvent extraction, making the hardening temperature increasing not necessary. Further, by comparing the Fig. 3.3 (a) and the Fig. 3.3 (b), it is possible to notice how the improved emulsion stability pursued by

maltose introduction, determines a drastically improved porosity percentage within the PLGA matrix. In fact, despite the very low solvent extraction process at 30 °C, the emulsion stability is suitable enough to guarantee a good final porosity level. As visible from the comparison between the Fig. 3.3 (b) and 3.3 (e), in the case of maltose containing systems, the long term emulsion stability determines also a not conspicuous rise of the porosity level from the atmospheric to vacuum treatment, allowing in this way to obtain a good porosity by means of the simplest hardening process, i.e. at temperature close to the room one. The effect of vacuum is visible from the pore size distribution (Fig. 3.3 (g)): the vacuum can improve the monodispersity of this latter distribution.

Improved emulsion stability

In order to elucidate the reasons at the basis of the experimentally observed improved stability of the PLGA emulsion containing maltose in the dispersed phase, the density and the interfacial properties of the aqueous phases/polymer solution systems were evaluated. The obtained results are summarized in Tab.3.1.

Phase	Density (g/ml)	Interfacial Tension (mN/m)
PLGA/DMC 25% wt/v	1.15	-
Pure water	1	7.2±0.25
Water/maltose	1.13	8.5±0.38
Water/lecithin	0.964	4.7±0.3
Water/lecithin/maltose	1.098	7.3±0.6

Table 3.1: *Density and interfacial tensions of the phases of the water containing studied emulsions.*

First, the interfacial tensions of the aqueous phases without surfactant within the polymer solutions were measured: the higher value obtained for the water/maltose system shows how the maltose negatively interacts with the PLGA, causing a destabilization of the interface between the two phases. This latter evidence means that a higher level of energy is needed in order to expand the interface of the dispersed phase. The addition of lecithin as a surfactant determines a lowering of the interfacial tension in both cases, as expected, but, again, the pure water-containing system results more stabilized than the water/maltose one. This conclusion appears in opposition with the observed longer time stability of the emulsion in the presence of maltose. Indeed, the higher interfacial tension for the maltose-containing system could determine a larger size of the dispersed droplets, because of the higher level of

energy needed for interface stabilization: it is well known how the larger are the dispersed drops, the higher is their tendency to cream, with consequent lowering of the emulsion stabilization. Conversely, from the observation of the density values of the phases, it appears clear how the emulsion containing maltose is characterized by a lower difference in density between the continuous and the disperse phase, leading to a reduction in the creaming tendency. From the experimental observation confirming less creaming in presence of maltose, it is possible to conclude that the density effect is strong enough to counteract the higher creaming tendency due to the bigger droplet size with respect to the system containing no maltose.

Theoretically, the settling or creaming velocity *U* of droplets within an emulsion can be estimated by means of the following relation:

$$U = \frac{2a^2|\Delta\rho|g}{9\mu} \tag{3.1}$$

where a, $\Delta\rho$, g and μ are respectively the droplet radius, the difference in density between the disperse and the continuous phases, the gravitational constant and the continuous phase viscosity. So, in constancy of the dispersing phase viscosity, the settling rate is proportional to the product:

$$a^2|\Delta\rho| \tag{3.2}$$

As a confirmation of the observed higher creaming rate of the emulsion without maltose, by assuming as radii for the droplets the mean values of the distributions in Fig.3.3 and for the densities the values in Tab.1, from the formula (3.2) it is possible to obtain:

- emulsion containing no maltose: $(1.5\cdot10^{-6})^2\cdot(1150-964) = 4.2\cdot10^{-10}$ Kg/m
- emulsion containing maltose: $(2.5\cdot10^{-6})^2\cdot(1150-1098) = 3.2\cdot10^{-10}$Kg/m

i.e. a reduction of the creaming rate by adding maltose.

Therefore, also theoretically, it is confirmed that the maltose introduction contributes to the kinetic stability of the PLGA emulsion.

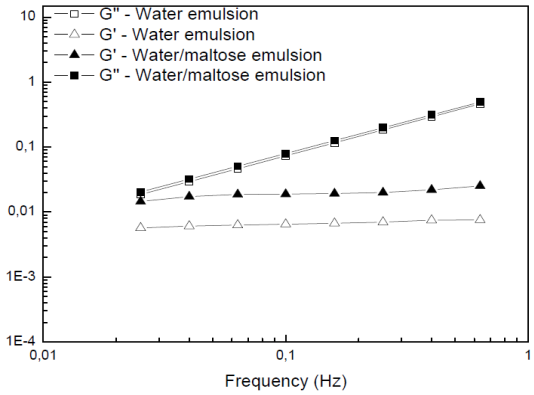

Figure 3.4: *Frequency dependence of the storage modulus G' and loss modulus G'' for the studied water phase containing emulsions.*

In Fig. 3.4 the results of the frequency sweeps, carried out on the emulsions in terms of storage (G') and loss (G'') moduli as functions of the oscillations frequency, are reported. In almost the whole range of investigated frequencies, the samples show a viscous liquid-like behavior (G''>G'), because of the low volume fraction of the dispersed phase (in the studied case this latter volume fraction is 0.15). The loss modulus trend is almost the same for the two studied samples, being the viscous component mainly due to the continuous phase. About the storage modulus, a higher value for the emulsion containing maltose was found: the elastic component, due to the surface contribution arising from the dispersed phase, is higher in the presence of maltose dissolved in the aqueous domains. This latter evidence is in agreement with the lower tendency of the maltose-containing system to kinetic destabilization by means of coalescence, which would increase the size of the drops with a further acceleration of the creaming process.

Porous electro-drawn microneedles

The maltose containing emulsion was then employed in order to obtain PLGA microneedles, by means of the ED technique, by depositing the just prepared emulsion on PDMS pillars, to the aim of employing the advantages of the maltose containing emulsions for optimizing the internal microstructure of the microneedles. Also for the microneedles, the best individuated hardening treatment was employed (1 h, 30° C under vacuum).

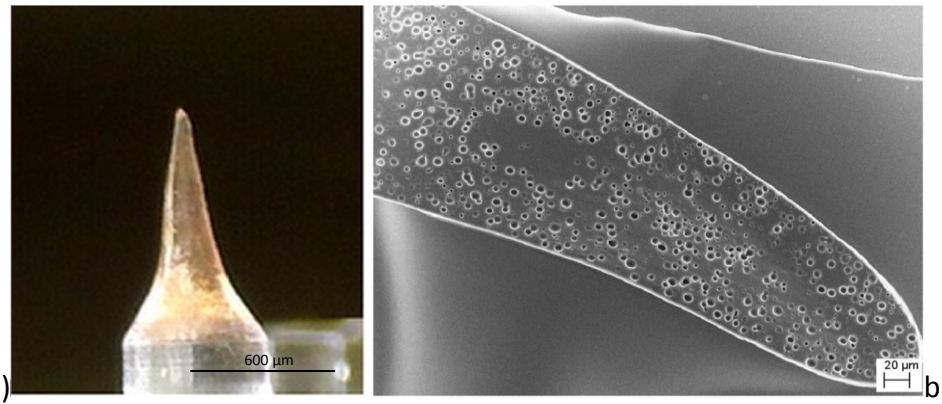

Figure 3.5: *Optical image (a) and SEM image of a longitudinal section (b) of a maltose containing PLGA porous microneedle produce by Electro-drawing.*

From the Fig. 3.5 a) it is possible to notice how the emulsion macroscopically behaves as the same of the simple PLGA solution under the electric field action, conventionally used for the ED, giving rise to a good macroscopic shape of the microneedle. Furthermore, from the Fig. 3.5 b), it appears clear how the porosity within the microneedles is homogeneously distributed along the cone and how it replies the good features found within the flat PLGA films, hardened without being electro-drawn. In other words, the electric field action does not affect the internal microstructure of the microneedle, being it controlled by the only emulsion templating process.

3.4.3 Microneedles with internal lipid compartments

As anticipated in the previous paragraphs, an emulsion made up of lipid disperse compartments was also tested for the electro-drawing of PLGA microneedles. The microneedles, consolidated as the same for 1h at 30°C under vacuum were studied in terms of internal microstructure.

a) 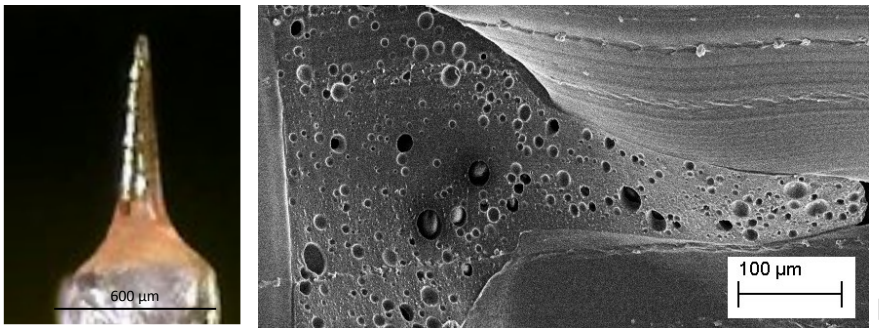

b)

Figure 3.6: *Optical image (a) and SEM longitudinal section image of a porous electro-drawn PLGA microneedle with lipid compartments.*

As shown in Fig. 3.6 a) also the emulsion with lipid compartments appears suitable for the ED process, producing microneedles with a good shape. From the SEM image in Fig. 3.6 b) a well distributed porosity along the cone clearly appears.

3.4.4 Microneedles with interconnected porosity

A process based on TIPS was carried out on PLGA matrices and microneedles in order to obtain an interconnected internal porous structure. As anticipated in the introductive paragraph, the interconnected porosity can dramatically increase the loading capability of microneedles, and can be suitable in order to modulate the drug release kinetics. In fact, in this way, the drug release can occur both following the PLGA degradation and diffusing across the void channels.

The TIPS process was achieved by rapid quenching the PLGA matrices and microneedles in a liquid nitrogen bath. In this way, the solvent crystallization was determined, with the consequent expulsion of the polymer, which generated the continuous porous structure, according to the demixing of the initial monophasic solution.

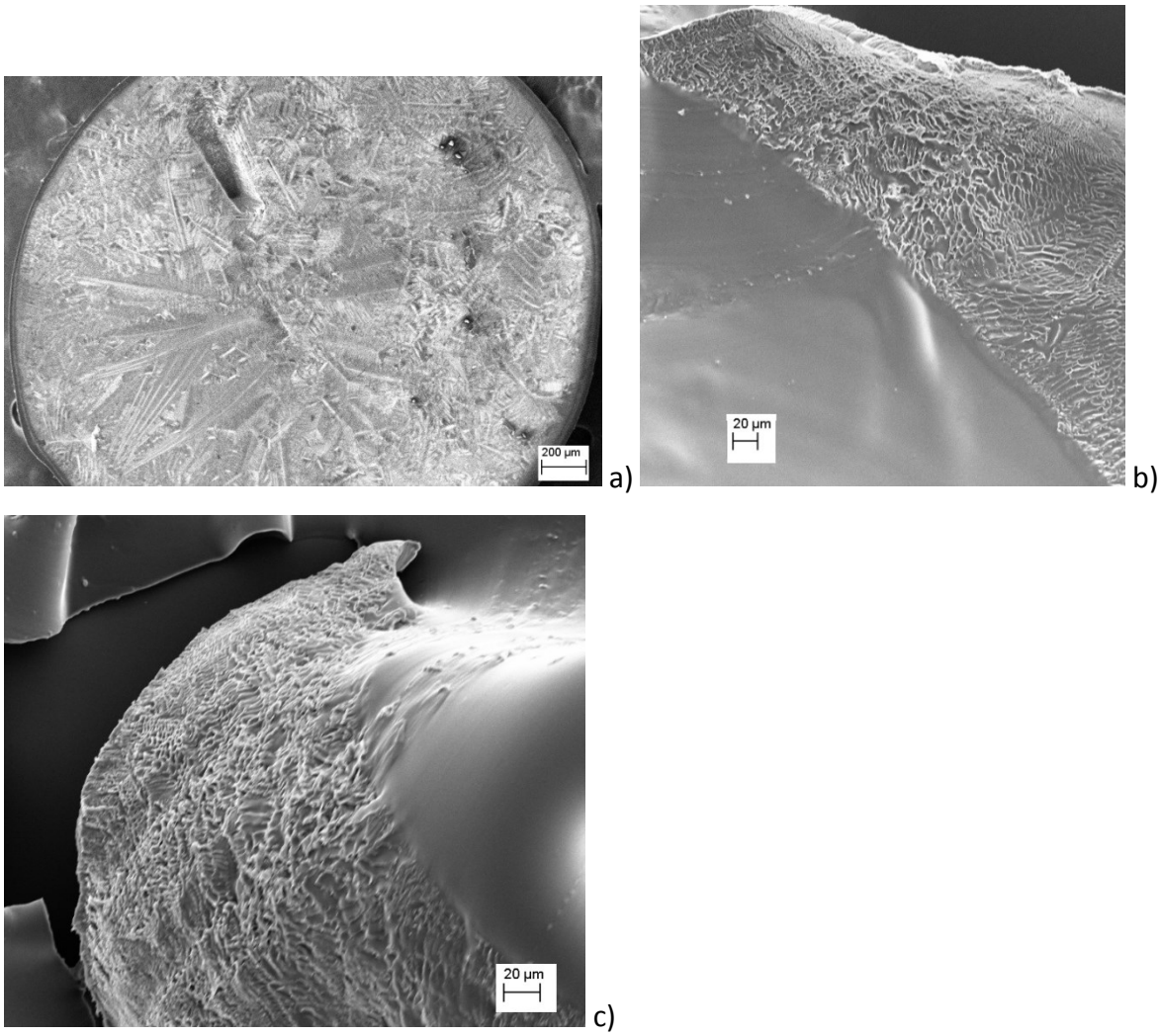

Figure 3.7*: SEM images of porous PLGA matrices and microneedles obtained by TIPS; a) surface porosity; b-c) internal porosity.*

From the comparison between the images in Fig. 3.7 and the ones presented in the previous paragraphs, it appears clear how by inducing a TIPS process on just shaped microneedles, the obtained pores are well interconnected while in the case of emulsion templating they are well isolated from each other. Depending on the desired final application, one can chose closed pores or interconnected pores. It is proper to specify how the interconnected porosity via TIPS can be successfully achieved only if the microneedles are rapidly drawn, before the most of the solvent contained in the starting solution evaporates. In fact, the lower is the solvent content, the lower will be the chance of obtaining a good interconnected porosity. Anyway, as discussed in the previous chapter, the novel proposed ED set-up, based on an engineered driving plate, is suitable to ensure a rapid microneedle shaping, leading to the possibility of preserve enough solvent within the microneedles before their quenching in liquid nitrogen.

3.5 Conclusions

In this chapter, several strategies for the fabrication of polymer microneedles with an internal microstructure, by means of the electro-drawing technique, were proposed. Micropores within the PLGA matrices were obtained by emulsifying a water or a lipid phase in the PLGA continuous phase. In the case of the water dispersed phase, in order to keep a good uniformity of the pore distribution by counteracting the intrinsic tendency to the destabilization of the emulsion system, maltose was dissolved in water as densifying agent. The improved stability was demonstrated both experimentally, from the morphologically analysis of the polymer systems, and theoretically, by means of tensiometry and rheology. The improved stability, in terms of minor tendency to coalescence and creaming, allows consolidating the porous structure by means of mild temperatures, very close to the room one. Further, also the possibility of good microporous structures with lipid compartments, obtained by means of mild consolidation temperature, was demonstrated. A TIPS process was then employed in order to obtain an interconnected porosity within the PLGA matrices. All the discussed strategies were finally demonstrated to be suitable in order to obtain porous electro-drawn PLGA microneedles.

References

[1] M. Okamoto, B. John, Synthetic biopolymer nanocomposites for tissue engineering scaffolds, Progress in Polymer Science, 38 (2013) 1487-1503.

[2] Z. Pan, J.D. Ding, Poly(lactide-co-glycolide) porous scaffolds for tissue engineering and regenerative medicine, Interface Focus, 2 (2012) 366-377.

[3] K. Seunarine, N. Gadegaard, M. Tormen, D. O Meredith, M. O Riehle, C.D.W. Wilkinson, 3D polymer scaffolds for tissue engineering, Nanomedicine, 1 (2006) 281-296.

[4] F. Danhier, E. Ansorena, J.M. Silva, R. Coco, A. Le Breton, V. Preat, PLGA-based nanoparticles: An overview of biomedical applications, Journal of Controlled Release, 161 (2012) 505-522.

[5] W.L. Jiang, R.K. Gupta, M.C. Deshpande, S.P. Schwendeman, Biodegradable poly(lactic-co-glycolic acid) microparticles for injectable delivery of vaccine antigens, Advanced Drug Delivery Reviews, 57 (2005) 391-410.

[6] F.C. Pavia, V. La Carrubba, S. Piccarolo, V. Brucato, Polymeric scaffolds prepared via thermally induced phase separation: Tuning of structure and morphology, Journal of Biomedical Materials Research Part A, 86A (2008) 459-466.

[7] D.P. Go, D.J.E. Harvie, N. Tirtaatmadja, S.L. Gras, A.J. O'Connor, A Simple, Scalable Process for the Production of Porous Polymer Microspheres by Ink-Jetting Combined with Thermally Induced Phase Separation, Particle & Particle Systems Characterization, 31 (2014) 685-698.

[8] R. Vecchione, S. Coppola, E. Esposito, C. Casale, V. Vespini, S. Grilli, P. Ferraro, P.A. Netti, Electro-Drawn Drug-Loaded Biodegradable Polymer Microneedles as a Viable Route to Hypodermic Injection, Advanced Functional Materials, 24 (2014) 3515-3523.

[9] N. Khayata, W. Abdelwahed, M.F. Chehna, C. Charcosset, H. Fessi, Preparation of vitamin E loaded nanocapsules by the nanoprecipitation method: From laboratory scale to large scale using a membrane contactor, International Journal of Pharmaceutics, 423 (2012) 419-427.

[10] K. Whang, C.H. Thomas, K.E. Healy, G. Nuber, A NOVEL METHOD TO FABRICATE BIOABSORBABLE SCAFFOLDS, Polymer, 36 (1995) 837-842.

[11] V. La Carrubba, F.C. Pavia, V. Brucato, S. Piccarolo, PLLA/PLA scaffolds prepared via Thermally Induced Phase Separation (TIPS): tuning of properties and biodegradability, International Journal of Material Forming, 1 (2008) 619-622.

[12] Y.S. Nam, T.G. Park, Porous biodegradable polymeric scaffolds prepared by thermally induced phase separation, Journal of Biomedical Materials Research, 47 (1999) 8-17.

[13] H. Ghanbar, C.J. Luo, P. Bakhshi, R. Day, M. Edirisinghe, Preparation of porous microsphere-scaffolds by electrohydrodynamic forming and thermally induced phase separation, Materials Science & Engineering C-Materials for Biological Applications, 33 (2013) 2488-2498.

[14] K.C. Shin, B.S. Kim, J.H. Kim, T.G. Park, J. Do Nam, D.S. Lee, A facile preparation of highly interconnected macroporous PLGA scaffolds by liquid-liquid phase separation II, Polymer, 46 (2005) 3801-3808.

Chapter 4

Thermodynamics of polymer solutions for the control of microstructure morphologies from TIPS

The experimental part of this chapter is based on the paper *"Experimental Investigation and Thermodynamic Assessment of Phase Equilibria in the PLLA/Dioxane/Water Ternary System for Applications in the Biomedical Field",* Ruggiero F., Netti P.A., Torino E., published on *Langmuir*, 2015, 31, 13003 – 13010[1].
The simulations results are, instead, in phase of organization for writing a new paper.

4.1 Introduction

As described in Chapter 1, Thermally Induced Phase Separation (TIPS) represents a widely used technique, in order to obtain porous architectures starting from polymer systems, for manifold applications, among which the fabrication of porous media obtained as biodegradable and biocompatible scaffolds for tissue engineering or of several drug delivery systems, such as micro and nanoparticles, but also for biodegradable microneedles, as shown in the previous chapter. Among the advantages offered by TIPS technique, there is the possibility of obtaining a large variety of pore size and/or interconnectivity, by controlling the process parameters[2]. In particular, the TIPS can occur according two different mechanism: nucleation and growth of droplets of the less abundant phase in the continuous one, or spinodal decomposition, giving rise to a co-continuous morphology of the demixed system. The mechanism followed and, as a consequence, the final features of the porous system, depends on several parameters of the TIPS process, such as quenching speed, final temperature reached and initial solution composition. For this reason, in order to produce final porous polymer structures with the desired features, phase diagrams, in terms of binodal and spinodal curves, can be used to gain some information about critical conditions for the observation and the control of phase separation processes in binary or ternary polymer solutions. In order to determine liquid-liquid phase boundaries for this latter systems, cloud point measurements have been widely used[3]: it is the point at which, by slowly cooling the polymer solution, it becomes cloudy, due to the formation of two phases,

characterized by different compositions and optical properties. Thermo-optical analysis provides, in fact, a simple, rapid and reliable experimental method for determinations of cloud-point curves of binary and ternary systems, together with their upper or lower critical solution temperature. Anyway, although it represents a widely used technique, cloud-point measurement provides only qualitative and not quantitative information.

Among the other techniques reported in literature for the determination of thermodynamic interaction parameters in solution, Isothermal Titration Calorimetry (ITC) has been employed for the study of partial molar enthalpies and excess enthalpies for liquid mixtures[4]. This type of thermodynamic investigation has been extended to polymer solutions in a recent work by Mohite et al.[5] where a correlation based on the generalized Flory-Huggins model, which relates the activity data of aqueous solutions of poly(ethylene glycol) to the binodal curve, has been developed, estimating the enthalpy of the solutions by means of ITC.

ITC experiments have also been used by Hamedi et al.[6], in order to determine the solid-liquid equilibrium line in ternary systems containing the solute to precipitate and an aqueous mixed solvent.

In the literature work on which part of this chapter is based[1], thermodynamic investigations on the ternary system polylactic acid/dioxane/water, widely used for scaffold fabrication, have been carried out for the first time by means of ITC, in order to study the interactions between polymer and water as nonsolvent. Indeed, the mechanism of the polymer-solvents interactions have been extensively hypothesized as reported by Su et al.[7] and Tsuji and co-workers[8-10]. In the perspective of adding some explanations in terms of energetic contributions to the system specified above, a study aimed to investigate the thermodynamics of the interaction among the species of the considered ternary system has been carried out, leading to a better understanding of the basic energetic phenomena of the phase separation, used to control the structure of biomaterials. In particular, the goal has been to monitor the behavior of the polymer at different solvent/nonsolvent ratios, focusing on the study of its solvation process. Considerations about phase diagrams can be done starting from these results, to support the classic optical methods for thermodynamic studies on polymer solutions.

Miscibility studies on binary or ternary polymer containing systems, can be done by quantifying the Gibbs free energy of the system[11,12]. Two contributions to this energy are reported, respectively controlled by the energetic and the entropic properties of the system;

while for the energetic contribution estimation, several experimental methods appear to be suitable, the task seems to be harder for the entropic contribution to the free energy. In particular, in the case of macromolecules-containing systems, the high molecular weight and the possibility for the long chains to experience a high number of conformations in solution, are additional features that should be taken into account when studying thermodynamics, in terms of entropic contribution to free energy, of polymer solutions. Often, in applications linked to nanomedicine and nanotechnologies, the macromolecules are forced in a reduced volume, smaller than their natural size[13-22]. In particular, confining constraints (such as the imposition of volume constraints) applied to a free unperturbed polymer chain, reduce the number of available conformations for the macromolecules and could introduce additional interactions between the chain segments and the confining interface[23]. Among other properties, this reduction influences the conformational entropy of the polymer chain, determining a change in many characteristics of a polymer, such as its mobility and its miscibility[24].

To date, the effects of spatial confinement have been extensively modeled by means of both simulations and theory[25]. In particular, in order to study the conformational properties of a macromolecule under confinement, many different variants of the Monte Carlo simulative method (MC method) have been employed and manifold are also the models employed for the chain description.

While in the first part of this chapter considerations about the energy contribution to the free energy are provided starting from experimental calorimetric tests, the second part is aimed to understand how the thermodynamic behavior of a polymer solution can be influenced by the presence of a 3D confining interface, focusing on the individuation of critical conditions, in terms of *degree of confinement*, for observation of the effects on the chain entropy due to the presence of the interface. Among several applications, this task seems to be of crucial importance in studying the phase separation processes involving polymer-containing systems.

By varying the degree of confinement of the system, the reduction of conformational entropy can make energetically favored chain conformations characterized by a high order degree. The degree of confinement can be used as a controlling parameter for the morphologies of the phase separated systems, due to its influence on the thermodynamics and, consequently, on the mechanism of the phase separation process. The presented study

is focused on the thermodynamic behavior of a single polymer chain in an athermal solution in diluted conditions, confined by a 3D interface, paying particular attention to the chain conformational entropy penalty arising from the excluded volume effects. In order to reach this goal, the static Monte Carlo (MC) simulation method is employed, and applied to a modification of the Self Avoiding Walk (SAW) model.

In conclusion, the work presented in this chapter is aimed to give some tools for the study of thermodynamics of polymer solutions, taking into account both enthalpic and entropic contributions to the system free energy. In fact, a better understanding of thermodynamics of polymer solutions is of fundamental importance in order to control morphologies of systems fabricated by means of phase separation processes. While for the enthalpic contribution, an experimental approach is presented (at this aim, one of the most used ternary systems for porous microstructure is taken into account), for the entropic one, a simulation approach is discussed.

4.2 Materials and methods

4.2.1 Materials

Poly-L-lactic acid (PLLA or Resomer L209 S), with an average molecular weight of 125 000 Dalton was purchased from Evonik Industries. Diethylene dioxide (1,4 dioxane) of analytical quality and without any further purification, provided from Sigma-Aldrich, was used as a solvent for the chosen polymer. Milli-Q water was used as a nonsolvent for it.

4.2.2 Polymer solution preparation

PLLA in solid pellets was added in weight/volume (w/v) percentages 0.5%, 1% and 1.5% to pure dioxane in an Erlenmeyer bulb, immersed in a silicone oil bath on a stirring hot plate. A thermocouple was used to control the oil bath temperature, set at 116 °C, in order to allow the polymer pellets to dissolve. The solution was maintained at this temperature for at least 2 h. The system was kept in continuous stirring (300−350 rpm). Temperature of 116 °C is higher than the dioxane boiling point (101 °C); thus, during the dissolution of the polymer, evaporation of dioxane was expected, with consequent undesired changes in system composition. To avoid this drawback, a glass Liebig condenser was installed on the top of the

Erlenmeyer bulb. When the solution appeared transparent because of the dissolution of the polymer, without stopping the stirrer, the system temperature was finally lowered to 80 °C and maintained at this value for at least 1 h before starting the experiment.

4.2.3 Isothermal Titration Calorimetry experiments

Titration experiments of PLLA/dioxane solutions with pure water were carried out by means of a Nano ITC Low Volume calorimeter (TA Instruments); the principles of operation have been exhaustively described previously in literature[26]. Before starting the experiment, the instrument idle temperature was set to the desired value and several minutes were needed to reach the heat flow stability corresponding to the new temperature. When such stability was reached, the syringe holder was removed and the sample cell (its volume of reaction 170 µL) was filled with the PLLA/dioxane solution previously prepared and degassed, while the reference cell was filled with pure dioxane. The titration syringe (maximum volume 50 µL) was charged with degassed pure water and restored in the buret; at this point the buret was inserted in its accommodation and the calorimeter was closed. Before starting the experiment, the stirring rate was set to 250 rpm, and several minutes elapsed again so that the heat flow stability was restored, then the experiment definitively started. All the experiments were carried out with an equilibration time of 600 s, initial and final baselines of 120 s, and a titration program made up of 25 injections, each of 2 µL of pure water (the instrument automatically sets an actual volume of 1.96 µL). The stirring rate was fixed at 250 rpm; the time elapsed between two successive injections was set to 800 s for the first six injections, to 600 s for the following 10 injections (the ones going from the seventh to the 15th), and to 420 s for the remaining ones. The injection volume was chosen after some optimization experiments, in order to avoid the drawback linked to the instrument full scale; some preliminary experiments were needed to identify the time for the heat flow signal to return to the baseline in order to determine the time between two successive injections. The polymer percentages of the starting solution were chosen in order to the avoid heat flow signal reaching the full scale. For all the experiments, the starting solution was made up of PLLA in pure dioxane, and the final solvent/nonsolvent ratio was equal to 74.8/25.2. This final value was chosen in order to cover the practical interest range, according to the typical ratios used for scaffolds fabrication in previous literature studies[27].

4.2.4 Model for polymer chains

In order to investigate the entropic properties of a single polymer chain in an athermal solvent in presence of a confining tridimensional interface, a reticular model based on a cubic lattice was adopted, following the theoretical approach developed by the Flory-Huggins theory for unconfined solutions; for the chain a modified Self Avoiding Walk (SAW) model was used. The whole solution was modeled as a tridimensional lattice with cubic cells, of which each vertex is occupied by a polymer chain segment or a molecule of the low molecular weight species, representing the solvent or the non-solvent. The edge of each cell was chosen as unit length, while the boundaries of the simulation domain represented the confining interface: therefore, periodic boundary conditions were not be used, but the boundaries of the whole cubic lattice were be treated as solid obstacles. For the macromolecular chain, a modification of the SAW model was used. The classic SAW model has been exhaustively described in literature[28]: it consists of the construction of a random sequence of lattice sites, without ever returning twice to the same site and never intersecting the path already traced. However, instead of the standard SAW model, in which each chain segment links two consecutive nodes in the lattice, in the presented algorithm, the segments of the chain were connected by vectors of the type [±a, ±a, 0], [0, ±a, ±a] or [±a, 0, ±a], where a represents the lattice constant, chosen for convenience equal to 1. In the following lines, this algorithm will be referred to as the (011) motion. This algorithm differs from the ones previously used in literature, both for polymers[29] and for polypeptides[30] for the maximum coordination number of segments: in this case the coordination number is equal to 12, in order to reduce the chain flexibility.

In this way, the chain generation path consisted of the following steps:

- the first chain segment was randomly allocated on a site within the lattice;
- the second chain segment was then allocated within the lattice by translating the first one of a random vector of the type specified above;
- a similar procedure was used for the segments following the second;
- at each step of the chain generation, it was necessary to check the respecting of the non-overlapping assumption of the model.

At the end of the chain generation, each occupied site represented a chain segment, while the vectors connecting two consecutive segments were the chemical bonds and defined the Kuhn length l_s of the modeled polymer chain. All the remaining vacant sites were then each occupied with a solvent molecule (with a solvent or a non-solvent molecule, in proportion equal to the solvent/non-solvent ratio characterizing the system, if the simulation of a ternary solution was desired). An example of chain generated following the described algorithm is shown in Fig. 4.1. The model for the chain generation took into account the excluded volume interactions; in particular, two different contributions for each segment were considered:

- the excluded volume linked to the non-overlapping of two or more chain segments;
- the presence of the confining interface, that reduces the available volume for the polymer chain.

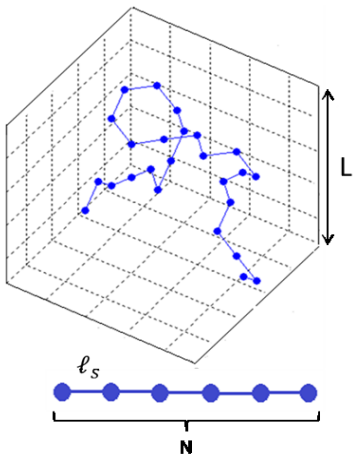

Figure 4.1: *Representation of the modified SAW model on a cubic lattice. A fragment of a single polymer chain (• single segment, ---- bond connecting two segments) is represented as a Self Avoiding Random Walk on a 3D cubic lattice. The remaining vacant sites are occupied by solvent molecules.*

It was assumed that the system behaves as an athermal one, giving estimation of the chain conformational entropy in the case of the theta condition of the solvent[31]: for this reason, long range interactions and local potential can both be neglected, but the model can be easily extended in order to take them into account. The cubic lattice boundaries were treated as a solid obstacle for the polymer chain; no chain adsorption was assumed; therefore, only the entropic contribution to the chain conformation due to the presence of the interface was taken into account. This assumption is more realistic in the case of a liquid interface confining the polymer solution; in fact, in this case the interactions between the

interface and the species in solution can be considered a lot weaker with respect to the case of a solid interface. The degree of confinement of the system is typically defined as the ratio of a chain characteristic length and a confining interface characteristic length[32]: only when the two dimensions become comparable, the confinement effects become significant. In the presented study, the degree of confinement D.C. was defined as the ratio between the length of the polymer chain when completely stretched and the length of the edge of the cubic lattice. The radius of gyration could represent an alternative choice for the characteristic length of the chain, but it loses its physical meaning when we assume an athermal solution. indicating with N the number of segments, each of length l_s, and with L the lattice edge, formally the degree of confinement was defined as follows:

$$\mathrm{D.C.} = \frac{\mathrm{N} \cdot \mathrm{l_S}}{\mathrm{L}} \tag{4.1}$$

The edge of the single cell of the lattice was chosen as unit length: for this reason L was equal to the number of segments composing the edge of the 3D cubic confining interface, further referred to as n. Calculations of chain conformational entropy were carried out by varying the degree of confinement using two different parameters: the number of Kuhn segments N composing the polymer chain, and the cube edge length L. The first case is equivalent to increasing the molecular weight of the polymer chain, while the second one corresponds to varying the volume allowed to the chain disposition in solution.

4.2.5 Simulation method

For the implementation of the described chain generation method, a code was written using Matlab and Simulink (Release R2013a, The MathWorks, Inc., Natick, Massachusetts, United States). Polymer chains of up to 800 segments were generated, and the degree of confinement was changed from 0.1414 up to 28 by varying both the cubic lattice characteristic length and the chain length.

During the chain generation, for each segment the coordination number ω was calculated as the number of sites available for the allocation of the successive segments, i.e. the number of adjacent sites free from other chain segments or the confining interface: for each segment, according with the algorithm definition, $\omega \leq 12$.

As for the Static Monte Carlo simulation method[33], a sequence of statistically independent chain conformations was generated, using the code implementing the procedure described above. For each chain conformation, the coordinates of the site allocating the first segment were identified by means of a generator of random integers, uniformly distributed in the interval [1, *number of sites for edge - 1*]; the successive segments were allocated choosing the components of the random vectors specified above by means of a generator of random integers in the interval [-1,1].

For each segment the coordination number was then averaged on 10^3 chain conformations, statistically independent from each other.

4.2.6 Calculation of chain conformational entropy

The conformational entropy of the confined and the unconfined single polymer chain was calculated using the Statistical Counting Method - a type of Monte Carlo method well described in literature[34] - in order to estimate the entropy of chains terminally attached to a surface[29]. According to this method, the calculation of the chain conformational entropy is based on the following definition:

$$\Omega(i)=\frac{\Omega(i+1)}{\Omega(i)} \tag{4.2}$$

where Ω(*i*) e Ω(*i*+1) represent the number of accessible conformations for the chain consisting of *i* and of *i* + 1 segments, respectively; ω(i) can be interpreted as the number of allowed allocation for the segment $i+1$, i.e. the coordination number for the *i-th* segment; as described above, in the studied case

$$\omega(i) \leq 12 \text{ for } i = 1,2,\ldots,N$$

(with N number of chain segments), in accordance with the chosen (011) algorithm.

If the coordination number $\omega(i)$ is known for each chain segment, starting from the definition (2), it is possible to calculate the number Ω of possible conformations for a polymer chain made up of N segments, using the following equation:

$$\Omega(N) = \prod_{i=1}^{N-1} \omega(i) \tag{4.3}$$

In order to calculate Ω(N), in the presented work, the values of ω(i) averaged on a set of 10^3 chain conformations, generated by the MC sampling method described above, were inserted in the formula (3).

Then, the conformational entropy S of the unconfined or confined single polymer chain can be calculated using the Boltzmann equation:

$$\frac{S}{k_B} = \sum_{i=1}^{N-1} \ln \omega(i) \tag{4.4}$$

where k_B is the Boltzmann constant and ω(i) is still the averaged coordination number for the segment i.

In other words, the formula (4) is the purely conformational entropy of a single polymer chain, calculated as the sum of the logarithms of the coordination numbers calculated at each step of the SAW chain generation. These coordination numbers represent the number of free lattice sites allowed for the following segment allocation: they are calculated by subtracting the number of sites occupied by other chain segments or by the confining interface from the theoretical coordination number.

In the calculation of the conformational entropy, the excluded volume contributions from the chain and from the interface are both taken into account.

All the calculation of the normalized entropy S/k_b were carried out on 10 different set of 10^3 chain conformations, obtaining a standard error in the order of 0.25%. As a consequence, we conclude that the accuracy of the method is satisfactory.

4.3 Results and discussion

4.3.1 Enthalpy of mixing and interaction parameters

The aims of the calorimetric measurements were to study and to thermodynamically characterize the interaction between PLLA and water. Referring to blank test water/dioxane, first results were obtained by carrying out titrations of pure dioxane with pure water, both at 333.15 K and at 313.15 K, until a final dioxane (D) to water (W) ratio of about 75/25 was reached. Then, the same titrations were carried out for initial solutions prepared by dissolving PLLA in pure dioxane, which is a good solvent for the selected polymer. Three different initial polymer percentages were used, 0.5/1/1.5 % wt/v, but in all the cases the dilution due to the titration gave a reduced final polymer percentage.

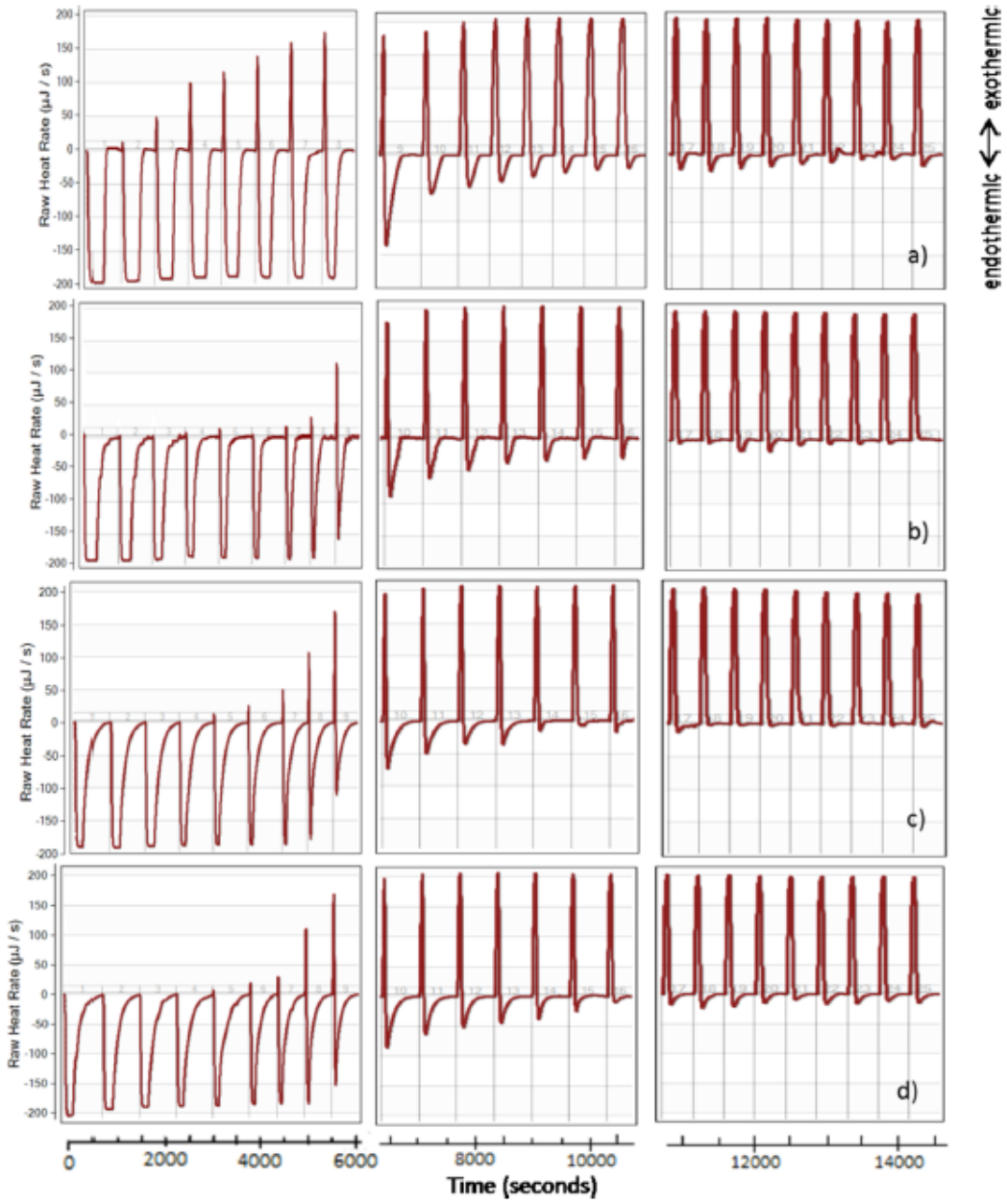

Figure 4.2: *Titration experiments results at 333.15 K. Titration of pure dioxane with pure water (a); titration, with pure water as titrant, of PLLA/dioxane solutions, at different polymer percentages: 0.5 wt %/v (b), 1 wt %/v (c), 1.5 wt %/v (d).*

The Fig. 4.2 shows the results of the titration experiments carried out at 333.15 K in terms of power released or adsorbed from the reaction cell of the calorimeter as a function of the time (peaks above the baseline represent exothermic phenomena while peaks under the baseline represent endothermic phenomena); to better understand the differences between the different cases, the diagrams are organized in a matrix form. In detail, Fig.4.2 a) represents the result of the titration of pure dioxane with pure water (blank test) while, Fig. 4.2 b–d) show the diagrams of the titration of a PLLA/dioxane solution (at different w/v% of

PLLA) with pure water. The differences among the first diagram (Fig. 4.2 a) and the following figures (Fig. 4.2 b–d) are due to the contribution of the heat involved in the interactions PLLA/water, which overlaps the interaction dioxane/water. The PLLA/water contribution was then isolated and quantified in Fig. 4.3.

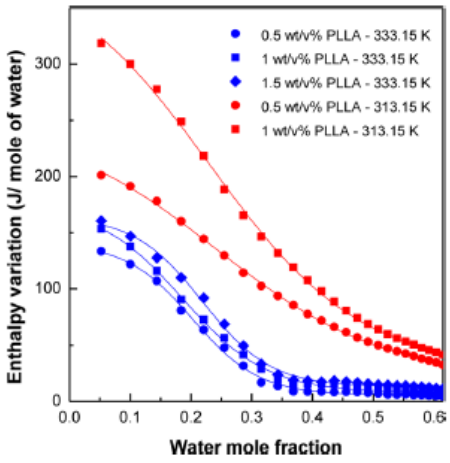

Figure 4.3: *Enthalpy variation for PLLA–water interaction as a function of the water mole fraction in the binary solvent. The values for the specific enthalpy variation were obtained by subtracting the blank test results from the results of the polymer solutions titrations.*

Generally, in each of the result diagrams shown in Fig. 4.2, it is possible to recognize three different regions (not strictly corresponding to the diagram matrix cells): each region represents a different state of the interaction phenomena developing in the sample cell between the species in solution. In particular, in the first region, it is possible to notice that the initial injections give rise to purely endothermic peaks, whose area is approximately the same, showing that all the injected titrant interacts with the solution in the cell and such interaction has the same intensity for all initial injections. The second region is characterized by the evolution of the interaction phenomena involved in the mixing process between the water and the PLLA/dioxane solution: the peaks show the overlap of an endothermic phenomenon and an exothermic one, whose intensity changes with the increase in the number of injections. This competition makes the shape of the peaks changing at each injection, showing the evolution of the solvation phenomena for the species involved in the system: it appears clear as a growing number of the polymer sites, available for the solvation, become saturated. The third region shows peaks the same height: they represent the saturation of the interactive phenomenon; the addition of further titrant determines only a dilution of the system. The “boundaries” of each region, in terms of number of

injections or in terms of dioxane/water ratio, change with the polymer content of the initial solution and/or the temperature of the titration experiment. The outputs obtained for the titration experiments of PLLA/dioxane solutions are the overlapping of several phenomena and do not represent the pure heat contribution of the interaction polymer/water: they include also the heat of dilution of water in dioxane. In order to evaluate the only contribution deriving from PLLA/water interactions, the output of a blank test (consisting of a titration experiment of pure dioxane with pure water as titrant) must be subtracted from the titration results of the polymer solution. After this subtraction, it is possible to evaluate the only heat involved in the interaction between PLLA and water. To this aim, the blank tests were carried out at 313.1K and 333.15 K. From the comparison between the strips of Fig. 4.2, it appears clear as all the results are qualitatively similar: they differ for the number of injections needed for the saturation of the power signal and for the relative importance of the endothermic and exothermic phenomena, that is, for the relative height of the peaks, under and above the baseline. For the studied polymer percentages, these differences are not very relevant; this evidence can be attributed to the high thermal energy content of the system: the polymer chains have enough mobility in solution to arrange themselves in new conformations by adding water to the system. In the case of lower temperature, the differences in terms of saturation of the interaction phenomena become more relevant.

In order to evaluate the heat involved in the mixing phenomena between the PLLA target molecules and the water, the power signal was integrated in time for each peak, until the baseline is reached again after each injection; this way, the heat generated or absorbed at each water injection was calculated. Fig. 4.3 shows results for the enthalpy variation, reduced to the only contribution due to the interaction phenomena occurring between the target molecules (PLLA chains) and the water used as titrant, to focus on the interaction between the polymer and its nonsolvent. These results were obtained by subtracting the blank test results from the titration results obtained for the polymer solution. For all the investigated conditions, in terms of both temperature and polymer initial percentage, the trend is almost monotonically decreasing and, in particular, it is well fitted by a Boltzmann sigmoid. Furthermore, the enthalpy variation is always positive, that is, the process of mixing between PLLA and water is always endothermic, in accordance with the hydrophobicity of the polymer. Focusing the attention on a single temperature, and in particular on the results obtained at 333.15 K, the changing in the initial polymer percentage does not greatly affect

the enthalpy variation. Indeed, by increasing the PLLA content, only small increments in the enthalpy variation are observed for the whole binary solvent composition range studied. Switching on the study of the results obtained at 313.15 K, it is possible to notice that the same increment in the polymer percentages determines an increase in enthalpy variation (at a fixed binary solvent composition) higher than the one determined at 333.15 K. By comparing the curves obtained at 313.15 and 333.15 K for the same initial PLLA percentage, it is possible to notice at a fixed water mole fraction the enthalpy variation is higher at 313.15 K; that is, the process of mixing is more endothermic[35-38]. Experiments at 313.15 K were performed for polymer percentages until 1 w/v% PLLA, instead of 1.5, to avoid the occurring of potential phase separation phenomena (as for example the reaching of cloud point) or PLLA precipitation within the ITC sample cell. Indeed, in that case, measurements could be affected by different undesired heat contributions. In fact, the aim of the work was to estimate the interaction parameters of the species in solution, and not the thermodynamic parameters during phase separation processes.

The interactions between PLLA and water can be explained in terms of hydrogen bonding phenomena, in accordance to the molecular structures of the considered species. There are several different types of hydrogen bonding involved in the mixing process: the PLLA−water hydrogen bonds, the intramolecular PLLA hydrogen bonds and the water−water hydrogen bonds. From literature[39], it is well-known that PLLA is a hydrophobic polymer, and that its interaction with water is characterized by a positive Gibbs free energy variation; but it is important to keep in mind that the Gibbs free energy variation of a mixing process is made of an enthalpic contribution and an entropic one, in accordance to the following law:

$$\Delta G_M = \Delta H_M - T\Delta S_M \tag{4.5}$$

As shown in Fig. 4.3 for the studied systems, the enthalpy variation is always positive; by increasing the water content, the fraction of PLLA−water hydrogen bonds increases, giving an endothermic contribution. On the other hand, the enthalpy variation decreases during the titration because of the intramolecular PLLA hydrogen bonding that gives the enthalpy variation a contribution that is opposite to the previous one. At the end, the asymptotic value is reached when the polymer hydrogen bonding sites are saturated and only water−water hydrogen bonding occurs. The intramolecular PLLA interactions occur because the polymer chains are “forced”, by the increasing water content and because of their

hydrophobicity, to take a conformation characterized by a reduced radius of gyration in solution, thus encouraging the intramolecular PLLA interactions.

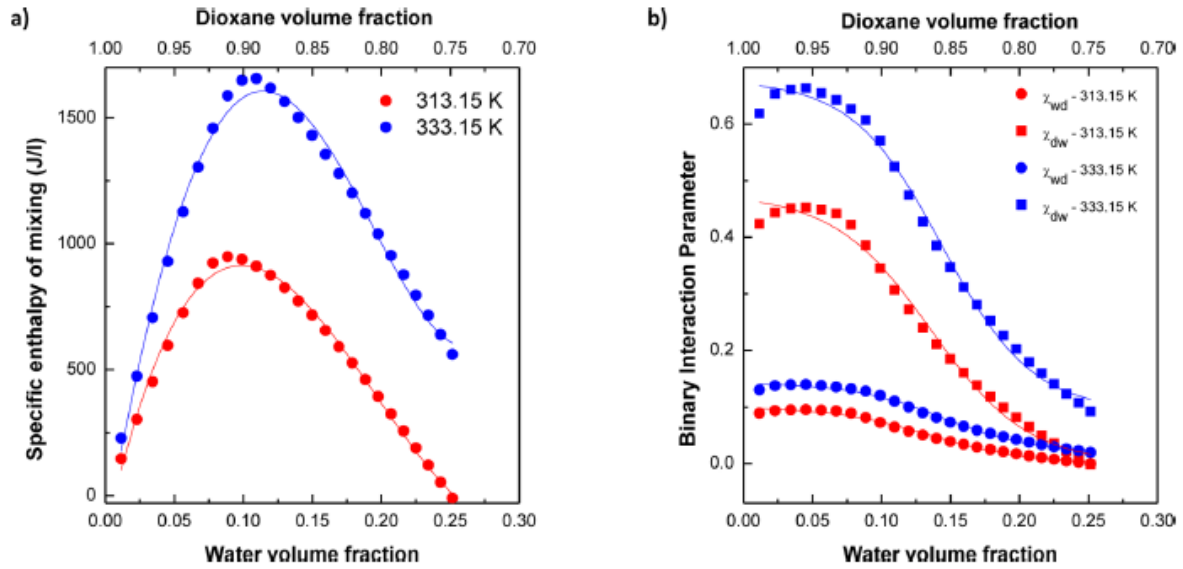

Figure 4.4: *Specific enthalpy of mixing (a) and binary interaction parameter (b) as functions of the water volume fraction in the dioxane/water binary solution. (a) Enthalpy variation is shown for both the studied temperatures. (b) the figure shows the interaction parameter of dioxane in water and that of water in dioxane, at the two studied temperatures; symbols represent the experimental data and lines represent the fitting curves.*

Fig. 4.4 a) shows the excess enthalpies of mixing for the binary solution made of solvent and nonsolvent, at 313.15 and 333.15 K, as a function of the solution composition. The excess is always positive in the studied composition and temperature conditions, showing that the mixing process is endothermic: the trend passes through a maximum and then begins to decrease. The number and strength of hydrogen-bonding between water and 1,4-dioxane might be affected on enthalpy behavior very strongly, as also reported by Suzuki et al.[40]. This behavior can be explained in terms of hydrogen bonding networks between the species. In detail, at the beginning of the experiment, we have a large amount of 1,4-dioxane, and therefore, hydrogen bonding between 1,4-dioxane and water mostly occurs. On the contrary, for higher water contents, the water−water hydrogen bonding becomes relevant. In this concentration region, the solution might consist of a cluster of water and 1,4-dioxane within the solution. The Flory−Huggins lattice model for the enthalpy of mixing[31] was then employed in order to calculate the binary interaction parameters for the couple

dioxane/water, further referred to as χ_{wd} and χ_{dw} starting for the excess enthalpy values. Their evolution as a function of the water volume fraction is shown in Fig. 4.4 b).

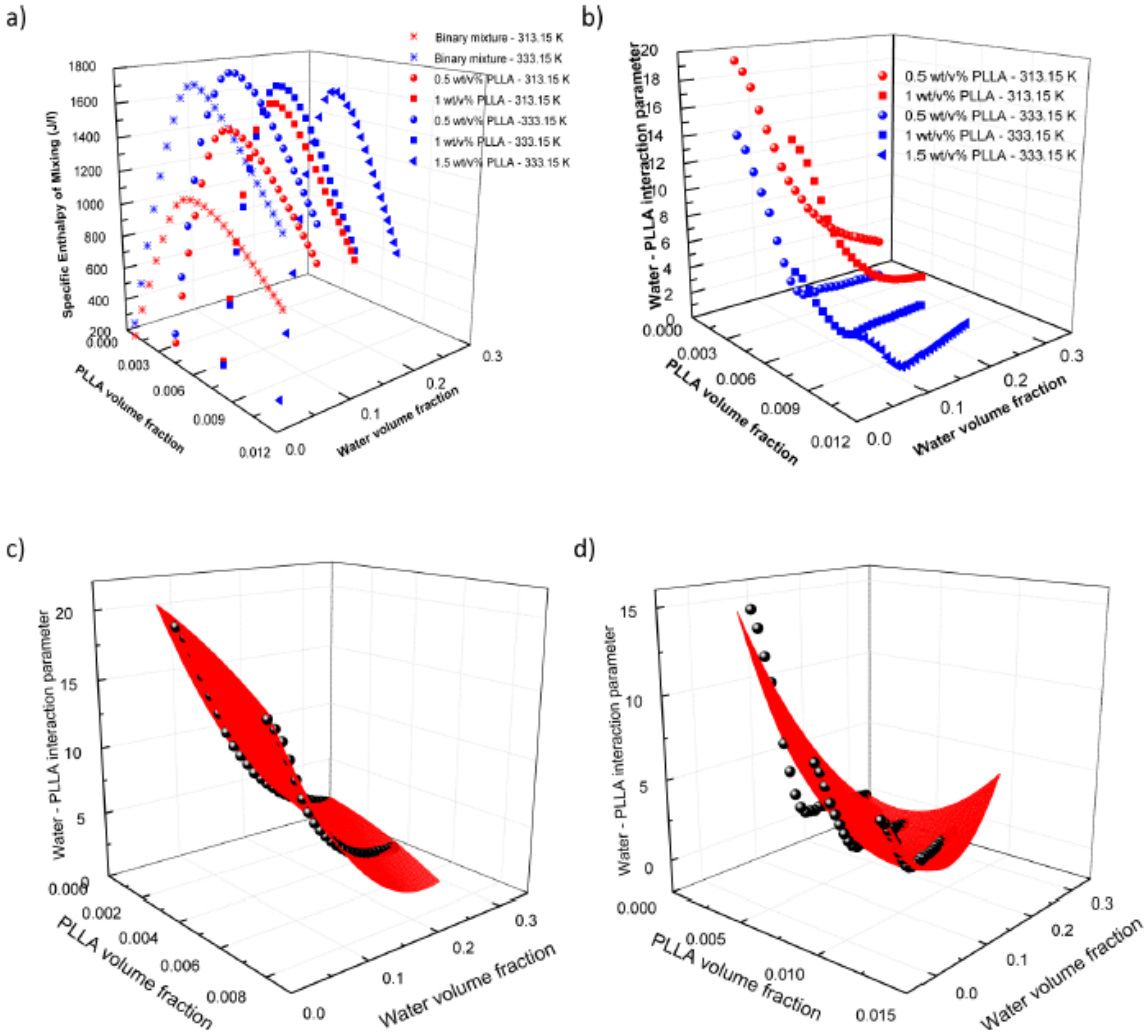

Figure 4.5: *Specific enthalpy of mixing (a) and water–PLLA interaction parameter (b) as a function of both water and PLLA volume fraction in the ternary solution; fitting surfaces for water–PLLA interaction parameters: (c) data at 313.15 K and (d) data at 333.15 K.*

In Fig. 4.5 a), the excess enthalpy values for the mixing curves for the ternary solutions are shown. The curves for the binary solutions are also reported, in order to make comparisons. For all studied ternary solutions the enthalpy of mixing is positive; that is, in the range of temperatures and compositions investigated, the mixing process is endothermic. At 333.15 K, the enthalpy values for the ternary solutions are not very different from the binary mixtures ones; at 313.15 K, at a fixed value for the water volume fraction, the enthalpy of mixing increases by increasing the PLLA volume fraction in solution, according to the polymer hydrophobicity. Starting from these results for the enthalpy variation of mixing, by means of the extension to the Flory lattice model for ternary systems[31], the water–PLLA

interaction parameters were estimated by means of the following expression for the enthalpy of mixing of the ternary solution made of the species i, j, and z:

$$\frac{\Delta H_M}{RT} = \chi_{ij} n_i \phi_j + \chi_{iz} n_i \phi_z + \chi_{zj} n_z \phi_j \quad (4.6)$$

The values obtained for the interaction parameters are shown in Fig. 4.5 b). For the solvent/nonsolvent interaction parameter, the results shown in Fig. 4.4 b) were used, while for the PLLA–dioxane interaction parameter a value from literature[3] was used, assumed to be constant both with temperature and solution composition (it was chosen equal to 0.2). The numerical values are summarized in Tab. 4.1.

Water volume fraction	PLLA volume fraction	χ_{wp} (313,15 K)	χ_{wp} (333,15 K)
0,05633	0,0037	15,05627	9,10295
	0,00741	11,40259	3,67066
	0,01111	-	3,12585
0,09911	0,00354	10,25006	2,53203
	0,00707	7,22581	1,12687
	0,01061	-	0,9237
0,12991	0,00341	8,11505	1,92621
	0,00683	5,553	0,90421
	0,01024	-	0,70184
0,14986	0,00334	7,10514	1,97179
	0,00667	4,67684	0,85316
	0,01001	-	0,70589
0,207	0,00311	5,25411	1,67607
	0,00622	3,30029	0,56214
	0,00934	-	0,58366

Table 4.1: *Water–PLLA Interaction Parameters in the ternary system.*

For each temperature value studied, the data of water–PLLA interaction parameters were fitted by means of a two independent variable functional form, in order to model its dependence from the ternary solution composition, that is, PLLA and water volume fractions. In particular, the data were fitted by means of the following equation:

$$\chi_{wp} = \chi_0 + A\phi_p + B\phi_w + C\phi_p^2 + D\phi_w^2 + E\phi_p\phi_w \quad (4.7)$$

The surfaces fitting the data and the model parameters, are summarized in Fig. 4.5 c-d) and in Tab. 4.2, respectively. In Tab. 4.2, the values for the adjusted coefficient of determination are also reported: they reveal that the model (4.7) gives a very good fitting of data at 313.15 K, while for data at 333.15 K the fitting is less accurate, but still satisfactory.

T (K)	χ_0	A	B	C	D	E	$\bar{R}^2$
313,15	24,14	-224,97	-155,03	-74659,09	311,90	1510,36	0,996
333,15	22,95	-2501,47	-158,78	95713,26	326,63	5982,96	0,917

Table 4.2*: Fitting parameters for the model (4.7).* $\bar{R}^2$ *represents the adjusted squared coefficient of determination for the considered model.*

4.3.2 Entropy of polymer chain

According to previous works[34,41], through the comparison with the Exact Enumeration (EE) method and the Renormalization Group (RG) theory, the Statistical Counting (SC) method gives good results for the conformational entropies of (001) SAW chains. Also for (112) SAW chains, the model appeared to give good estimation of the conformational entropy - for both free chains and chains irreversibly terminally attached to a surface[29] - for numbers of chain segments up to 1000.

In this work, it was employed the SC method for (011) SAW chains, up to 800 segments each, in the presence of a 3D confining interface. To validate the model for the confined system, simulations for free chains were performed first, and then for different degrees of confinement, i.e. for different values of the confining interface characteristic length. The first results of the SC method, applied to (011) SAW chains, were obtained for the calculation of the averaged coordination number for free chains up to 800 segments; then the calculations were repeated for chains of the same length, but in different confinement conditions obtained by varying the cube characteristic length. All the results are shown in Fig. 4.6, in terms of dependence of the segment averaged coordination number (referred to as the coordination number in the following discussion) as a function of the number of segments composing the generated SAW.

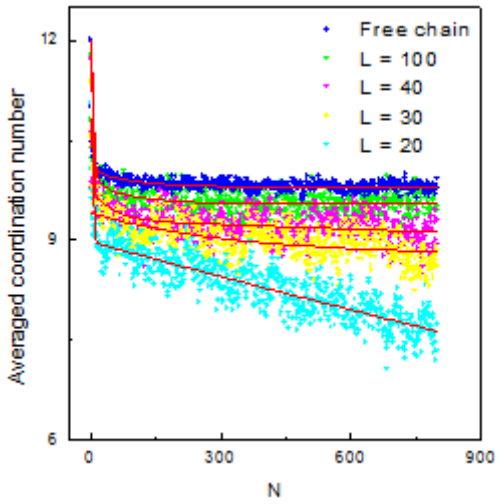

Figure 4.6*: Averaged coordination number vs. chain length N, resulting from Monte Carlo calculations. The results are shown for 800 segments SAW, in absence of confinement and for 4 different values of the characteristic length of the confining interface, i.e. of degree of confinement D.C.; dots are simulations results; red lines are data fitting.*

Fig. 4.6 shows how, in the case of free chains, for several initial segments the coordination number value is very close to the maximum (ω = 12) allowed for the chosen modification of the SAW, then it decreases for the successive segments until an asymptotic value is reached: for the free chain this value is 9.8 and it is reached after allocating 150 chain segments. In this case the deviation of the calculated coordination number from its maximum value is only due to the excluded volume effects arising from the non-allowed overlapping of two or more chain segments on the lattice. The same trend observed for the free chain is also found for chains confined in cubic cells of L = 100, 40, 30, corresponding to increasing degrees of confinement, but in this case the asymptotic values reached by the coordination number and the number of segments needed for its value saturation are quite different: they are respectively equal to 9.54 (reached after allocating 420 segments), 9.13 (reached after allocating 700 segments), and 9.82 (reached after allocating 750 segments). If the volume available for the macromolecule in solution is further reduced choosing a cube with L = 20, a modification in the coordination number trend is observed: in this case, after allocating 800 segments in the lattice, the coordination number is still decreasing, proving that the presence of the interface brings the chain to assume very contracted conformations. From the comparison of the curves in Fig. 4.6, an observation of general validity can be made: choosing a fixed number of segments allocated in the lattice, i.e. fixing a value for N, the coordination number decreases by increasing the degree of confinement, i.e. choosing a

smaller edge for the cube. This gap estimates the contribution to the excluded volume interactions arising from the solution confinement, allowing to distinguish the latter from the contribution linked to the segment-segment interaction.

The results obtained for the coordination number were employed to obtain conformational entropies using the Statistical Counting method described above, for different degrees of confinement, applied to chains with different lengths. The results were then compared with the ones obtained for the free chain, in order to evaluate the effect of confinement.

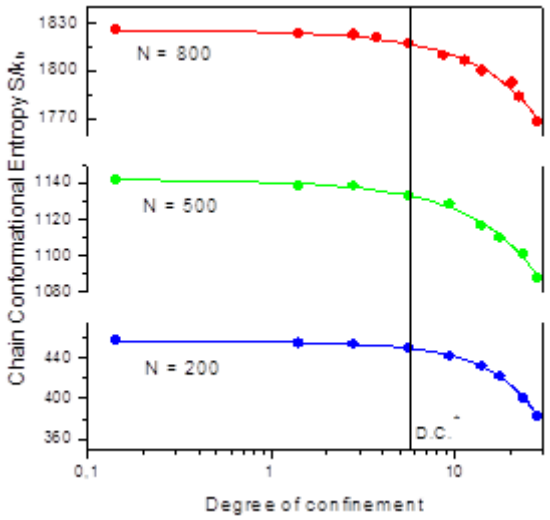

Figure 4.7*: Chain conformational entropy as a function of the dimensionless degree of confinement, for 3 different chain lengths.*

The Fig. 4.7 shows the trend of the conformational entropy of a single polymer chain, of a fixed number of segments N, in solution as a function of the degree of confinement, varied changing only the cube edge length L, while N is kept constant.

The calculations of conformational entropy, starting from the coordination numbers, were repeated for 3 different chain lengths, N = 200, 500, 800, for degrees of confinement going from 0.141 up to 28.28. For all the 3 chain lengths, the trend is qualitatively similar: it is monotonically decreasing and it is well described by the following second order polynomial law:

$$S/_{k_b} = A_0 + A_1 \cdot D.C. + A_2 \cdot (D.C.)^2 \qquad (4.8)$$

N	A_0	A_1	A_2	$\bar{R}^2$
200	456,272	-0,935	-0,060	0,999
500	1141,923	-1,531	-0,013	0,993
800	1825,743	-1,464	-0,019	0,988

***Table 4.3**: Fitting parameters for the model (4.8). $\bar{R}^2$ represents the adjusted squared coefficient of determination for the considered model.*

The parameters for the model (4.8) are listed in Tab. 4.3. The trend is almost constant for the initial points, and then begins to decrease significantly: in other words, for degrees of confinement under 5.7 the entropic penalty with respect to the free chain of the same length is very small and it is of the same order of the standard error reported in the calculations of conformational entropies linked to the chosen method. Over the value of 5.7, conformational entropies significantly decrease, meaning that the effect of the presence of the confining interface becomes relevant. For this reason, the value D.C.* = 5.7 can be interpreted as a threshold to exceed, in order to make the presence of the interface to have an effect on the chain conformations. By comparing the three curves in Fig. 4.7, it appears clear as the value of D.C.* is equal for all the cases, giving to the identified threshold a general validity.

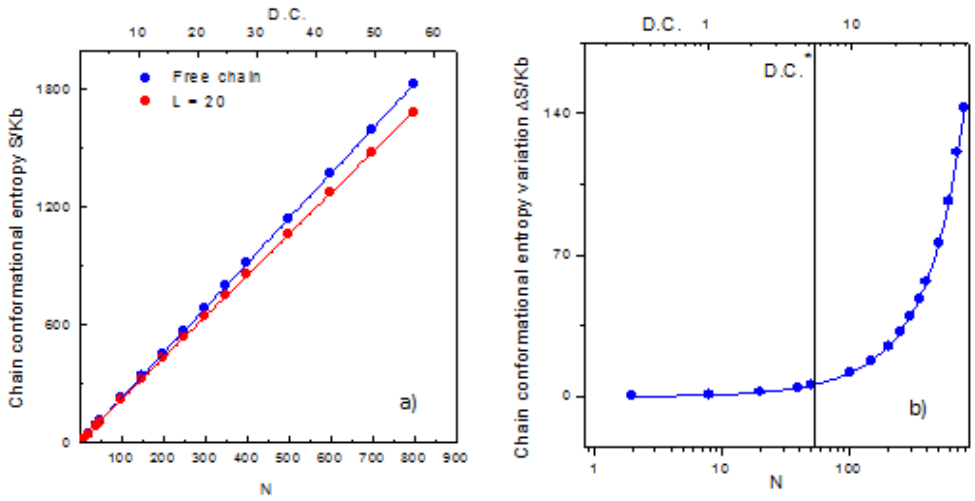

Figure 4.8: *a) Comparison between free and confined chains, for SAWs with a different number of segments N: for the confined chain, all the results are obtained in a lattice with L = 20; D.C.* represents the threshold value for the confining effects; b) entropy variations obtained as the difference between the two curves in Fig. 4 a); the symbols represent simulation results and the lines fitting models.*

In order to validate the existence of a threshold in the meaning described above, Fig. 4.8 a) shows a comparison between confined and unconfined chains, in terms of purely conformational entropy. The data were generated by fixing the confining interface characteristic length and varying the number of chain segments (the polymer molecular weight); a double scale for the independent variable was chosen in order to monitor how the degree of confinement is varied by means of the N variation, at a fixed L. The figure shows that S/K_b grows linearly with the number of chain segments N, for both free and confined chains. This growth is related to the saturation of all the lattice sites. Furthermore, the figure shows that, once fixed a value for N, the free chain presents higher conformational entropy than the confined entropy. A further observation of the data reported in Fig. 4.7 suggests that the three curves can overlap each other by applying a shifting factor to the model (4.8). In particular, employing the curve relative to N = $\overline{\mathrm{N}}$ as a reference, the curves relative to all N' values different from $\overline{\mathrm{N}}$ can be directly deduced from the expression of the conformational entropy variation for the case chosen as a reference, by applying a shifting law. The shifting law can be generalized as follow:

$$\left(S/\mathrm{k_b}\right)_{\mathrm{N}'} = \left(S/\mathrm{k_b}\right)_{\overline{\mathrm{N}}} + \phi_{\mathrm{N}'} \tag{4.9}$$

where $\phi_N = \phi_N(N)$ is the shifting factor and it is found to be a linear function of N. If the curve relative to N = 200 is chosen as a reference, the expression of the shifting factor assumes the form:

$$\phi_N = 2.283 \cdot \mathrm{N} - 456.67 \tag{4.10}$$

The comparison between the data directly obtained from the simulations and the ones predicted by the model (4.9), reveals that the latter give an estimation of the values of conformational entropies with a standard error lower than 2% in almost the whole range of D.C. values studied. For this reason, the model (4.9) is assumed to satisfactorily predict the conformational entropy values. The entropic gap represented by the shifting factor between the curves at different N values can be interpreted as the different contributions to the chain conformational entropy arising from the difference in the number of internal degree of freedom of the chain, determined by the different number of segments, i.e. of the number of points of flexibility. This interpretation is confirmed by noticing the linearity of the shifting factor as a function of the number of segments, as predicted for the entropy of free chains

as a function of N by the RG theory and confirmed by simulations[34]. By shifting all the curves on the reference one, it is possible to estimate the only contribution to the entropy variation linked to the confinement effects; the results can be expressed by a single master curve, independently from the chain length.

Numerical analysis of the simulation results obtained for the free chain and shown in Fig. 4.8 a) reveals that the relationship between the chain conformational entropy and its number of segments can be well described by the following formula, derived from the RG theory[42]:

$$S/k_B = \ln(C_0) + (\gamma - 1)\ln(N) + N\ln(\bar{\omega}) \quad (4.11)$$

where C_0 and $\bar{\omega}$ are parameters dependent on the microscopical details of the network used for the simulative model and γ is the universal exponent. The values for the parameters obtained from the regression of the data in Fig. 4.8 a) for the free chains are respectively: $C_0 = 0{,}076$, $\bar{\omega} = 9{,}81$ and $\gamma = 1{,}45$. The value obtained for γ is close to the value 7/6 predicted by the RG theory, indicating that the algorithm and the method employed for the conformational entropy calculations give satisfactory results. Moreover, the fitting model gives satisfactory results in terms of standard error only for free chains with a number of segments higher than 100, according to the validity of the model (4.11) from the RG theory only for $N \to \infty$. As regards the estimating of the threshold for the confinement effects, Fig. 4.8 b) shows the variation of conformational entropy arising from the confinement of polymer chains of different lengths in a cubic lattice with L = 20, calculated by punctually subtracting the two straight lines in Fig. 4.8 a). If it is assumed that also the trend of the chain conformational entropy as a function of N, at a fixed value of L, can be described by the model (4.11) (this assumption being justified by the linear trend of the results), the entropy variation linked to the confinement of the polymer chain can be expressed as:

$$S/k_B = \ln(C_c/C_0) + (\gamma_c - \gamma)\ln(N) + N\ln(\bar{\omega}_c/\bar{\omega}) \quad (4.12)$$

where C_c, γ_c and $\bar{\omega}_c$ are the parameters for the confined chain. Moreover, the best fit of the data for the entropy variation is given by the polynomial model:

$$\Delta S/k_B = B_0 + B_1 \cdot N + B_2 \cdot N^2 \quad (4.13)$$

In the case of L = 20, the values obtained for the parameters are: B_0 = - 0.144, B_1 = 0.105 and B_2 = 9.45 E-5. From the results in Fig. 4.8 b), it is possible to identify a threshold in terms of degree of confinement (referred to as D.C.*), starting from which the presence of confinement becomes relevant in terms of conformational entropy gap between the

confined and the unconfined chain; in fact, starting from $D.C.^*$, the gap between the two calculated values of conformational entropy becomes significant and it can no longer be attributed to the numerical fluctuation linked to the simulative method chosen. Also in this case, the value found for $D.C.^*$ is equal to 5.7, in agreement with the estimation from the results in Fig. 4.7: it is therefore possible to conclude that this threshold has general validity, and its value is independent from the parameter chosen for the degree of confinement modulation. Indeed, the threshold value can be univocally determined by varying the 3D interface characteristic length, keeping constant the chain length, or *vice versa*.

4.4 Conclusions

In this chapter, an experimental and simulation study of thermodynamics of polymer-containing systems was presented. In the first part, the isothermal titration calorimetric approach was demonstrated to be a suitable route in order to gain information about the energy contributions linked to polymer-solvents interactions, involved in mixing processes of ternary systems. In order to make considerations about the free energy of the ternary system, i.e. about its equilibria, these energetic contribution have to be joint to entropic ones. At this aim, a simulation approach, based on a Monte Carlo method, was developed in order to gain information about the conformational entropy of chains in solutions. The model was extended to cases of confinement of the polymer chains, often encountered in applications linked to nanomedicine and nanotechnologies. These data are of fundamental importance in order to predict phase separation processes, and therefore to control for final morphology features of several polymer architectures used for drug delivery systems.

References

[1] F. Ruggiero, P.A. Netti, E. Torino, Experimental Investigation and Thermodynamic Assessment of Phase Equilibria in the PLLA/Dioxane/Water Ternary System for Applications in the Biomedical Field, Langmuir, 31 (2015) 13003-13010.

[2] Y.S. Nam, T.G. Park, Porous biodegradable polymeric scaffolds prepared by thermally induced phase separation, Journal of Biomedical Materials Research, 47 (1999) 8-17.

[3] P. vandeWitte, P.J. Dijkstra, J.W.A. vandenBerg, J. Feijen, Phase behavior of polylactides in solvent-nonsolvent mixtures, Journal of Polymer Science Part B-Polymer Physics, 34 (1996) 2553-2568.

[4] C. Duce, M.R. Tine, L. Lepori, E. Matteoli, Thermodynamic study of (perfluoroalkane plus alkane) mixtures: Excess and solvation enthalpies, Journal of Chemical Thermodynamics, 39 (2007) 1346-1353.

[5] L.V. Mohite, V.A. Juvekar, Quantification of thermodynamics of aqueous solutions of poly(ethylene glycols): Role of calorimetry, Fluid Phase Equilibria, 278 (2009) 41-53.

[6] M.H. Hamedi, J.P.E. Grolier, Solubility diagrams in solvent-antisolvent systems by titration calorimetry, Journal of Thermal Analysis and Calorimetry, 89 (2007) 87-92.

[7] Y. Jin, W. Wang, Z.H. Su, Spectroscopic study on water diffusion in poly(lactic acid) film, Polymer Chemistry, 3 (2012) 2430-2435.

[8] L. Cartier, T. Okihara, Y. Ikada, H. Tsuji, J. Puiggali, B. Lotz, Epitaxial crystallization and crystalline polymorphism of polylactides, Polymer, 41 (2000) 8909-8919.

[9] H. Tsuji, A. Mizuno, Y. Ikada, Properties and morphology of poly(L-lactide). III. Effects of initial crystallinity on long-term in vitro hydrolysis of high molecular weight poly(L-lactide) film in phosphate-buffered solution, Journal of Applied Polymer Science, 77 (2000) 1452-1464.

[10] J.M. Zhang, H. Tsuji, I. Noda, Y. Ozaki, Structural changes and crystallization dynamics of poly(L-lactide) during the cold-crystallization process investigated by infrared and two-dimensional infrared correlation spectroscopy, Macromolecules, 37 (2004) 6433-6439.

[11] v.E. P.T., C.A. Smolders, Phase Separation in Polymer Solutions. I. Liquid - Liquid phase separation of PPO poly (2,6 - Dimethyl 1,4 - Phenylene Oxide) in binary mixtures with toluene and ternary mixtures, in, J. Polymer Sci.: PART C, 1972, pp. 73 - 86.

[12] V.J. Klenin, Thermodynamics of systems containing flexible - chain polymers, in, Elsevier, Amsterdam, 1999.

[13] D. Marenduzzo, C. Micheletti, E. Orlandini, Biopolymer organization upon confinement, Journal of Physics-Condensed Matter, 22 (2010) 16.

[14] W. Reisner, J.N. Pedersen, R.H. Austin, DNA confinement in nanochannels: physics and biological applications, Reports on Progress in Physics, 75 (2012) 34.

[15] H. Kumar, Y. Lansac, M.A. Glaser, P.K. Maiti, Biopolymers in nanopores: challenges and opportunities, Soft Matter, 7 (2011) 5898-5907.

[16] A. Meller, Dynamics of polynucleotide transport through nanometre-scale pores, Journal of Physics-Condensed Matter, 15 (2003) R581-R607.

[17] A.M. Yoffe, P. Prinsen, A. Gopal, C.M. Knobler, W.M. Gelbart, A. Ben-Shaul, Predicting the sizes of large RNA molecules, Proceedings of the National Academy of Sciences of the United States of America, 105 (2008) 16153-16158.

[18] S.C. Harvey, A.S. Petrov, B. Devkota, M.B. Boz, Viral assembly: a molecular modeling perspective, Physical Chemistry Chemical Physics, 11 (2009) 10553-10564.

[19] A.S. Petrov, S.C. Harvey, Structural and thermodynamic principles of viral packaging, Structure, 15 (2007) 21-27.

[20] J.P. Fu, J. Yoo, J.Y. Han, Molecular sieving in periodic free-energy landscapes created by patterned nanofilter arrays, Physical Review Letters, 97 (2006) 4.

[21] R.B. Schoch, J.Y. Han, P. Renaud, Transport phenomena in nanofluidics, Reviews of Modern Physics, 80 (2008) 839-883.

[22] R.M. Robertson, D.E. Smith, Strong effects of molecular topology on diffusion of entangled DNA molecules, Proceedings of the National Academy of Sciences of the United States of America, 104 (2007) 4824-4827.

[23] M. Daoud, P.G. De Gennes, Statistics of Macromolecular Solutions trapped in small pores, in, Journal de Physique, 1977, pp. 85 - 93.

[24] T.M. Madkour, S.A. Salem, S.A. Miller, The role of the deformational entropy in the miscibility of polymer blends investigated using a hybrid statistical mechanics and molecular dynamics model, Physical Chemistry Chemical Physics, 15 (2013) 5982-5991.

[25] C. Micheletti, D. Marenduzzo, E. Orlandini, Polymers with spatial or topological constraints: Theoretical and computational results, Physics Reports-Review Section of Physics Letters, 504 (2011) 1-73.

[26] I. Wadso, R.N. Goldberg, Standards in isothermal microcalorimetry (IUPAC technical report), Pure and Applied Chemistry, 73 (2001) 1625-1639.

[27] F.J. Hua, G.E. Kim, J.D. Lee, Y.K. Son, D.S. Lee, Macroporous poly(L-lactide) scaffold 1. Preparation of a macroporous scaffold by liquid-liquid phase separation of a PLLA-dioxane-water system, Journal of Biomedical Materials Research, 63 (2002) 161-167.

[28] K. Binder, Applications of Monte Carlo methods to statistical physics, Reports on Progress in Physics, 60 (1997) 487-559.

[29] W. Nowicki, G. Nowicka, J. Narkiewicz-Michalek, Influence of confinement on conformational entropy of a polymer chain and structure of polymer-nanoparticles complexes, Polymer, 50 (2009) 2161-2171.

[30] P. Romiszowski, A. Sikorski, Properties of star-branched and linear chains in confined space. A Monte-Carlo study, Journal of Molecular Modeling, 11 (2005) 335-340.

[31] P.J. Flory, Principles of Polymer Chemistry, in, Cornell University Press, 1953.

[32] M. Fosnaric, A. Iglic, D.M. Kroll, S. May, Monte Carlo simulations of a polymer confined within a fluid vesicle, Soft Matter, 9 (2013) 3976-3984.

[33] A. Sokal, Monte Carlo and molecular dynamics simulations in polymer science, in, Binder, K., editor, New York: Oxford University Press, 1995.

[34] D.L. Zhao, Y. Huang, Z.R. He, R.Y. Qian, Monte Carlo simulation of the conformational entropy of polymer chains, Journal of Chemical Physics, 104 (1996) 1672-1674.

[35] P. vandeWitte, P.J. Dijkstra, J.W.A. vandenBerg, J. Feijen, Phase separation processes in polymer solutions in relation to membrane formation, Journal of Membrane Science, 117 (1996) 1-31.

[36] M. Aratono, A. Ohta, N. Ikeda, A. Matsubara, K. Motomura, T. Takiue, Calorimetry of surfactant solutions. Measurement of the enthalpy of mixing of tetraethylene glycol monooctyl ether and water, Journal of Physical Chemistry B, 101 (1997) 3535-3539.

[37] C. Schugens, V. Maquet, C. Grandfils, R. Jerome, P. Teyssie, Polylactide macroporous biodegradable implants for cell transplantation .2. Preparation of polylactide foams by liquid-liquid phase separation, Journal of Biomedical Materials Research, 30 (1996) 449-461.

[38] J.S. Chen, S.L. Tu, R.Y. Tsay, A morphological study of porous polylactide scaffolds prepared by thermally induced phase separation, Journal of the Taiwan Institute of Chemical Engineers, 41 (2010) 229-238.

[39] D. Garlotta, A literature review of poly(lactic acid), Journal of Polymers and the Environment, 9 (2001) 63-84.

[40] T. Suzuki, M. Fujisawa, S. Takagi, T. Kimura, Excess enthalpies of water+1,4-dioxane at 278.15, 298.15, 318.15 and 338.15 K, Journal of Thermal Analysis and Calorimetry, 85 (2006) 545-550.

[41] W. Nowicki, Structure and entropy of a long polymer chain in the presence of nanoparticles, Macromolecules, 35 (2002) 1424-1436.

[42] P. Cifra, A. Romanov, ON THE ENTROPY OF SINGLE FLEXIBLE POLYMER-CHAINS, Makromolekulare Chemie-Macromolecular Chemistry and Physics, 187 (1986) 2289-2297.

Overall conclusions

In this work, a novel set up for the Electro-Drawing (ED) technique was presented, in order to extend its advantages to the simultaneous fabrication of polymer microneedles in an array configuration. It was based on the patterning of an integrated electric circuit directly onto the pyroelectric crystal, needed in order to generate the electrohydrodynamic (EHD) action responsible of shaping the starting PLGA solution sessile drops in microneedles. Therefore, this engineered device acted as drawing plate for the ED. Preliminary simulation studies allowed to choose the best configuration for the integrated circuit, which determined the uniform heating of a large surface area of the crystal, in order to obtain the simultaneous and homogeneous activation of the EHD action over multiple drops. The designed device was then fabricated by means of a laser lithographic process, followed by an evaporated Ti film deposition.

The novel ED set up was then tested, in order to study the morphology of the fabricated microneedles. A first analysis was carried out on single microneedles. It was found how the engineered driving plate determines an optimized microneedle shape, in terms reduction of the basis pedestal and tip radius of curvature. Further, it was observed how the new solution is suitable for the electro-drawing of microneedles with different height, i.e. fitting different applications. This new shape, combined with a PAA layer interposed between the needle basis and the PDMS support, allowed the release of microneedles from the patch few minutes after the application. Finally, the in parallel ED was demonstrated for multiple PLGA drops, dispensed by means of a μ-contact technique.

Several strategies for tuning the internal morphology of the electro-drawn microneedles were presented. In particular, it was demonstrated how, by acting on the formulation of a W/O emulsion, it is possible to obtain a high porous structure, nevertheless a room temperature hardening process was carried out on the PLGA structures. Also the possibility of provide lipid compartments within the PLGA microneedles was shown: this solution is of practical interest for several applications, including vitamin delivery. If in the case of the ED of emulsions the final porosity was found to be characterized by closed compartments, it was also shown how by conducting a TIPS process on the just shaped microneedles by rapidly quenching them, an interconnected porosity can be achieved.

In the last part of the work, it was demonstrated how Isothermal Titration Calorimetry is an effective strategy in order to gain information about the energy contributions to mixing processes of ternary polymer systems, in terms of interaction parameters between species. A simulative approach, based on Monte Carlo method, was then proposed for entropic estimations on these systems, also in cases of the presence of a confinement. In this way, a thermodynamic characterization useful in predicting the morphologies of the porous systems fabricated by means of phase separation processes can be obtained.